UNIVERSITÁ DEGLI STUDI DI PADOVA

DIPARTIMENTO DI INGEGNERIA INDUSTRIALE

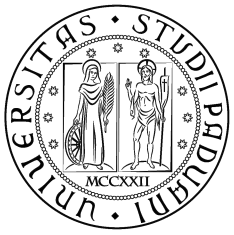

Effects of Surrounding Aircraft Structures on the Noise Produced by Propulsive Jets

Tesi di Laurea Magistrale in Ingegneria Aerospaziale

Laureando: Boris Battistin

Relatore Italiano:	Prof. Antonello Marco
Relatore Estero:	Dr. Jordan Peter (CEAT Laboratory)
Co-Relatore Estero:	Dr. Erwan Collin (ENSMA)

Anno Accademico 2012-2013

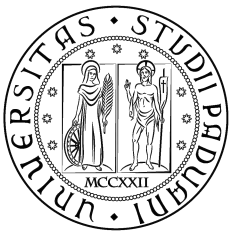

UNIVERSITÁ DEGLI STUDI DI PADOVA

DIPARTIMENTO DI INGEGNERIA INDUSTRIALE

Tesi di Laurea Magistrale in Ingegneria Aerospaziale

Effects of Surrounding Aircraft Structures on the Noise Produced by Propulsive Jets

Laureando: Boris Battistin (626556-IAS)
Relatore Italiano: Prof. Antonello Marco
Relatore Estero: Dr. Jordan Peter (CEAT Laboratory)
Co-Relatore Estero: Dr. Erwan Collin (ENSMA)

Anno Accademico 2012-2013

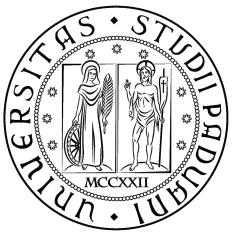

Declaration of Authorship

I undersigned BATTISTIN BORIS, declare that this thesis titled :

'Effects of Surrounding Aircraft Structures on the Noise Produced by Propulsive Jets'

and the work presented in it are my own.

I confirm that:

- This work was done while in candidature for a Master Science (MSc.) degree at the University of Padova.
- Where any part of this thesis has previously been submitted for a degree or any other qualification at this University or any other institution, this has been clearly stated.
- Where I have consulted the published work of others, this is always clearly attributed.
- Where I have quoted from the work of others, the source is always given.
- I have acknowledged all main sources of help.
- Where the thesis is based on work done by myself jointly with others, I have made clear exactly what was done by others and what I have contributed myself.

Date:

_____

Signed:

_____

Disclaimer

All the available data, obtained during the simulations and reported into the presented work, as to be taken "as it is" and, as such, it comes to the reader **WITHOUT ANY KIND OF WARRANTY**. Although the author has put a remarkable effort in trying to keep this Thesis Paper as much scientific as possible and to bring proof, whenever he got a chance, for the statements made and the assumptions considered, he **CAN NOT GUARANTEE IN ANY WAY and BY ANY MEANS** neither the *RELIABILITY* of the presented data, nor their *ACCURACY*.

Edited @ CEAT laboratory,
43, route de l'Aérodrome
86036 Poitiers Cedex, France
in 2012-2013.

Printed in May 2013.

Requests for any permission should be directly e-mailed to the author at the following mailboxes: ***boris.battistin@studenti.unipd.it*** , ***boris.battistin@gmail.com***

“ ...Although the velocity signal is random, one should expect to see intermittently a rather regular spatial structure in the shear layer [...] ”

“ It is suggested that turbulence, at least as far as some of the lower order statistical measures are concerned, may be more regular than we may think it is, if we could only find a new way of looking at it.”

Mollo-Christensen, (1967)

Abstract

The work presented in this thesis paper is the result of a seven-months Thesis Project for obtaining the title of Master Science Degree in Aerospace Engineering at the University of Padova, Italy. It does include the work done during the six-months stage experience, conducted at CEAT laboratory, during the Erasmus exchange program that I made from October 2012 to March 2013, with the ISAE-ENSMA School of Engineering in Futuroscope, Poitiers France.

The work reported is based on the trace of the **"Stage report"** (see Chapters 3 to 6) handed in at the **CEAT laboratory** in Poitiers, where I had physically carried out the stage, under the supervision of **Dr. Peter Jordan** (Chief Researcher of CEAT) and **Dr. Erwan Collin** (Prof. at ENSMA and Researcher at CEAT).

The paper is organized in three main parts.

Part I is an introductory part, with a general overview, in which a thorough **literature review** (Chapter 1) and **theory background** of the discipline of aeroacoustics, the problem of aircraft noise & sources identification, as well as a brief introduction on noise regulations and noise reduction strategies (Chapter 2), are presented, both from a physical perspective, as well as a more mathematical point of view.

In Part II, after Chapter 3, in which a brief **overview of the stage project work** is given - describing the main objectives & achievements during the stage experience -, and Chapter 4, where it is possible to find detailed information concerning the **CEAT laboratory and test facility used**, is well reported in detail, (respectively in subsequent Chapter 5 and Chapter 6), the **effective project work description**, from both, the point of view of the **practical tasks carried out** in the "Bruit & Vent" facility and from the point of view of **data analysis, post-processing and numerical simulations run.**

In the third and last part of the thesis - Part III -, some **conclusions** regarding the work presented in Part II are drawn (Chapter 7), as well as some **future perspectives** for further studies (Chapter 8).

Acknowledgements

I personally want to thank everyone who supported me in these years of hard work, starting from **My family**, for all the help and support they have provided me with, through all these years of study.

Follows a list of all "The Ones" that I would like to thank and a short statement of why...

My Italian thesis project supervisor, ***Prof. Antonello Marco****, for giving me blank check on the whole Thesis Paper Project, as usual and* ***Prof. Marino Quaresimin*** *for giving me this life opportunity with the ERASMUS project.*

• The following People for having me directly helped on my Thesis project:

Dr. Peter Jordan *and* ***Dr. Erwan Collin****, for the help and supervision during the period of stage;* ***Dr. André V.G. Cavalieri*** *for giving me help and precious hints on the thesis subject and for letting me have access to his data, project, thesis paper etc.* ***Prof. Yves Gervais*** *for the help and the material from his course at ENSMA/ENSIP;* ***Alex Royer*** *and* ***Dr. Steve Gerard*** *for all their help, both professional and personal, for being such good friends, in and out of the lab and for all the beers they had offered me and all the great time we had and we had spent together.*

Dr. Guillaume Daviller*,* ***Dr. Alessandro Savarese****,* ***Dr. Remy Maury****,* ***Dr. Gilles Tissot****,* ***Selene Piantanida*** *for being in the office with me and always being ready to confront and share ideas, helping hints and beers;* ***Paolo Rizzato*** *for all the previously mentioned topics, for being a wise presence of faith in my life in these 6 months and for having shared this experience together, in good times and bad ones.*

• The following People and institutions for the help they gave me during my whole staying in France:

The ***ENSMA****;* ***M.me Sacristani****, as a valid representative of the international relations office of the school; the* ***CEAT****, because it gave me such a great opportunity to learn and to become a better man. The* ***University of Poitiers****, its facilities and all the people from this great university that have made my experience possible; the* ***city of Poitiers*** *and all its citizens, for giving me such a great time and welcome in France.*

• Finally I want to personally thank **all the People I met during these unforgettable 6 months.**

Thanks a lot to everyone, May 2013

Contents

List of Figures

List of Tables

Abbreviations

BR or **BPR**	**B**ypass **R**atio
LBPR	**L**ow **B**ypass **R**atio
HPBR	**H**igh **B**ypass **R**atio
UHBR	**U**ltrahigh **B**ypass **R**atio
AA or **AAC**	**A**ero-**A**coustics
CAA	**C**omputational **A**ero-**A**coustics
CAD	**C**omputer **A**ided **D**esign
CFD	**C**omputational **F**luid **D**ynamics
ISAE	**I**nstitut **S**uperiéur de l'**A**éronautique et de l'**E**space
ENSMA	**É**cole **N**ationale **S**uperiéure de **M**ecanique et **A**érotecnique
CEAT	**C**entre d' **É**tudes **A**érodinamiques et **T**hermiques
LEA	**L**aboratoire d'**É**tudes **A**érodinamiques
TAMCO	**T**urbulence **A**nalysis **M**odeling and **C**ontrol
WP	**W**ave **P**acket
NF	**N**ear **F**ield
FF	**F**ar **F**ield
a/c	**A**ircraft
BBN	**B**road **B**and **N**oise
LE	**L**eading **E**dge
TE	**T**railing **E**dge
ICAO	**I**nternational **C**ivil **A**viation **O**rganization
EU	**E**uropean **U**nion
PAS	**P**rimary **A**ntenna **S**tructure

SAS	**S**econdary **A**ntenna **S**tructure
PCB	**P**rinted **C**ircuit **B**oard
AC	**A**lternate **C**urrent
DC	**D**irect **C**urrent
LDV	**L**aser **D**oppler **V**elocimetry
PIV	**P**article **I**mage **V**elocimetry
FWD	**F**ramework **P**rogram
DSP	**D**igital **S**ignal **P**rocessing
NBW	**N**oise **B**and**W**idth
HSL	**H**ighest **S**ide-**L**obe
SLRO	**S**ide-**L**obe **R**oll-**O**ff
PFFX	**P**icket **F**ence **E**ffect
SNR	**S**ignal to **N**oise **R**atio
DFT	**D**iscrete **F**ourier **T**ransform
FFT	**F**ast **F**ourier **T**ransform

Physical Constants

Gravity acceleration	g	=	$9.81\ ms^{-2}$
Speed of sound (@ T_{amb})	c_0	=	$340.29\ ms^{-1}$
Air density (@ T_{amb})	ρ_0	=	$1.18415\ kgm^{-3}$
Air viscosity (@ T_{amb})	ν	=	$14.61 \times 10^{-6}\ m^2s^{-1}$
Ref. Sound Intensity (@std. conditions)	I_0	=	$1 \times 10^{-12}\ Wm^{-2}$

Symbols

t	time	s
f	frequency	s^{-1}
v	velocity	ms^{-1}
v_∞	free stream velocity	ms^{-1}
c_0	std speed of sound	ms^{-1}
p	pressure	Pa
p_∞	free stream pressure	Pa
∇p	pressure gradient(s)	Pa
ρ	density	kgm^{-3}
ρ_∞	free stream density	kgm^{-3}
μ_0	dynamic viscosity	$kg(ms)^{-1}$
ν_0	kinematic viscosity	m^2s^{-1}
l	generic length	m
L	characteristic length	m
h	generic height	m
t	generic thickness	m
u$'$	velocity perturbation	ms^{-1}
p'	pressure perturbation	Pa
ρ'	density perturbation	kgm^{-3}
U_c	phase velocity of convected wave packet	ms^{-1}
M_c	Mach number based on U_c	-
kL	axial compactness parameter	-

Re	Reynolds number	-
Ma	Mach number	-
St	Strouhal number	-
He	Helmholtz number	-
I	acoustic intensity	Wm^{-2}
I_{dB}	acoustic intensity	dB
I_D	dipole acoustic intensity	dB
I_D	quadrupole acoustic intensity	dB
P	total acoustic power output	W
P_D	total dipole acoustic power output	W
P_Q	total quadrupole acoustic power output	W
SPL	sound pressure level	dB
G_0	free field Green's function	-
G	Green's function	-
λ	wavelength	m
k_H	axial wavenumber	m^{-1}
k_a	acoustic wavenumber	m^{-1}

Dedicated to my whole family and all the people I met during this great life-experience ...

Part I

Theory Background and Literature Review

Chapter 1

Literature Review

1.1 Introduction

1.1.1 General Overview on Aircraft's Noise Problem

One of the first acknowledgments of **the problem of aircraft noise** dates back as early as 1927 when a note taken from an aviator's scrapbook - Leon Cuddeback - a chief pilot of Varney airlines, was received by a predecessor of the United Airlines. In this note it is briefly underlined the potential problem of the a/c noise especially the one from the jet engine, that would be the cause of severe headaches to pilots.(Ref. [1])

Although **internal noise** has been one of the major concerns of aircraft acoustic engineers for many years, nowadays the **noise produced by the aircraft engines** has become a dominant factor in the *acceptability* of an airplane, considering the fact that this kind of noise is not only directed and perceived **in the cabin** by crew and passengers, but also it is experienced **on the ground**, especially during **take-off** and **landing** procedures.

With the later development of **high bypass ratio (HBPR) engines** though, noise due to other sources has become important as well, as the previously mentioned one. In fact, at present, engineers are working really hard in order to reduce other sources and components of noise, such as: **turbo-machinery** noise - namely the noise generated by fan, compressor and turbine in the engine - **combustion** noise and especially **jet noise**, being this very last one, the subject of this paper.

Noise **generated aerodynamically** over wings and structures, needs a special mention as well though, because at present, it poses a great challenge that seems will last also for many future years.

Some preliminary solutions to the underlined problems are the following:

• **Internal noise** is treated by placing the engines in *optimized positions* in order to minimize the noise directly radiated to the cabin; most of the time, *the wing is used as a* ***noise shield*** for protecting the fuselage and, moreover, **acoustically insulating materials** are placed over the entire surface of the flight deck and passenger compartments, in order to reduce at minimum the discomfort due to the noise that could be heard inside the airplane.

• **External noise** though, is very difficult to treat and is affected by the *relative location of* ***source*** *and* ***observer***, engine's **level of thrust** that is being throttled during a particular phase of cruise or maneuver and a number of **other factors** that emerge from peculiar aircraft/engine configuration, matching and design.

1.1.2 Detailed Description of Aircraft Noise Sources

As can be easily found in literature or reported in many articles such as, for instance, in Ref. [2] or in Ref. [3], it is possible to categorize the **sources of aircraft noise** in two macro categories, namely:

1. **Engine noise**
2. **Airframe noise**

While the first category concerns the first three broad subsets that will be described below (namely the **turbo-machinery noise**, the **combustion noise** and the **jet noise**), the second category deals almost exclusively with the very last subset reported below, i.e. the **aerodynamic noise**.

- **Turbo-machinery noise**; mainly **fan noise** and **compressor noise** are due to all the mechanical parts that make up the engine and the propulsion system; this source of noise often includes *discrete tones*, associated with blade passage frequencies and their *harmonics*.
- **Combustion noise**: noise generation associated with acoustic sources within the "jet pipe" (i.e. the combustor); it is due to the fast oxidation processes of the jet fuel and its subsequent energy release.
- **Jet noise**: noise generation due to the mixing of high speed exhausts gases - with speed that exceeds $100\,[m/s]$ - with the relatively slower and cooler ambient

surrounding bulk of air; noise generation caused by turbulent eddies produced by shearing flows.

As can be read in various articles and books (see for instance Ref. [4]), this mixing initially occurs in an annular shear layer, which grows with the distance from the nozzle's exit. The mixing region generally fills the entire jet, at an approximate distance of four or five diameters downstream the nozzle's exit. The **high-frequency components** of the emitted sound and their sources are mainly localized in this zone, close to the nozzle, called the near field (NF), where the dimensions of the turbulence eddies are small compared with the nozzle exit diameter. Moving further down the jet axis line, the eddy size approaches the dimension of the jet diameter at nozzle's exit: this is the zone where **lower frequency sources** are found and begin to emit.

- **Aerodynamic noise**: is the noise produced by the rapid airflow over all aircraft's body parts and **aerodynamic appendages**: *fuselage, wings, landing gear, control surfaces* and *airframes* or *structures*, exposed to the airflow, in general.

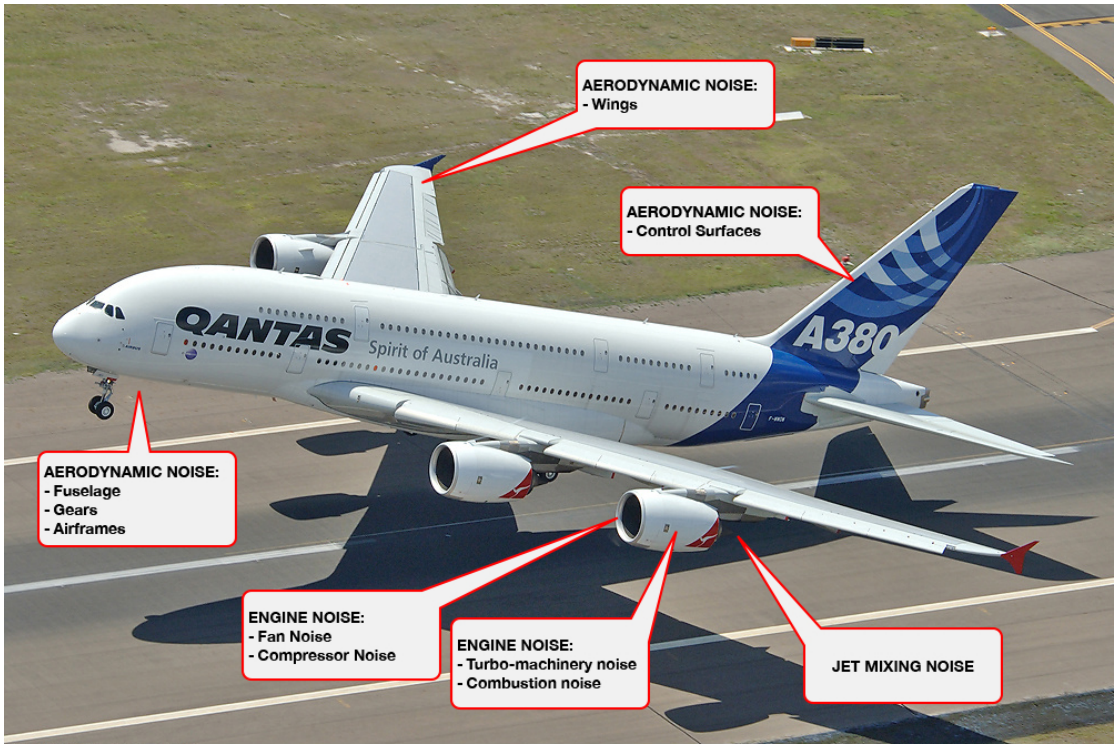

FIGURE 1.1: Sources of aircraft noise (airliner Airbus A380).

In Figure 1.1 are summarized the **aircraft noise macro categories** previously underlined and their mutual localization on an Airbus A380 airliner; the qualitative analysis of each **noise source respective contribution** is reported in Figure 1.2 as found in

Ref. [3] and Ref. [1], while in Figure 1.3 are approximately and qualitatively sketched the **engine noise sources** that it is possible to find in a common turbofan jet engine.

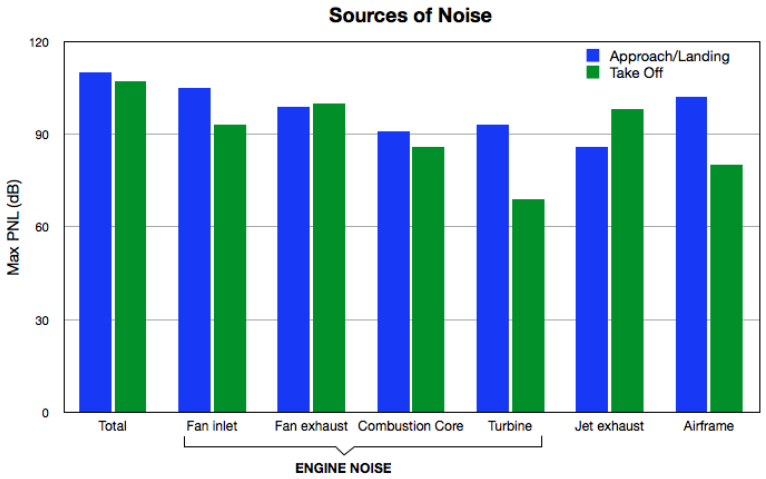

FIGURE 1.2: Various sources contribution to aircraft noise (qualitative analysis graph).

As a matter of fact, the **shear of the boundary layer**, the **unsteady vortex shedding** spawned from landing gears, their bay doors and **other separated flows** - such as those from flap and control surface edges - contribute to a significant part of the acoustic energy emitted from aircrafts, nowadays, especially for large ones and, above all, during **take-off** and **landing** maneuvers as it has already been stated. This is why **aerodynamic noise** is indeed a current challenging area of acoustic research in the field of **aircraft noise reduction** because, as engine noise emissions are reduced, aerodynamic noise can still be considered as a *major acoustic source of future generation aircrafts*.

In Figures (1.4), (1.5) are reported for a quick visual comparison, the **directivity patterns** of two turbojet engines of the types used nowadays respectively in the military

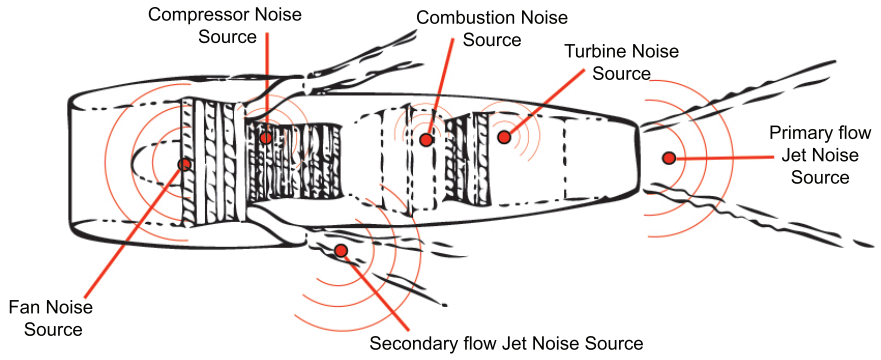

FIGURE 1.3: Sources of engine noise in a turbofan engine.

field (LBPR jet engines) and in the civil one (HPBR jet engines).[1]

As can be seen from cited images, in the LBPR engine of Figure (1.4) the **Jet noise** and **Shock noise** are two very loud sources, quite scattered at high angles backward and below the motor itself, while **Compressor source of noise** and **core/turbine** are of a smaller entity and while this second is scattered only *behind the motor*, the first one obviously radiates its field also *forward*.

In the case of the HBPR jet engine of Figure (1.5) though, there is obviously no shock radiation pattern - because of the lower Mach number ranges at which these types of engine operate - while there is a **consistent Jet noise source radiation**, whose **directivity** is well concentrated at *lower axial angles* than the previous type of engine; one new powerful source of noise in this HPBR engine, is the noise component due to the **fan**, that is both scattered *forward* and *backward* with respect to the engine fan position. **Compressor, Turbine** and **core noise sources** are yet still present in this type of motor and they present a bigger directivity pattern than in the previous engine type.

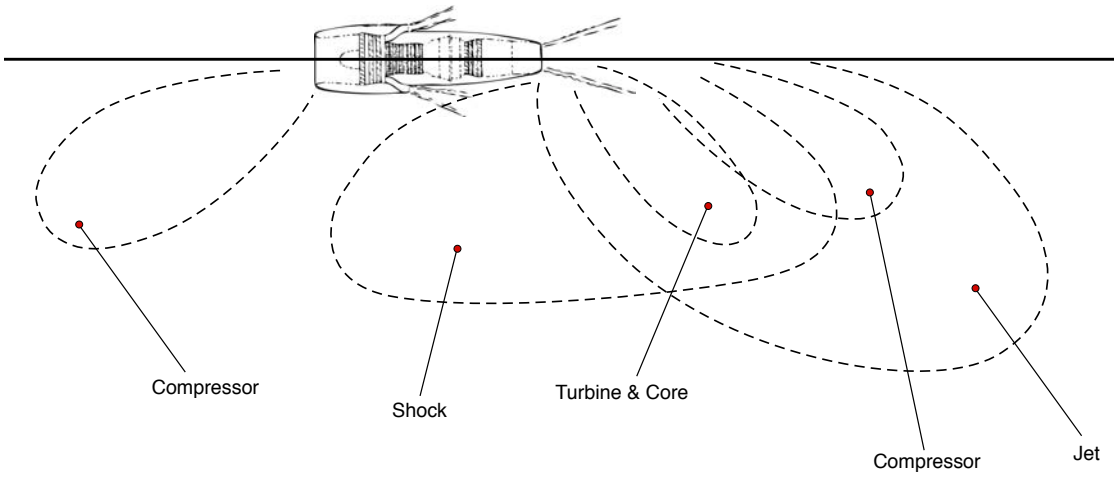

FIGURE 1.4: Directivity of Noise sources in a LPBR Engine (e.g. Military a/c).

1.1.3 International Regulations & Concerns with Aircraft Noise

Aircraft manufacturers and airlines companies are experiencing nowadays great pressure from authorities in order to keep as low as possible the **levels of noise** of aircrafts in airports for **safety purposes** and to maintain the **quality of life** of both, the working personnel and the people living in the surroundings.

[1] These images are a readaptation of those found in Ref. [5]

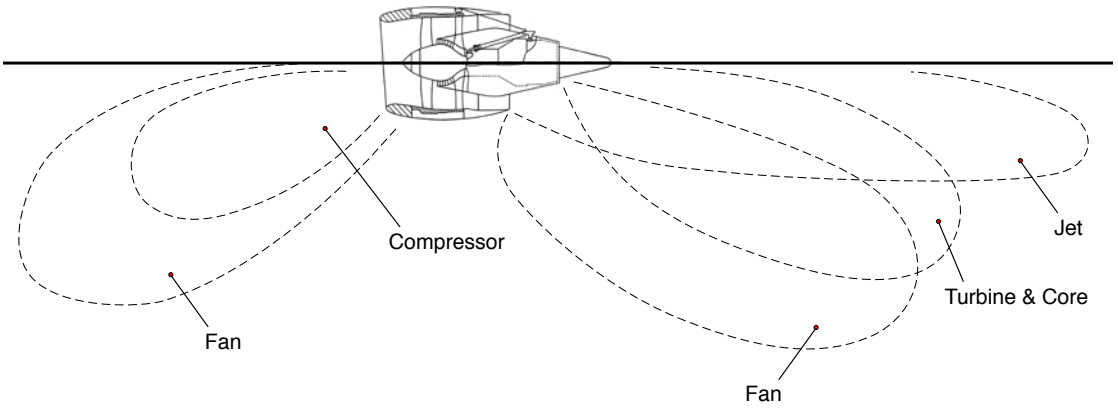

FIGURE 1.5: Directivity of Noise sources in a HPBR Engine (e.g. Civil a/c).

The **ICAO** is the International Civil Aviation Organization, its objective is that of promoting the understanding and security through cooperative aviation regulation; this organization emits every ten years, its updated policies, in order to **reduce the maximum noise level** that an airplane can produce before it can be certified and sold to the public.

The **reduction of noise at the source** is one of the four explored paths; i.e one of the four ways chosen by ICAO in order to reduce the **overall noise problem at airports**. As can be read directly on ICAO's regulations and web site, airplanes and helicopters built today are required to meet the noise certification standards adopted by the Council of ICAO. These are contained in *"Annex 16 - Environmental Protection, Volume I - Aircraft Noise to the Convention on International Civil Aviation"*, while practical guidance to certificating authorities on implementation of the technical procedures of Annex 16 is contained in the *"Environmental Technical Manual on the use of Procedures in the Noise Certification of Aircraft (Doc 9501)"*.

After the last regulation issue, which happened in 2010, aircrafts are barely able to meet the current levels, nowadays. When the noise level threshold will drop again in a few years, no one has a ready-made solution, yet, to directly face the problem.

Always speaking about directives, noise official regulations in FAR Part 36, Stage 3 include **restrictions on noise** in all the 3 following conditions:

1. **Take-off noise**: that is defined as the noise measured at a distance of 21,325 ft (6500 m) from the start of the take-off roll, *directly under* the airplane.

2. **Sideline noise**: that is measured 1476 ft (450 m) *from the runway centerline* at a point where the noise level after liftoff is greatest.

3. **Approach noise**: that is also measured *under the airplane* when it is at a distance of 6562 ft (2000 m) from the runway threshold.

For each of these conditions the **maximum noise level** is a function of **maximum takeoff gross weight**, and for the take-off case the limits depend also on the **number of engines.**

1.1.4 Noise Reduction Strategies

In order to fulfill the always increasing stringent regulations presented and cited above and in order to **reduce noise impact** either on the community or the environment, governmental agencies, aircraft manufacturers as well as engine companies, are exploring various ways to reduce aircraft noise in all its forms.

The main key points on which it is vital to operate now, have been identified in the following list:

- **6 dB** *reduction from previous technology*, for what concerns **interior noise** and **engine noise**.
- **4 dB** *reduction from previous technology*, for what concerns **airframe noise**.
- **50 %** *improvement from previous technology*, in **nacelle liner efficiency**.
- *Community noise impact minimization* through strictly planned **rescheduling of aircraft operations**.

To accomplish this, engineers are working at 360 degrees to develop *higher bypass ratio engines* to **reduce exhaust velocities**, as well as *improve nacelle treatments*, and *plan precise schedules* for operating the aircraft with **take-off power cutbacks** and **2-segment approaches**.

From the point of view of **mechanical design** and **fluid dynamics optimization**, both industries and research laboratories are studying nowadays **passive systems** as well as **active** ones in order to **reduce or control turbulence** and thus **obtain noise emission reduction**. Two of the most commonly studied and used system at the present, are the following state of the art strategies:

1. **Passive system:** use of **mechanical "chevrons"** and jet exit nozzle shaping
2. **Active system:** use of **microjet systems** for turbulence reduction and control.

In Figure 1.6 are reported two examples of both the aforementioned systems, relatively taken from Boeing website and NASA SHJAR Project website.

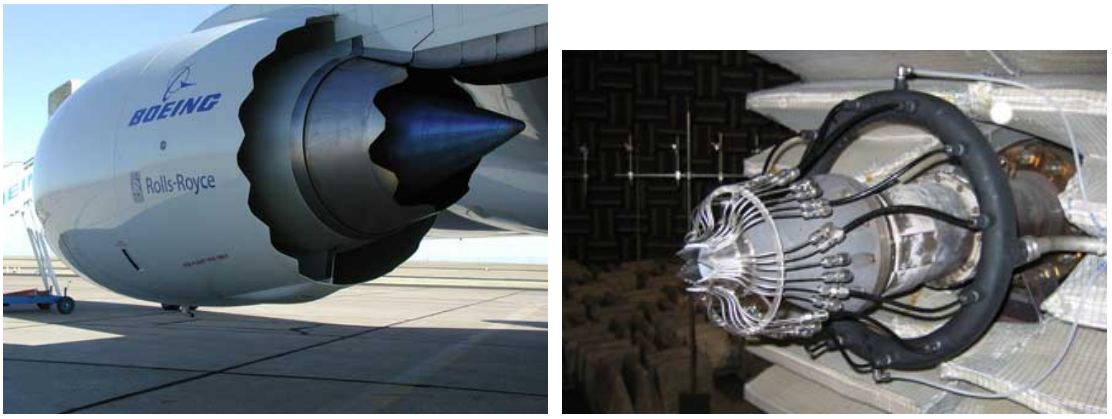

FIGURE 1.6: Example of chevrons and microjet systems for reducing jet noise.

1.2 Brief Introduction to Aeroacoustics

The science of aeroacoustics deals with the **investigation of acoustics phenomena** strongly coupled with the **aerodynamics of the problem** that has to be studied (i.e. it researches the bond between the **sound generation** that occurs in the flow - or that is generated by - and the **fluid mechanics** that underpins the studied topic).

The three major typical processes in aeroacoustics are the following:

- **noise generation by a flow**
- **noise generated by free turbulent flows**
- **noise generated by wall turbulence**

For a more complete description see Ref. [6]. But a part from these, there are more phenomena, related to this particular science such as:

- the combined **volumetric and wall turbulence's effects** on the sound-field
- the **noise propagation in a flow**
- the in-flow **acoustic waves propagation**

- phenomena of **convection, refraction, diffraction of waves** by velocity/temperature flow's gradients or boundaries in the fluid
- the **generation of a flow by sound**
- etc.

One of the main objectives of this discipline is the **reduction and control** of serious problematics related to environmental noise emissions, primarily due - in the aerospace field - to the following categories: **jet exhaust noise**, **jet fan noise**, **airframe/air-structures noise**, as it has already been pointed out in previous introductory paragraphs.

The science of aeroacoustics is obviously concerned with the **sound generated by aerodynamic forces** or **in-flow originating motions**, in contrast with the classical acoustic science which deals with sound generated by externally applied forces or motions.

A few examples of aeroacoustic sound generation are those produced by :

- **unsteady aerodynamic forces** on *propellers, fans, compressor blades*, etc.
- **turbulent flows** at *jet's outlets*
- **acoustic propagation** in *ducts*
- **unsteady aerodynamics** in general

These are in indeed only a small number of examples; many other physical problems or situations that fall within the category of aeroacoustics phenomena, can be found in nature. In fact, as can be read in literature, the term **"Aeroacoustic sound production"** introduced by one of the founding fathers of the modern aeroacoustic science, Sir James Lighthill, is also frequently used in Goldstein (Ref. [4]) in order to address this kind of phenomena.

Finally, it has to be noted that **three perturbation modes** are coexistent in a fluid flow in general:

- **hydrodynamic mode** (i.e. **hydrodynamic instabilities**); there are *pressure fluctuations*, but no *density fluctuations*; in this mode, the *hydrodynamic velocity fluctuation* are convected downstream by the *mean flow*.
- **acoustic mode**: has both *pressure* and *density fluctuations*;
- **entropic mode**

1.3 Deeper Overview of Jet Noise Sources

Understanding the complexity of phenomena like **jet noise** and **turbulent mixing noise** and their sources, is critical both for **jet exhaust nozzles design** and in order to be able to **deliver the next generation of green low-noise jet engines.**

As already pointed out in previous paragraphs, in fact, **Jet noise source of noise** is mainly due to the mixing of high speed/high temperature exhausts gases, with the relatively slower and cooler ambient surrounding bulk of air, downstream the engine's exit nozzle. Moreover, downstream the wings, this phenomenon of jet mixing, generates **very strong turbulence** that is the **main cause of noise emission for subsonic jets.**

The main general characteristics of this type of noise are the following:

1. The main **generation area** is located at the *back of the engines*, at a distance equivalent to a few nozzle diameters - as it will be described later on, in subsequent chapters -.
2. **Noise directivity** is strong, heading mainly *backwards* with respect to aircraft's motion direction, but it can also be pointing *forward*, in some special cases.
3. The noise generated **does not contain remarkable tones**, and its frequency band is quite wide.
4. It is a **broad band noise source**, with most of the energy directed *aft of the engine at an angle between 20 and 45 degrees* from the engine axis.

1.4 Jet Noise Interaction with Surrounding Structures

As can be easily inferred by reading the introductory overview just presented, when studying jet noise, another major concern that arise, is that the engine is actually **mounted on the aircraft**, so every single part of the plane that surrounds the engine itself, can be a **potential source of acoustic waves**. In fact these would be *noise sources of secondary type*: meaning, with this term, that fuselage, wings, engine nacelles, landing gears etc., are **noise reflecting/scattering surfaces** and thus they are not **direct emitters** by themselves, but rather they reflect noise produced and scattered by *primary sources* like the ones visible in Figure 1.3.

One of the main topics of this thesis project is the study of the **interaction phenomena** between *jet noise scattered* by jet's turbulence acoustic sources and the *surrounding aircraft structures*, namely the wing - more precisely the **wing's trailing edge** -.

When considering jet noise problems of this kind, the **greatest interaction effects** are seen and are proven to be when the engines - especially those UHBPR turbofans already mentioned - are positioned in **close proximity of the wings**, especially in **underwing-mounting configurations**.

In this case, in fact, the wing causes both a **shielding effect** and an **effect of interference**: the sound waves, *reflected* and *diffracted* by wing's surface, are scattered downstream and combine thanks to superposition, with jet noise from turbulence direct sources. (check both Figures 1.7 and 1.8 for sketches of the described phenomena).

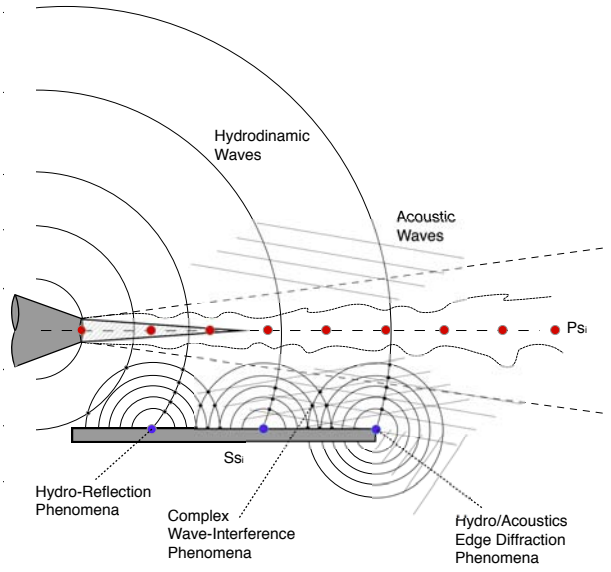

FIGURE 1.7: Sketch of the complex interference mechanisms in the jet+plate problem.

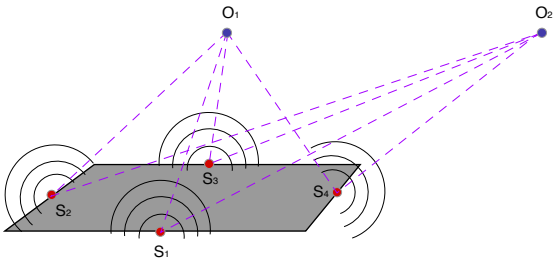

FIGURE 1.8: Simplified sketch of the edge sources distribution on the plate.

This is mainly why in some theories that will be cited lately (see Chapter 2, Curle, Ffowcs Williams and Hall) the wing acts as a **surface distribution of dipoles**, modifying the total sound field spawned, especially when considering the **far field**.

Experiments like those conducted by Mead and Strange, (reported in Ref. [29]) or better, those conducted by Dr. Peter Jordan and Dr. André Cavalieri of CEAT, in the "Bruit & Vent" facility, for the Jeronimo project[2] (reported in Ref. [33]) show these **effects of superposition of sound waves** and in particular, the **increase in the values of the spectra (SPL)**, in some precise frequency bands, as a result of the interference of the scattered sound waves, with those directly emitted by the primary jet source. These higher level of local sound intensity are peculiar in the zones where **no sound cancellation phenomena** occur.

1.4.1 The Problem of Engine Placement

As can be found in literature (see Ref. [1], for instance) **three** are the major and most common types of **engine mounting** and positioning in an aircraft:

- **Wing-mounted** Engine configuration
- **Aft Fuselage** Engine Placement
- **Three-Engine/Tail Designs**

Considering the first of these three cited configurations and focusing on the **suspended mounting of the nacelles on pylons below the wings**, it is possible to see that, in order to minimize wing structural damage in the event of a turbo-machinery disks or blades failure, nacelles can be placed in a **wing-mounted position**, so that the gas generator is placed well forward and off the front spar (i.e. with the front air intake placed well ahead the wing's leading edge (LE)).

In Figure 1.9 are reported a sketch of a LBPR engine, mounted in an **under-wing position** (taken from Ref. [1]) and a technical drawing of a HBPR engine, always in the same installation configuration. (from Ref. [22]).

Additional increase of protections (e.g. enhanced armoring of the nacelle) or even re-design, is sometimes needed during normal operations of reconfigurations or update of older aircraft engines, in order to prevent catastrophic results following turbine blade

[2] see Appendix A and Appendix B for details on the Jeronimo Project.

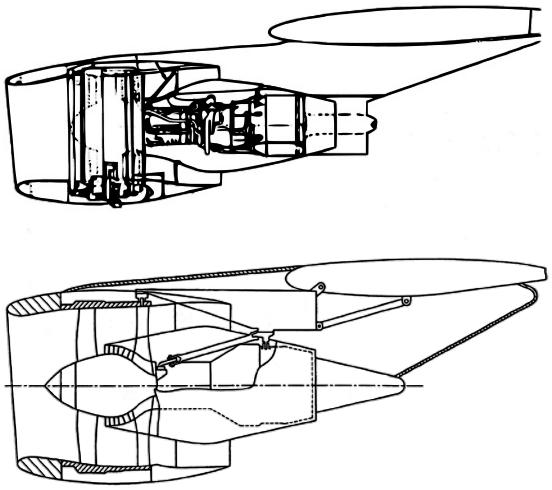

FIGURE 1.9: Sketch and technical drawing of underwing mounted LBPR and HBPR engines.

failure. This is mainly due to the fact that some old original configurations do not permit this new type of engine installation after reconfiguration - such as, for instance, the original 737 design -.

The preferred underwing positioning of the air-breathing engine is sought to be one with the inlet well ahead of the wing leading edge and away from the high upwash flow that can be found near it (compare Figure 1.9). With this setup, it is also relatively simple to obtain a high ram recovery effect in the inlet, since its angle of attack is minimized and no wake is ingested.

Though it was considered once reasonable to leave a gap of about 1/2 of the engine diameter between the wing and the nacelle, in the early days of **LBPR turbofans** (see for instance in Ref. [1] the sketch of the DC-8 underwing engine installation), as these have increased to values of approximately 6 to 8 over time, a large gap is not acceptable anymore. To permit the update of older aircraft that did not present very long gears, with larger diameter turbofan engines, substantial work had been done in order to **minimize the required wing-nacelle gap** and **fit the new bigger HBPR turbofans in the older underwing position**.

Furthermore, as can be read in the above cited articles, current **CFD-based design approaches** have made it possible to install the engine very close to the wing as shown in literature. As one of the more visible results nowadays, the 737 benefited especially from the closely mounted engines, permitting this older aircraft design to be fitted with HBPR engines, despite its short gear original configuration.

Considering some effects of **aerodynamics interference**, it has to be keep in mind that nacelles must be placed wisely, in order to avoid superposition of induced velocities

from the fuselage and the nacelle itself, or from the adjoining nacelles. This problem is even greater if the wing-pylon-nacelle mutual interference has to be considered and requires nacelle locations to be sufficiently forward and low, to avoid drag increases from high local velocities and especially premature occurrence of local supersonic velocities.

Chapter 2

Theory Background

2.1 The Physics of the Problem

The physics behind jet noise, its interaction with structures and in general any problems concerning aeroacoustics, has roots in both, aerodynamics phenomena and acoustic ones and concerns each one of these domains, as the combined name of this *"new science"* suggests.

Sound wave propagation in **compressible media** and all those phenomena regarding waves (such as reflexion, refraction, diffraction and scattering, absorption etc...) are similar - and thus treated equally - to those found in classical acoustics problems and applications, but are approached also with a critical eye, always considering the aerodynamic aspect of the treated problem.

2.1.1 Fundamentals of Aerodynamic Noise Generation: Introductory Thoughts

One of the earliest pioneers of aeroacoustics, was Sir M. J. Lighthill, who wrote in 1952 one of the most successful articles on **aerodynamics noise generation** : *"On Sound Generated Aerodynamically. I. General Theory"* (see Ref. [31]) which proved itself to be a very useful theory for the study of aeroacoustics phenomena in general and especially those related to jet noise.

Large scale commercial jet airliners were flying the skies in those years and **aerodynamic noise production** soon became a matter of serious concern, both from civil and military operations point of view: there was a growing interest in these phenomena

concerning aerodynamic noise production, both in aeronautical and naval applications such as, for instance, in the detection of ships, submarines and aircraft's.

Soon engineers became interested in understanding the **by-products of fluid flow turbulence** that does not modify much over the internal dynamics of the fluid flow itself; in fact, small energy drains in form of acoustic or structural waves had been observed firstly in those years and it was that subject indeed that captured scientists' attention.

A very important question that soon began to arise was that regarding the possibility of *"decoupling the fluid flow dynamics, from sound wave motion"*, but the lack of deeper knowledge of flow's features, posed some serious problems at the time.

As Sir. Lighthill himself reported in his cited paper, since both the prediction and the measurements of turbulent flows quantities are hard tasks to fulfill, caution must be employed when doing approximations, especially in flows where the value of **Mach number is small** and the corresponding **acoustic energy** is a very little fraction of the **total flow energy**.

As today, noise levels are known to vary far more widely than flow parameters; for instance, doubling the speed of a turbojet engine - by acting on its throttle - causes an **increase in the emitted noise intensity** by 24 dB, that corresponds to a factor of 250.

One of many studies carried out by researchers in laboratories, is that concerning the **identification of dimensional trends and scaling laws** that govern such phenomena, in order to enable data to be shared between experiments and these, to be designed and, later on, interpreted on physical bases, to justify one theory or another, concerning the **origins and sources of aerodynamic noise generation**.

Both phenomena of **generation** and **propagation of sound** are most of the time **highly coupled**, especially if one has to study or take into consideration the case of sound generation by **unsteady fluid flow**.

Sound propagation phenomena are indeed various and complex events to study - such as those regarding light propagation and other wave-like quantities -.

In fact, sound propagates around diffracting obstacles and through refracting and scattering media; so not only **direct propagation** and **reflections** occur, but also **refraction**, **diffraction** and **scattering**, as well as other ways of spreading in space and time can be involved, thus complicating the study of the sound propagation itself.

Yet, when speaking about these ways of propagation, some phenomena are shared amongst different processes: in fact, it is possible to observe, for instance, that in both, **jet-exhausts shear layer** analysis and **flow-through-ducts** studies, a common denominator can be found: the refracted sound propagation in the shear layer is not always and necessarily an **energy consuming process**.

Shear layer instabilities triggered in these cases by sound waves, can be responsible for **additional release of acoustic energy**, in a sort of a *"chain-process"*, experienced in both the aforementioned situations.

One of the main results of Lighthill theory is that it gives a way to define and quantify the **acoustic Intensity** I and **total acoustic power output** P radiated by free turbulent flows, in absence of solid bodies, generated by a **source distribution of quadrupoles**.

More advanced extensions and developments of this early theory and results, are those proposed and obtained by other famous authors like Curle, Ffowcs Williams and Hall, that takes into account also the presence of proximity boundaries and describes the scattered sound field as a result of a combination of a **volume quadrupole sources distribution** superimposed to a **surface distribution of dipole sources**, i.e. taking into account the **diffraction theory** that tries to explain how purely passive surfaces can convert **local hydrodynamics energy** into sound and trying to understand the mechanisms of sound generation by the wall nearby turbulence. (See Paragraph 2.2, Refs. [31],[24] for more details).

Inhomogeneities in the flow like solid boundaries or bodies or bubbles and vortices, in underwater flows, pose other great complications to these theories.

As can be read in books like Goldstein (Ref. [4]), many concepts and techniques used in aeroacoustics, have been taken directly from classical acoustic analysis theory, or from the more recently developed *"acoustics of moving media"*. All fluids possess two important properties:

- **Elasticity**: that causes the fluid to resist the compression.
- **Inertia**: that causes the fluid to overshoot when displaced.

These particular features of fluids, permit either to **pressure** or to **density fluctuations**, occurring anywhere in the fluid, to propagate outward from their **sources** and to be communicated to the surrounding medium. As these pressure and density **through-air-traveling disturbances** propagate, they get to human ears and cause vibrations of the eardrums that are immediately transmitted via the auditory nerve up to the brain: it is thank to this process that humans recognize **sound**.

If the fluids of concern have very *small viscosity* and *thermal conductivity* (such as, for instance, **air** and **water**) some effects can be neglected as long as the **disturbances** are not allowed to propagate over *excessively large distances*. Another important point is that, if the **spatial gradients** are very weak and never much larger than disturbances themselves, it is possible to approximate the real case fluid and neglect some other features of minor interest as it is well described and reported in Ref. [4]

Basic acoustics equations follow from the **linearization** of full equations of **mass momentum** and **state equation** (or *entropy/energy equation*) (as will be discussed later in Paragraph 2.2).

Another hypothesis is that the fluid is a Newtonian fluid[1] and to neglect both the effects of **molecular relaxation** and **diffusion**. By carrying out these simplifications, **stresses** involved simply consist of **normal pressure stresses**, and the stress tensor can then be roughly approximated with these types of forcing effects. Another useful simplification is that **entropy** is regarded as *constant*, so the pressure depends only on density (see Goldstein, Ref. [4] and P. Jordan, Ref. [20] for deeper insights on the subject).

For the **subsonic propulsive cold jet** (that is the most extensively studied jet type, in terms of sound emissions) the **characteristic eddy dimension** is of the order of *one jet diameter* D_j, which approximates the **vorticity thickness of the mixing layer** until the **potential core's end**.

The **potential core** is defined nowadays as the most important region of the jet in terms of sound production and it was not known at Lighthill's time. (see Figures 2.1, 2.2) In fact, the central region of a jet of the described types, is called the **potential core**; it spans approximately downstream for about $4 \div 6$, D_j - depending on the precise Mach number of the flow - and it is mainly characterized by the fact that the **mean velocity** is *constant* and the **fluctuation levels** are *low*. Moreover, the flow in the conical region of the potential core, can be roughly approximated as being *irrotational*, thus allowing the definition of a **velocity potential** in that same region.

The outer zone, which is referred to as the **entrainment region** and is characterized by *low mean velocity* values, can also be assumed as *irrotational*; in this region, though, as the name suggests, the predominant phenomenon is the one of ambient **air entrainment by the jet**; characterized by *small*, *inward radial* **flow velocities**.

It has to be noted that the mixing layer will be **turbulent** if the boundary layer near to the jet's nozzle exit presents characteristics of turbulence, otherwise, it will be **initially**

[1] i.e. if the viscous stresses that arise from its flow, at every point, are proportional to the local strain rate.

laminar with a **later transition to turbulence**, *downstream*. As the author points out in his work Ref. [12].

> *" The transition process is initiated by the Kelvin-Helmholtz instability of the inflexional velocity profile [...] "*

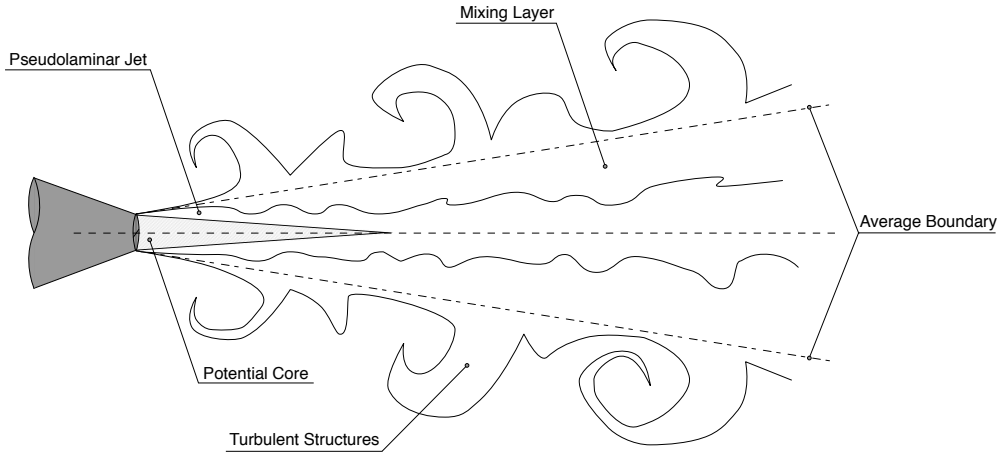

FIGURE 2.1: Boundary structure of the mixing layer.

Lighhill's first estimates of the **acoustic intensity radiated** take into account the fact of having a characteristic frequency of $f = U_j/D_j$ and a Mach number given by $M = U_j/c_0$, giving a relation of proportionality (that will be discussed better in subsequent paragraphs) like the following:

$$I \propto U_j^8 \tag{2.1}$$

which underlines the very strong dependence of the **radiated sound power** to the jet velocity and jet exit Mach number.

From the point of view of jet noise control strategies, this theory's main result states that, in order to achieve **significant reductions of the radiated sound power**, M and U_j must be reduced and possibly, if a reduction of sound power has to be targeted without notable losses on the thrust (which is proportional to U_j) larger jet diameters are required.

This is mainly why between years 1950 and 2000 the introduction and later optimization of new LBPR & HBPR jet engines lead to a **20 dB reduction** in the radiated sound power at take off (as can be read in Refs. [1], [2], [3]).

2.1.2 Jet-Flows Physics & Behavior

In this paragraph are briefly presented the most salient fluid mechanics aspects of jets that will be relevant to understand how does the sound generation process works.

Considering the classical turbulent jet configuration (as can be seen in Figure. 2.1, or better, in Figure. 2.2 readapted from Ref. [4]) and a subsonic jet of air, flowing out of a convergent nozzle, that has the following properties:

- uniform velocity U_j
- high Reynolds numbers
- stationary fluid

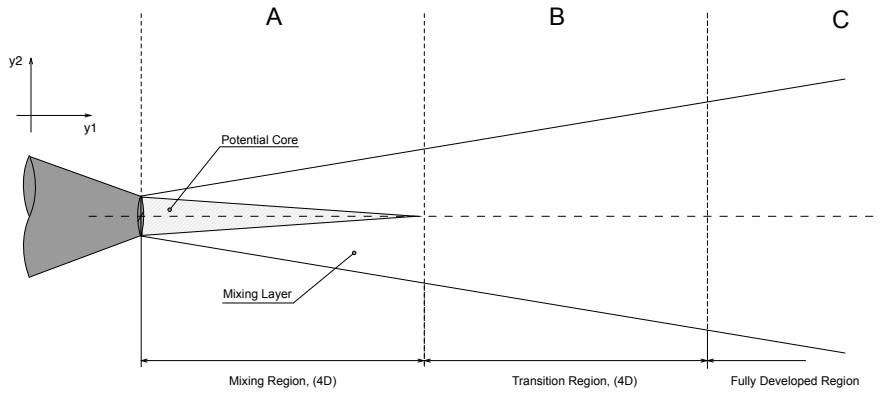

FIGURE 2.2: Sketch of a typical jet structure

It is easy to visualize the jet flow behavior in the 3D space, as it *expands downstream*, filling the surroundings. One can assess the following key points of the jet flow behavior:

1. the jet that leaves the nozzle, forms an annular mixing layer between the moving fluid and the surroundings (see Figure 2.7).
2. The flow becomes turbulent at about $0.5\,D$ downstream (**Zone A** in Figure 2.2).
3. The flow spreads then, linearly, in both directions, filling the entire jet at about $4 \div 5\,D$ - in this zone (**Zone A** in Figure 2.2), the thickness of the mixing layer is approximately $0.2\,y_1$ or $0.25\,y_1$.
4. there is a laminar motion within a conical domain, enclosed by turbulent flow: this zone is the so-called potential core (**Zone A** in Figure 2.2).
5. the boundary of the mixing layer is not straight but rather ruffle, because of turbulence and convection effects.

6. Once passed the mixing region just described, the jet develops into two more regions:

   - the transitional region from 4 to 8 D (**Zone B** in Figure 2.2)
   - and the fully developed region $> 8\,D$ (**Zone C** in Figure 2.2)

In this very last region of fully developed flow, it reaches a state of *self preserving fluid*, with mixing layer thickness that grows again, linearly, with y_1 but at a different growing rate from the previous zone.

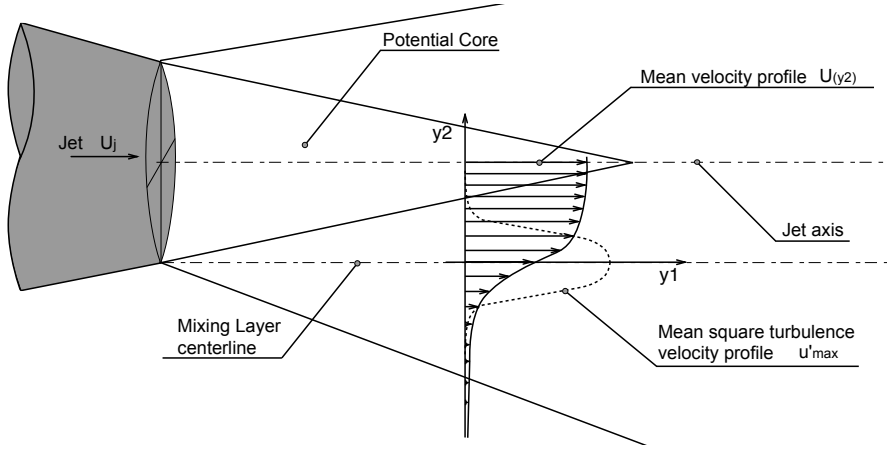

FIGURE 2.3: Mixing layer velocity profiles.

In Figure 2.3 are sketched roughly to scale - as taken from Ref. [4] - the **mean velocity profile** $U_{(y_2)}$ and the **mean square turbulence velocity profile** u'_{max} whose variations are shown across the mixing layer.

As can be seen from the figure, the **peak turbulence intensity** occurs at the *centerline* of the mixing layer, it is fairly constant and approximately equal to Eq. 2.2, until well-into the transition region, then it finally falls off as y_1^{-2} in the fully developed region.

$$u'_{max} \approx 0.16 \cdot U_j \tag{2.2}$$

Most of the turbulent energy is confined to a fairly narrow region located at the center of the mixing layer, and the turbulent eddies in this region are believed to be elongated in the flow direction.

It is thus possible to define the **eddy convection velocity** in the mixing region as U_c, that is given by Equation 2.4 and it is demonstrated to vary across the mixing region but not nearly as much as the mean velocity does.

Always in Ref. [4] is reported the following expression for the eddy convection velocity at the center of the mixing region where the peak of turbulence energy is concentrated, independently of axial distance from jet exit :

$$U_c = 0.62 \cdot U_j \tag{2.3}$$

$$U_c = c_0 \cdot M_c \tag{2.4}$$

It has to be noted though that there are other values in literature - based on other theories - for the convective velocity proportionality coefficient (namely U_c/U_j), other than that in Eq.2.3; these are well discussed and analyzed by Dr. Cavalieri in his article (Ref. [27]) where he points out that different azimuthal mode is described by a different and defined coefficient (see Table 6 in the cited Ref. article).

The value used in this thesis paper for the simulations with the **tweaked wave packet (WP) model** written by the author himself, and reported in Chapter 6 is that of Eq. 2.5, that corresponds to the azimuthal mode zero, (i.e. $m = 0$).

$$\frac{U_c}{U_j} = 0.97 \tag{2.5}$$

Finally it is important to remember, from the point of view of the physics of jet noise, that as Goldstein writes in his book on aeroacoustics, Ref. [4], the **directional pattern** of the jet noise is primarily the result of the **convection factor** $(1 - M_c\, cos(\theta))^{-5}$ which arises from the relative motion of the turbulent eddies and the observer (i.e. the introduction of the moving frame correlation tensor) and it is therefore related to the motion of the aggregate of acoustic sources that fills a finite volume of space. This factor, present in the expression of the **average acoustic intensity** at **x** due to a unit volume of turbulence located at a point in **y**, gives birth, when integrated to obtain the total power emitted per unit volume of turbulence $P(y)$, at the group in Eq. 2.6, meaning that **source convection** causes a **greater radiation of power upstream rather than downstream** together with an **increased effective total energy**, emitted by the source itself.

$$\frac{1 + M_c^2}{(1 - M_c^2)^4} > 1 \tag{2.6}$$

2.1.3 Coherent Structures

Researchers have made big efforts during the last 60 years, in order to explain the physics of turbulent jets and their produced and **scattered sound field**, by combining theory,

experimental analysis and numerical simulations. Dr. P. Jordan hold a very interesting conference about these and other topics, whose "transcript" has been made available as lecture notes in Ref. [20].

One of the major long-term objective is that of **jet noise reduction** (as it has been already pointed out many times in this paper), both for the commercial and military aviation communities. In order to achieve this goal, methodologies for **real-time modeling** and **noise control strategies** for these types of jets, have been and yet have to be developed.

As can be read in Ref. [28]:

> *"Prior to the 1960s, the turbulent motions of a jet were supposed to be entirely stochastic, as were, consequently, the associated sound sources. The discovery of coherent structures changed this view, and it is the connection between these and the coherent acoustic waves in the far field..."*

This means that during the sixties, studies of free-jet **turbulent fluctuations** and jet dynamics and kinematics, were based upon a common belief that the **turbulence** itself, was composed by **eddies**, without any particular organization (i.e. an ***"entirely stochastic"*** phenomenon).

Later on, thanks to the advent of **more advanced measuring techniques** (such as, for instance, more detailed *near field pressure measurements* and flow visualization methods like *smoke seeding*, *Schlieren techniques* etc..) and also thanks to the new, **more powerful computational approaches** undertaken, this point of view began to change, as the existence of **more organized flow patterns**, the so called **"coherent structures"**, had been discovered.

In Figure 2.4 are reported some shadowgraphs depicting the cited coherent structures in the mixing layer of a turbulent jet evolving from a $D_j = 5\,[cm]$, from left to right; while in Figure 2.5 are shown some other shadowgraphs, that visually explain the effects of Reynolds number on the coherent structures in the mixing layer of a helium-nitrogen mixture; (pictures are taken from Brown & Roshko, Ref. [11]).

The research evolved toward the study of **natural jets** (or **free-jets**), with high Reynolds and Mach numbers; as these are those of major interest for aeronautical applications, where a *non-continuous behavior* of these structures had been observed.

As some researchers have pointed out in their papers (see Ref. [10]), the importance of these coherent structures in the aerodynamic noise generation process in turbulent jet

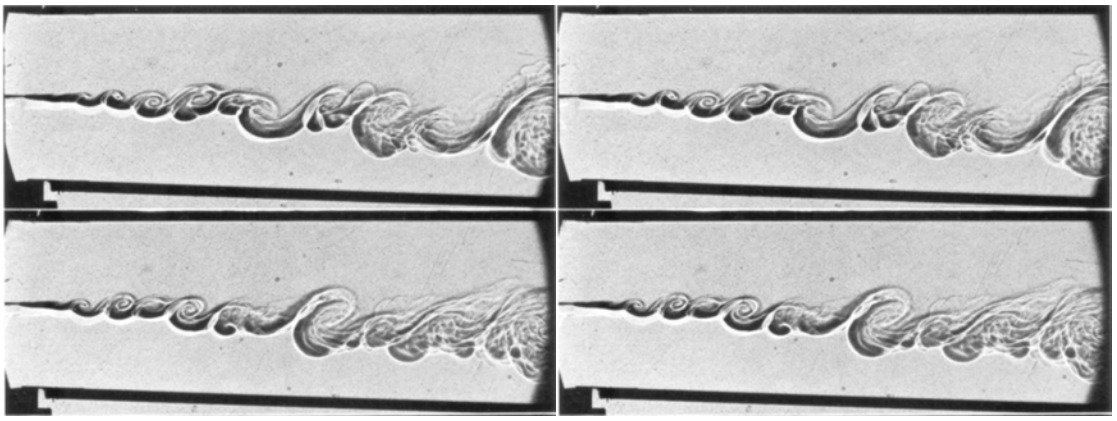

FIGURE 2.4: Shadowgraphs of coherent structures in the mixing layer.

flows, is crucial; most of the noise, in facts, originates from a zone near the end of the potential core, between $4 \div 8$ jet diameters (see Juvé, Sunyach & Comte-Bellot 1980).

A phenomenon know as **breakdown process** (depicted in Figure 2.6 taken from Hussain, Ref. [**10**]) which relates to the actual breakdown of the initial **toroidal structures** at the jet's exit (see Figure 2.7 from Ref. [**26**]), into *substructures* near the end of the potential core and their subsequent interactions, **seems to produce the greatest part of emitted noise** and it is thought to be its principal cause.

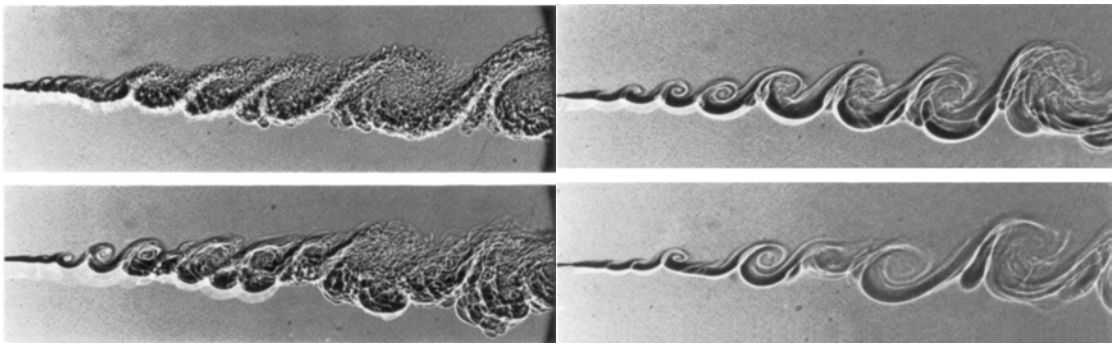

FIGURE 2.5: Shadowgraphs of coherent structures: Reynolds number effects in helium-nitrogen mixing layer.

Figure 2.7 shows the instantaneous experimental axial velocity fluctuations $u_x^{'}/U_j$ at $x/D_j = 2$ for the Mach number of the jet of the experiment (i.e. $M = 0.4$), reported in Ref. [**26**].

Another important aspect that needs not to be underestimated is the **intermittency** of these particular structures; in fact, their intermittent behavior implicates difficulties both, in their **experimental evaluation** and in that of the **numerical/computational simulations** (e.g. CAA), because of the complicated effects that they may generate in the radiated sound field, especially while multiple interactions are considered.

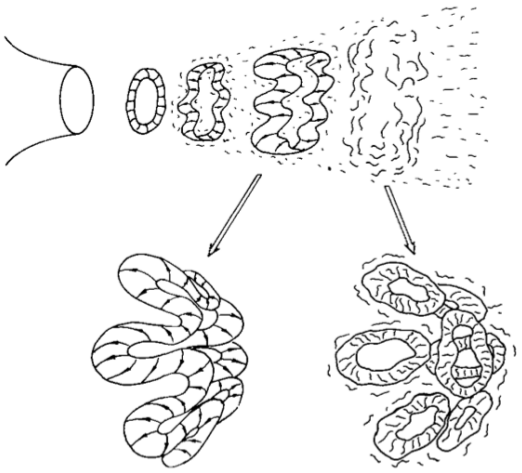

FIGURE 2.6: Idealization of the breakdown process in circular jets.

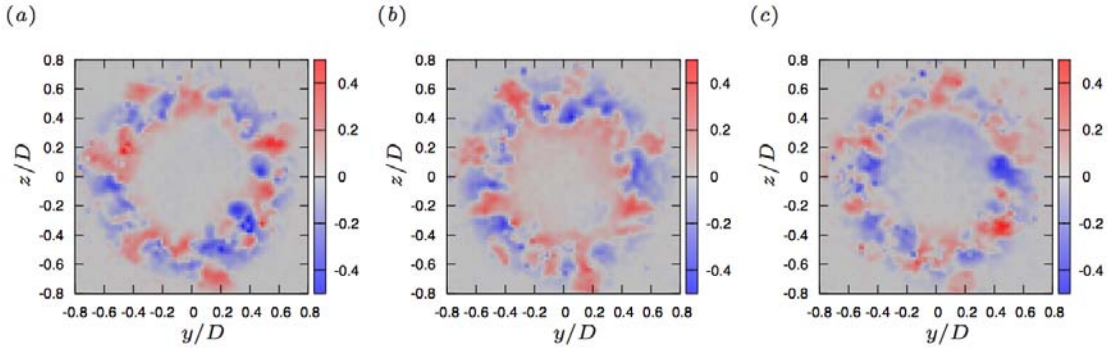

FIGURE 2.7: Toroidal structures observed in the mixing layer of subsonic round jets.

Other famous international researchers like Dr. P. Jordan, Dr. André V. G. Cavalieri, Dr. Daniel Rodriguez, Dr. Tim Colonius and Prof. Yves Gervais have demonstrated in many experiments and articles the *"wavy nature"* of these structures both in **longitudinal** and **azimuthal directions**, with some particular features like, for instance, the **space-time jittering characteristics**, well described by Dr. Cavalieri in article Ref. [34]. This is why it is so common to find reference to these coherent patterns as to the so called **wave packets**.

In the following images taken from Ref. [28] are respectively shown instantaneous and statistical renderings of wave packets from simulations and experiments: the first is from DNS calculations of Freund (2001) an instantaneous slice of the $M_j = 0.9$, $Re = 3600$ jet, while the second image of Figure 2.8 shows the stream-wise structure as a function of St number and azimuthal mode m, based on the cross-spectral density (CSD) of the pressure from a near-field caged microphone array (Suzuki & Colonius 2006) at $M_j = 0.5$, $Re = 700000$ as reported by this cited article's author, Dr. P. Jordan.

These kinds of structures appear in flow visualization methods such as what scientists

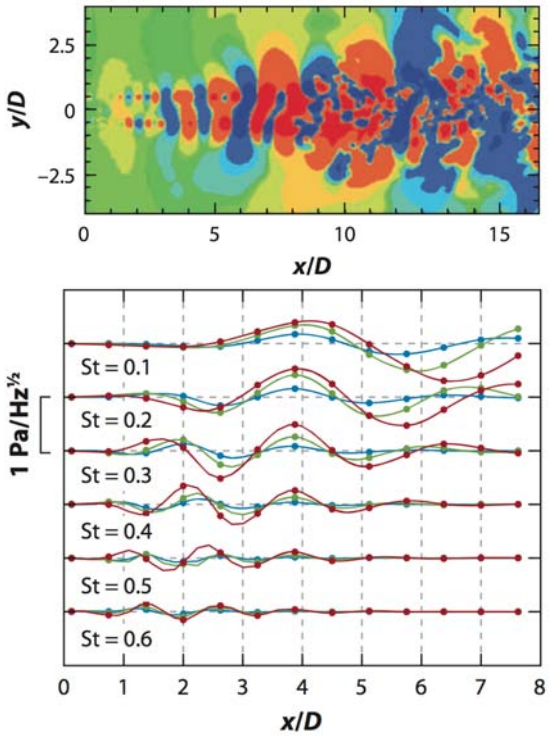

FIGURE 2.8: Instantaneous and statistical renderings of wave packets, from simulations and experiments.

call *"a train of puffs"*; it has been shown that these **"intermittent puffs" scale well with the jet diameter** D_j and present an average Strouhal number $St_{avg} \approx 0.3$ - always based upon D_j and U_j values -.

Once again, **near field pressure measurements** confirmed and highlighted the presence of **azimuthally coherent structures** or **wave packets** and permitted to draw the conclusion that natural jets comprise **hydrodynamic waves**, with significant downstream axial extent.

On the other hand, studies made on forced jets (e.g. conducted, for instance, by acoustically forcing the jet inside the nozzle, in order to impose a known periodicity in puffs formation) permitted to discover more details about these structures and to determine, for several excitation frequencies, **quantitative parameters** such as *wavelength*, *convection speeds* and the *excitation Strouhal number* value, that leads to **maximum fluctuations amplitude**, being like the one in natural and unforced jet (i.e. $St_{exc} \approx 0.3$).

See Ref. [11] for a deeper and thorough analysis regarding this topic.

2.2 The Maths of the Problem

2.2.1 Aerodynamic Sound and Lighthill's Theory

Any type of motion of a fluid flow continuum that has the properties of being:

1. **Compressible**
2. **Viscous**
3. **Heat conductive**

is governed by the subsequent system of equations which, respectively are, the:

- **continuity equation** (mass conservation equation):

$$\frac{\partial \rho}{\partial t} + \frac{\partial \rho v_i}{\partial x_i} = 0 \tag{2.7}$$

- **momentum conservation equation** (Navier-Stokes equations):

$$\rho \left(\frac{\partial v_i}{\partial t} + v_j \frac{\partial v_i}{\partial x_j} \right) = -\frac{\partial p}{\partial x_i} + \frac{\partial e_{ij}}{\partial x_j} \tag{2.8}$$

- **energy conservation equation**:

$$\frac{\partial S}{\partial t} + \mathbf{v} \cdot \nabla S = 0 \tag{2.9}$$

- the **state equation**:

$$\rho = \rho \left(p,\, S \right) \tag{2.10}$$

Refer to Appendix C (or alternatively see Dr. P. Jordan Ref. [20] or Goldstein Ref. [4]) for the complete derivation of the **wave equations**.

The above mentioned set of equations constitute a closed-form system of non linear partial differential equations for which a closed form, general analytical solution is not obtainable.

This system describes any possible class of motion of such an aforementioned fluid flow continuum from a generalized point of view and, as such, it ***does already intrinsically contains the description of the mechanisms upon which the generation of propagative acoustic energy is based***.

M. J. Lighthill, in its famous paper of 1951 Ref. [31] reported that experimental analysis had previously found frequencies in the flow structures, to be identical with those of sound produced by the flow itself; stating in fact that airflows may contain *fluctuation* as a result of *instabilities* that will induce a **regular eddy pattern**, in lower Reynolds number flows, or **very irregular turbulent motions**, in higher Reynolds number ones, leading, in both cases, to **sound production**.

Lighthill theory begins with stating that density fluctuations in the real flow must be exactly those that occur in a uniform acoustic medium subject to an external stress system given by the following for of the **Reynolds' stress tensor**:

$$\boxed{T_{ij} = (\rho v_i v_j + p_{ij}) - c_0^2 \rho \delta_{ij}} \tag{2.11}$$

This represents the **instantaneous applied stress** at any point of an arbitrary fluid in motion; i.e. it describes the difference between the **effective stresses in the real flow** and the **stresses in the uniform acoustic medium at rest**.

The propagation of sound in a uniform medium, in the case that *no sources of matter or external forces are present*, is governed by the following equations that are namely the **continuity equation** and an **approximate equation of momentum**:

$$\begin{cases} \dfrac{\partial \rho}{\partial t} + \dfrac{\partial (\rho v_i)}{\partial x_i} = 0 \\ \dfrac{\partial (\rho v_i)}{\partial t} + c_0^2 \dfrac{\partial \rho}{\partial x_i} = 0 \end{cases} \tag{2.12}$$

Combining and eliminating the *momentum density* (ρv_i) from the System 2.12, it is possible to obtain the already cited **homogeneous wave equation** as derived in Appendix C:

$$\boxed{\frac{\partial^2 \rho}{\partial t^2} - c_0^2 \nabla^2 \rho = 0} \tag{2.13}$$

Though, the exact equation of momentum in an arbitrary continuous medium under no external forces is the following, in Reynolds form:

$$\frac{\partial (\rho v_i)}{\partial t} + \frac{\partial \rho v_i v_j + p_{ij}}{\partial x_j} = 0 \tag{2.14}$$

Lighthill also rewrite the equations of this **arbitrary fluid motion** into the:

> *"**equations of the propagation of sound in a uniform medium at rest, due to externally applied fluctuating stresses** [...] "*

$$\begin{cases} \dfrac{\partial \rho}{\partial t} + \dfrac{\partial (\rho v_i)}{\partial x_i} = 0 \\ \dfrac{\partial (\rho v_i)}{\partial t} + c_0^2 \dfrac{\partial \rho}{\partial x_i} = -\dfrac{\partial T_{ij}}{\partial x_j} \end{cases} \tag{2.15}$$

and the wave equation becomes, in its inhomogeneous form, Eq. 2.16:

$$\boxed{\frac{\partial^2 \rho}{\partial t^2} - c_0^2 \nabla^2 \rho = \frac{\partial^2 T_{ij}}{\partial x_i \partial x_j}} \tag{2.16}$$

This last equation Eq. (2.16) is said to be the ***acoustic analogy*** because it considers the problem of sound radiation by sources - with an intensity of $\partial^2 T_{ij}/\partial x_i \partial x_j$ - in a medium at rest, to be analogous to sound generation by a turbulent flow, where the instantaneous applied stress T_{ij} is that of Eq. (2.11).

Equations (2.15) and (2.16) are the basics of the **theory of aerodynamic sound production**.

As suggested by Dr. P. Jordan in his paper (see Ref. [20]) the **inhomogeneous wave equation** (2.16) can be interpreted as a *source term* - in the right hand side of the equation - that drives density fluctuations (or alternatively, pressure ones), described by the left hand side of the same equation. The author also reports in his work that solution to this equation can be found by using the Green's function formalism, well described in Ref. [20] or Ref. [4].

In fact, taking into consideration the following solution for the **acoustic pressure field** at a distance R for a **small pulsating and radiating sphere**, it can be shown that it is related (as reported in Goldstein Ref. [4]) to the associated **volume flow** $Q(\tau)$ by Equation 2.17, that can be thought as a *"point source of sound"*:

$$p(\mathbf{R}, \tau) = \frac{\rho_0}{4\pi R} \frac{\partial}{\partial \tau} Q\left(\tau - \frac{R}{c_0}\right) \tag{2.17}$$

it is possible to express the **free-space Green's functions** as follow:

$$G^0(\mathbf{y}, \tau \,|\, \mathbf{x}, t) = \frac{1}{4\pi R} \delta\left(\tau - t + \frac{R}{c_0}\right) \tag{2.18}$$

$$G^0_\omega(\mathbf{y},\mathbf{x}) \equiv \frac{1}{4\pi R}\, e^{i\omega R/c_0} \tag{2.19}$$

Eq. 2.18 and Eq. 2.19 are related through the following:

$$G^0 = \frac{1}{2\pi}\int_{-\infty}^{+\infty} e^{-i\omega(t-\tau)} G^0_\omega \, d\omega \tag{2.20}$$

where R is the *distance* traversed by the pulse emitted by the sphere/point source, R/c_0 is the *time* it takes to traverse and the *altered variable* $\tau - (R/c_0)$ is the **retarded time** and represent the time at which the signal emitted from the point $\mathbf{x}$ arrives at the point $\mathbf{y}$.

As demonstrated in Ref. [4], that in order to get a solution to the inhomogeneous wave equation for a uniformly moving medium, it is possible to **superimpose** certain generalization of the point-source solution just mentioned and obtain a relation between the **source distribution** γ, the solution itself and the boundary values of pressure p as a generalization of the usual Green's formula (**generalized Green's formula**) used in classical acoustics.

In fact, in the case of aerodynamic sound problems, one is mainly interested in time-stationary processes; so it can be shown that the **acoustic pressure** p at an arbitrary point $\mathbf{x}$ and time t due to any *localized source distribution* γ, whose radiation field is **uninfluenced by solid boundaries**, can be computed with the following:

$$p(\mathbf{x},t) = \int_{-T}^{+T} \left(\int \gamma(\mathbf{y},\tau)\, G^0(\mathbf{y},\tau \,|\, \mathbf{x},t)\, d\mathbf{y} \right) d\tau \tag{2.21}$$

Where $G^0(\mathbf{y},\tau \,|\, \mathbf{x},t)$ represents the pressure at point $\mathbf{x}$ and time t caused by an impulsive source located at the point $\mathbf{y}$ and triggered at time τ

It is demonstrated always in Goldstein that:

> *" [...] any acoustic field can be thought of as the superposition of the fields due to a distribution $\gamma(\mathbf{y},\tau)$ of volume sources and a distribution $a(\mathbf{y},\tau)$ of boundary sources. "*

The T_{ij} external stress system incorporates various effects:

1. **generation of sound**

2. **sound convection** by the flow (in part of the $\rho v_i v_j$)
3. **sound propagation** with variable speed
4. **gradual dissipation** into heat by both, *thermal conduction* and *viscosity*

Speaking about these two last mentioned modes of **dissipation of the acoustic energy**, in fact, it can be easy to see how slow are these processes; thus, *viscosity stresses contribution* to T_{ij} can be neglected except for very large-scale phenomena, because they seem to cause just a *damping* of the sound field, due to the conversion of acoustic energy into heat, as stated in Kirchhoff analysis of Rayleigh's "Theory of Sound". (see Ref. [31])

Following this path, it is legit to consider the **approximated form** of the **equivalent applied stress field** as the one reported in Eq. 2.22:

$$T_{ij} \approx \rho_0 v_i v_j \tag{2.22}$$

with an error of $\varepsilon_{T_{ij}} \propto M^2$.

The hypothesis for carry on such an approximation are those valid for a **cold jet flow** with **low Mach number** in which it is possible to **assume negligible the viscous stresses** in the expression of the tensor T_{ij}.

2.2.1.1 Radiation Fields of Acoustic Sources and Multipole Source Types

If the expression of the free-space Green's function reported in Eq. 2.18 is inserted into Eq. 2.21 and the subsequent integration with respect to τ is carried out, the new expression for the sound field due to a localized distribution γ has the following form:

$$p(\mathbf{x}, t) = \frac{1}{4\pi} \int \frac{\gamma(\mathbf{x},\, t - R/c_0)}{R}\, d\mathbf{y} \tag{2.23}$$

From a practical point of view, it is possible to say, following Ref. [4], that the results obtained by expanding the integral I of Eq. 2.23 in a Taylor series (with respect to $R = |\mathbf{x} - \mathbf{y}|$, about the point $R = x$ and by assuming $y = const$), after performing some mathematical calculations - contained always in Ref. [4] - shows that:

> *" The lowest order poles in the multipole expansion, will contribute to the distant sound field emanating from a source region that is very small, relative to its wavelength [...] "*

i.e. the *typical wavelength* of given sound field is $\overline{\lambda} = c_0 T_p$, with T_p its *typical source period of oscillation.*

This is referred to as the **"condition of compactness"** and its equivalent to writing the following:

$$T_p \gg \frac{L}{c_0} \tag{2.24}$$

where L is the order of magnitude of the size confining the source γ. It is possible then to express $p(\mathbf{x}, t)$ in the following form:

$$p(\mathbf{x}, t) = \sum_{j,k,l=0} \frac{\partial^{j+k+l}}{\partial x_1^j \, \partial x_2^k \, \partial x_3^l} \frac{(-1)^{j+k+l}}{4\pi x} m_{j,k,l} \left(t - \frac{x}{c_0} \right) \tag{2.25}$$

where

$$m_{j,k,l} = \int \frac{y_1^j \, y_2^k \, y_3^l}{j! \, k! \, l!} \, \gamma(\mathbf{y}, t) \, d\mathbf{y} \tag{2.26}$$

Equation 2.26 is the **instantaneous multipole moment** with j, k, l the term of expansion, while Eq. 2.25 is the **multipole**, of order 2^{j+k+l}.

Each member of Eq. 2.25 is proven to be a solution of the **homogeneous wave equation** - Eq. 2.13 - being S and its derivative, a solution of this mentioned equation.

$$S = \frac{1}{4\pi \, x} m_{j,k,l} \left(t - \frac{x}{c_0} \right) \tag{2.27}$$

The following Equation 2.28 represents the expression for the considered **source distribution** $\gamma(\mathbf{y}, t)$:

$$\gamma \left(\mathbf{y}, t \right) = \sum_{i_1, i_2, \ldots, i_N = 1}^{3} \frac{\partial^N \psi_{i_1, i_2, \ldots, i_N}}{\partial y_{i_1} \, \partial y_{i_2}, \ldots, \partial y_{i_N}} \tag{2.28}$$

Any source region that can be expressed in these terms, is called a **multipole source** of order 2^N.

The **compact multipole sources** of higher order are *much less efficient emitters* than the lower order order sources; the amount of energy contained in the **near field** (the region closer to the source) will be approximately the same for all equal strength sources, regardless their order. This last fact, points out what Goldstein in his book calls: *some sort of* ***phase cancellation phenomenon"*** *that seems to occur at larger distances from higher order sources.* This would probably explain why **energy is prevented to be radiated as sound, in the far region**.

Order	Source Name
$N = 0$	Monopole or Simple Source
$N = 1$	Dipole
$N = 2$	Quadrupole (longitudinal or lateral)

TABLE 2.1: Multipole sources types & orders.

It has to be noted that each multipole source has its own **characteristic radiation pattern** of which a significative image is reported in Figure 2.9[2]

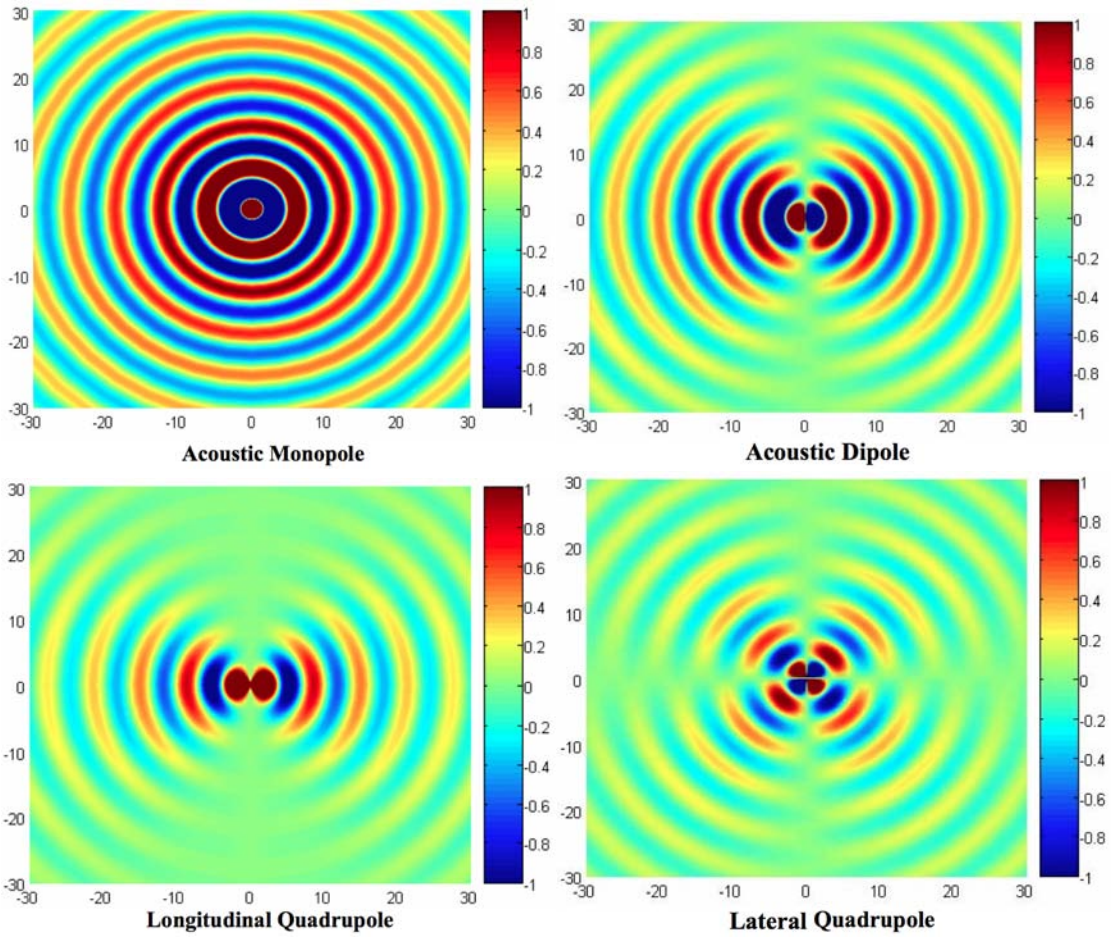

FIGURE 2.9: Radiative patterns of multipole acoustic sources.

Always in Ref. [4] it is possible to find the following expression for the behavior of **pressure fluctuations**, at *large distances* from any distribution of volume sources:

$$p(x,t) \sim \frac{1}{4\pi x} g\left(t - \frac{x}{c_0}, \theta, \phi\right) \tag{2.29}$$

[2] Reproduced with the code from Ref. [17]

The **radiation field** (or **far field** (FF)) is defined as the region of space where pressure fluctuations are fully characterized by the behavior reported in Eq. (2.29); this region must be far away enough from both, sources and interacting objects in terms of wavelength and source size.

2.2.1.2 Dimensional Analysis of Aerodynamic Sound Production

In order to co-ordinate experiments, compare data, rescale graphs and assess results from different experiments, some non-dimensional relations are needed; for **geometrically similar** mechanisms of flow, the **noise production** and the dependence of the sound field on typical parameters (such as for instance, typical flow velocity U_j, typical linear dimension l), can be studied, regarding also some other parameters as *constant* (e.g. gas related parameters such as ρ_0, c_0, ν_0, μ_0 etc.).

The classical Reynolds and Mach number are used and defined as follows:

$$R_e = \frac{Ul}{\nu_0} = \frac{\rho_0 Ul}{\mu_0} \tag{2.30}$$

$$M_a = \frac{U}{c_0} \tag{2.31}$$

In order to correctly relate the density variations expressed in Eq. 2.35 to the flow parameters cited above, it is necessary, as Lighthill reports in his paper, to know the typical frequencies of the flow, in order to link the fluctuations in $\partial^2 T_{ij}/\partial t^2$ to those in T_{ij}.

It is then possible to consider the so called **Strhoual Number** i.e. a non dimensional number that is inversely proportional to the *vortex spacing* in the turbulent flow and it is defined as follows:

$$S_t = \frac{k\,a}{c} = \frac{f\,l}{U} \tag{2.32}$$

with the given parameters:

- f **Frequency** of phenomenon (e.g. vortex shedding)
- l **Characteristic length** (e.g. jet diameter D_j, in case of jet noise studies)
- U **Field velocity** (e.g. jet exit speed U_j, in case of jet noise studies)

Another useful non-dimensional group used in these types of analysis is the **Helmholtz Number**, i.e. an a-dimensional number defined by the ratio of the *source scale length* ($\propto D$) and the *acoustic wavelength*. It gives idea of the **source compactness** and offers a measure of **interference effects** from different parts of the source. It is used in subsequent Chapter 6 graphs of the post-processing analysis made, in order to present a rescaled and peak aligned version of the Spectra plots SPL/St versus St computed.

$$H_e = \frac{D}{\lambda_a} = S_t \cdot M = \frac{f\,D}{c} \tag{2.33}$$

where the given parameters are the following:

- (U_c) phase velocity of convected wave
- (M_c) Mach number based on U_c
- (λ) Wavelength , (λ_a) acoustic wavelength
- (k) Wavenumber , (k_a) Acoustic wavenumber
- (ω) Frequency of the convected wave

and the **acoustic wavenumber** k_a is defined in Eq. 2.34:

$$k_a = \frac{\omega}{c} = \frac{2\pi}{\lambda} \tag{2.34}$$

2.2.1.3 Intensity, Power and Efficiency of the Radiated Sound Field

If one considers the following expression, *in terms of density fluctuations*, for the **radiated field of each quadrupole** to hold valid (always from Ref. [31]),

$$\rho - \rho_0 \sim \frac{1}{4\pi c_0^2} \int \frac{(x_i - y_i)(x_j - y_j)}{|\mathbf{x} - \mathbf{y}|^3} \frac{1}{c_0^2} \frac{\partial^2}{\partial t^2} T_{ij} \left(\mathbf{y}, t - \frac{|\mathbf{x} - \mathbf{y}|}{c_0} \right) d\mathbf{y} \tag{2.35}$$

it is possible to make the following approximation if the distance of evaluation is larger, compared to the dimensions of the flow:

$$\rho - \rho_0 \sim \frac{1}{4\pi c_0^2} \frac{x_i x_j}{x^3} \int \frac{1}{c_0^2} \frac{\partial^2}{\partial t^2} T_{ij} \left(\mathbf{y}, t - \frac{|\mathbf{x} - \mathbf{y}|}{c_0} \right) d\mathbf{y} \tag{2.36}$$

The **intensity of the sound field** is then computable with the following formula, as expressed by Lighthill in is paper - Ref. [31] - :

$$I(x) = \frac{c_0^3}{\rho_0}\sigma^2\{\rho(\mathbf{x}, t)\} \tag{2.37}$$

Intensity indicates the rate at which energy crosses the unit surface area at a point. Equation 2.37 states that the intensity of the sound at a point where the density is ρ_0 is c_0^3/ρ_0 times the **mean-square fluctuation** of ρ (i.e. the value $\overline{(\rho - \overline{\rho})^2}$ called the *variance*, which is written also like $\sigma^2\{\rho\}$ - where $\sigma\{\rho\}$ is the *standard deviation* -).

A convenient unit of measurements for the intensity is, a part from its natural one i.e. $[W/m^2]$, the decibel scale; the intensity level on the decibel scale is usually defined as follows:

$$I_{dB} = 10 \cdot log_{10}\left[\frac{I}{I_0}\right] \tag{2.38}$$

where $I_0 = 1\,[pW/m^2]$

Integrating the intensity over a sphere of large radius (compared with the average dimensions of the flow field considered) thus, considering valid the Equation 2.36 for the variations in density in this volume, it is possible to obtain the **total acoustic power output** of the field of flow.

Considerations reported in Ref. [31] give preliminary rough idea of the **sound production variation** with the flow constants and main parameters; Lighthill concludes that at a distance x from the flow center and in a given direction, the density variations Eq. 2.35 are *well approximated* using the following expression:

$$\rho - \rho_0 \approx \rho_0 \left(\frac{U}{c_0}\right)^4 \frac{l}{x} = \rho_0 M_a^4 \frac{l}{x} \tag{2.39}$$

where a dependence of the density changes in the sound radiation field on the *fourth power* of the Mach number is evident: describing the sound radiation as a **"Mach number effect"** due to the **quadrupole nature of the field**.

Always following Lighthill paper, it is possible to write Equations 2.40 and 2.41 for the **intensity** and the **total acoustic power output**, respectively:

$$\boxed{I_Q(x) \propto \rho_0 \frac{U^8}{c_0^5}\left(\frac{l}{x}\right)^2} \tag{2.40}$$

$$\boxed{P_Q \propto \rho_0 \frac{U^8}{c_0^5} l^2} \tag{2.41}$$

Where author's experiments suggest that the *sound intensity* **increases like a high power of the typical flow velocity** (in this case U^8) but this law has to be taken with caution because of the

> *"...approximate character of the arguments used to support them [...] "*

Also the **acoustic power coefficient** K and the **acoustic efficiency** η_Q are defined by Lighthill as follows, where P_{ac} is the acoustic power:

$$K = \frac{P_{ac}}{\rho_0 U^8 c_0^{-5} l^2} \tag{2.42}$$

$$\boxed{\eta_Q \propto \left(\frac{U}{c_0}\right)^5 = M_a^5} \tag{2.43}$$

Because in a steadily maintained flow, both the **energy per unit volume** and the **total rate of supply of energy** are roughly proportional respectively to $\rho_0 U^2$ and to $(\rho_0 U^2)(U l^2)$; giving birth to the concept of **aerodynamic sound production efficiency** and its approximated formula (Eq. 2.43).

It has to be kept in mind though, what this last equation says; (i.e. saying it with Lighthill's own words), that:

> *"Turbulence at low mach numbers is a quite exceptionally inefficient producer of sound."*

For a more advanced theory refer to Ref. [8] where it is exposed Lighthill's theory in a more complete and organized form, also in terms of the frequency domain space (x, ω).

2.2.2 Curle Extension to Lighthill's Theory

Curle wrote an interesting article - Ref. [32] - as an extension to Lighthill's general theory of aerodynamic sound production: he tried to incorporate the **influence of the presence of solid boundaries** in the computation of the sound field.

This theory deals both with the introduction of two features:

1. **Reflexion phenomena**
2. **Diffraction phenomena**

These in fact are mainly due to the fact that sound waves are *re-scattered* when they meet the **solid edges**.

Curle shows a **resultant dipole field** at the solid boundaries, as a limit to Lighthill's **quadrupole volume distribution**.

Dimensional analysis conducted in his paper, shows how **sound intensity**, namely $I(x)$ generated by **dipoles** and scattered in the **far-field** obeys the following *rule of proportionality*:

$$\boxed{I_D(x) = \frac{\rho_0 U_0^6}{c_0^3}\left(\frac{L}{x}\right)^2} \tag{2.44}$$

showing that *dipoles* should be **more efficient sound generator sources** than Lighthill's studied *quadruples*, in the case the Mach number is low enough. He also shows always in his paper that the **fundamental frequency of the dipole sound** is *one half of the frequency* of the quadrupole's one.

In this theory, dipoles correspond to externally applied forces, like the ones that are present at fluid-solid boundary interface, that are due to:

- the **impact of sound waves** from quadrupole sources on the solid surface (i.e. the **diffracted wave**)
- the **hydrodynamic flow itself** (including turbulence, etc..)

Thus, the general sound field is regarded as derived from:

1. **Quadrupole field** (from original *Lighthill's theory*) representative of the **fluctuating applied stresses**
2. **Dipole field** (*Curle's theory*) representative of the **fluctuating force action of solid boundaries**, on the fluid.

Another important fact is that *decreasing Mach number* implies *increasing importance* of the role of **dipoles** and **dipole-scattered field**.

Now, reconsidering the inhomogeneous wave equation system - namely Eq. 2.16 and Eq. 2.11 - its most **general solution** is, as reported in Ref. [32] (from Stratton 1941), the following:

$$\rho - \rho_0 = \frac{1}{4\pi c_0^2}\int_V \frac{\partial^2 T_{ij}}{\partial y_i \partial y_j}\frac{d\mathbf{y}}{|\mathbf{x}-\mathbf{y}|} + \frac{1}{4\pi}\int_S \left[\frac{1}{r}\frac{\partial \rho}{\partial n} + \frac{1}{r^2}\frac{\partial r}{\partial n}\rho + \frac{1}{c_0 r}\frac{\partial r}{\partial n}\frac{\partial \rho}{\partial t}\, dS(\mathbf{y})\right] \tag{2.45}$$

with quantities taken at *retarded times* $t - r/c_0$ where $r = |\mathbf{x}-\mathbf{y}|$ and $\mathbf{n}$ is the outward normal from the fluid.

The **retarded potential solution** as written in Eq. 2.45, indicates that the sound is radiated as if it was by a distribution of quadrupoles, of strength T_{ij} per unit volume, in a medium at rest. Curle proposed the following relation as a **solution for the sound field**:

$$\begin{aligned}\rho - \rho_0 &= \frac{1}{4\pi c_0^2}\left[\frac{\partial^2}{\partial x_i \partial x_j}\int_V \frac{T_{ij}\left(\mathbf{y}, t - \frac{r}{c_0}\right)}{r}\, d\mathbf{y} + \frac{\partial}{\partial x_i}\int_S \frac{1}{r} l_j p_{ij}\, dS(\mathbf{y})\right] \\ &= \frac{1}{4\pi c_0^2}\left[\frac{\partial^2}{\partial x_i \partial x_j}\int_V \frac{T_{ij}\left(\mathbf{y}, t - \frac{r}{c_0}\right)}{r}\, d\mathbf{y} - \frac{\partial}{\partial x_i}\int_S \frac{P_i\left(\mathbf{y}, t - \frac{r}{c_0}\right)}{r}\, dS(\mathbf{y})\right]\end{aligned} \tag{2.46}$$

with the following position in Eq. 2.47, in the special case that $\overline{v}_n = 0$ i.e. condition of zero normal velocity at boundaries and each surface is either fixed or vibrating in its own plane.

$$P_i = -l_j p_{ij} \tag{2.47}$$

Equations 2.46 and 2.47 are the **fundamental results of Curle's theory**; the *surface integral* represents the modification proposed to Lighthill's theory in order to **take into account solid boundaries presence and contribution**.

The sound field is that in a *uniform medium*, generated by a **distribution of dipoles** of strength P_i per unit area, located along the solid boundaries; the term in Eq. 2.47 is exactly the **force per unit area** exerted by the boundaries on the fluid, in the x_i direction.

Integrating this term on the whole surface it is possible to calculate with the following equation the **resultant force** exerted upon the fluid by the solid boundaries:

$$F_i(t) = \int_S P_i(\mathbf{y}, t)\, dS(\mathbf{y}) \tag{2.48}$$

The sound field is expressed in Eq. 2.46 as a **sum** of the respective fields generated by:

1. a **volume distribution of quadrupoles**
2. a **surface distribution of dipoles**

As already stated in previous paragraphs, parameters in the **external stress system** (T_{ij}) still incorporate the effects of the following phenomena:

- **generation of sound**;
- **sound convection**, with the main flow;
- **propagation** with variable speed;
- **dissipation** by conduction and viscosity

While the P_i term, (i.e. **the applied dipole field**), incorporates the effects of other two phenomena, namely:

- **Reflexion phenomena**
- **Diffraction effects at solid boundaries**

By the same **a-dimensional analysis** process made by Lighthill, Curle derives the following expressions for the **intensity** and the **total acoustic power output**:

$$\boxed{I_D(x) \propto \rho_0 \frac{U^6}{c_0^3} \left(\frac{l}{x}\right)^2} \tag{2.49}$$

$$\boxed{P_D \propto \rho_0 \frac{U^6}{c_0^3} l^2} \tag{2.50}$$

And comparing these equations with Eq. 2.40 and Eq. 2.41 respectively, for *Lighthill's quadrupole-solution expressions* of $I_Q(x)$ and P_Q, it is possible to see the following relations, between the two analysis:

$$\boxed{\frac{I_Q}{I_D} \sim \left(\frac{U}{c_0}\right)^2 = M_a^2} \tag{2.51}$$

which implies that

$$\boxed{I_D \approx \frac{I_Q}{M_a^2}} \tag{2.52}$$

In other words, Equation 2.52 means that at *low Mach numbers* the **contribution** to the sound field due to the **dipoles distribution** should be *greater* than that due to the **quadrupoles**.

Curle's expression for the **acoustic efficiency** is the following:

$$\boxed{\eta_D \propto \left(\frac{U}{c_0}\right)^3 = M_a^3} \tag{2.53}$$

2.2.3 Wave Packets Model for Coherent Structures

As recent studies have demonstrated the existence of these already cited more ordered features in the turbulent flow, new theories have been developed in order to physically and mathematically explain these *"new entities"*, sometimes referred to as **coherent structures** or, more frequently, **wave packets** (WP).

These wave packets are so called because of their structure: in fact they are **axially aligned waveforms** whose *wavelength* is of the order of magnitude of the jet diameter from which the turbulence has been generated.

It has been possible to clearly physically identify these coherent structures in the rather *"chaotic turbulent flow"*, by the aid of diversified techniques of **flow visualization** such as *Schlieren techniques*, *sheet illumination* and *carbon dioxide fog* and by viewing *time-averaged* and *conditionally-averaged images* of round jets at high Reynolds and Mach numbers respectively using *axisymmetric near-field pressure signature* as triggers, rather than a *single near-field microphone*; as reported in Ref. [20]

Further researches tried to investigate the connexion between **jet instability**, **related turbulence** and **wave emission of generated noise** by means of *measuring velocity* and *pressure fields* in the jet, both in the near and far fields. Researchers were trying to correlate these set of observations and measurements somehow, mainly using the **equations of sound propagation**.

Mollo-Christensen was able to discover in 1963 that the jet noise was mainly concerned with two types of characteristic emitted sound: **one dominating the very low frequencies band** and the other **one dominating the high frequencies band**.

He in fact discovered that collected data was pointing out some features of the fluctuating (hydrodynamic) pressure field, and tried to describe this behavior in terms of simple functions, building the basics for later studies that consider the jet itself as a **semi-finite antenna for sound emission**. He also pointed out the large scale transversal coherency of these newly discovered motions of the large eddies.

Following Dr. Jordan and Dr. Cavalieri, (see Ref. [20] and Ref. [34]), it is possible to express the **Reynolds stress tensor** with the model in Eq. 2.57[3]; this model is used to evaluate **temporal amplitude changes** of a time-localized wave packet with amplitude A, given by Eq. 2.56, always taken from Ref. [34]. This model would be used in conjunction with the field equations, expressed in one of the following two forms:

$$\rho(x,t) - \rho_0 = \frac{1}{4\pi c_0^2} \int_V \frac{1}{|x-y|} \left[\frac{\partial^2 T_{ij}}{\partial x_i \partial x_j} \right]_{\tau = t - |x-y|/c_0} dy \tag{2.54}$$

$$\rho(x,t) - \rho_0 = \frac{1}{4\pi c_0^4} \int_V \frac{(x_i - y_i)(x_j - y_j)}{|x-y|^3} \left[\frac{\partial^2 T_{ij}}{\partial \tau^2} \right]_{\tau = t - |x-y|/c_0} dy \tag{2.55}$$

$$A(\tau) = e^{-\tau^2/\tau_c^2} \tag{2.56}$$

$$T_{11}(\mathbf{y},\tau) = \left(2\rho_0 U \tilde{u} \frac{\pi D^2}{4} \right) \delta(y_2)\delta(y_3) \left[e^{i(\omega\tau - k y_1)} e^{\left(-y_1^2/L^2\right)} e^{\left(-\tau^2/\tau_c^2\right)} \right] \tag{2.57}$$

The convected wave has a **time-space modulation** that is mathematically represented by the **two Gaussian envelope functions** both in *space* and *time* with their relatives parameters L and τ_c

Other parameters are: ρ_0, the density of undisturbed fluid, U the jet velocity, $\tilde{u}$ the maximum amplitude of velocity fluctuations in the WP, D the jet diameter and $\delta(..)$ represent the Dirac delta distribution. **Convections parameters** are both the wave frequency ω and wavenumber k and the **convection velocity** is calculated as ω/k.

It has to be noted that T_{11} has a complex-valued expression but only the real part has physical meaning while the double Dirac delta distribution ($\delta(..)\,\delta(..)$) is needed in order

[3] (see Appendix E for detailed calculations of the model.)

to **reduce the dimension of the problem**: from a 3D problem to a one dimensional model, that underlines **source compactness features** in the *radial direction*.

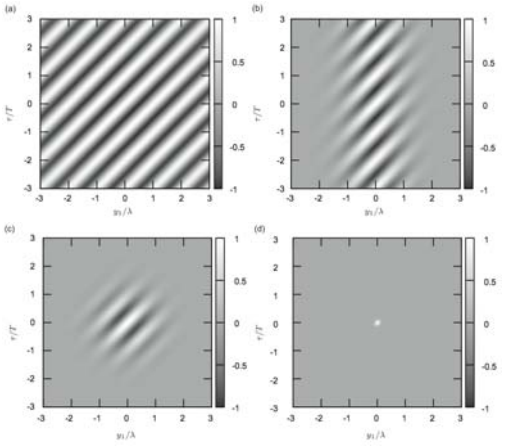

FIGURE 2.10: Space-modulated and time-modulated wave packets: from Dr. Cavalieri simulation code. (Ref. [34])

Following all passages reported in Appendix E , it is possible after making the **assumption of far field**, to derive an **analytical expression** for the **pressure in the far field** (as the one derived by Dr. Cavalieri in his paper) that matches *Crow's* and *Crighton models* (see Ref. [19] and Ref. [8]).

Always in his paper (Ref. [34]) the author presents a WP model for coherent structures in subsonic jets that has the following features:

1. **Time-dependent amplitude convected WP** with **spatial extent** as well. (i.e. the radiated sound field is function of both, the amplitude temporal variation of the wave and of its modulation in space).
2. **Intermittency features** are seen to be good in describing the behavior of subsonic jet turbulence, especially at the end of the potential core.

The presented model tries to explain **higher noise levels** and the **intermittent characteristic emission of the radiated sound mainly at low polar angles from the jet axis**.

The author has found an analytical expression for the radiated sound pressure; i fact, **temporally localized changes in WP** can lead to **directional radiation patterns** (or **highly directional** i.e. ***superdirective***) and **high amplitude bursts**.

Both analyzed features of **increased temporal localization** of the source and source radiated acoustic power over the fluctuations energy, give an idea of the **level of power of the source**.

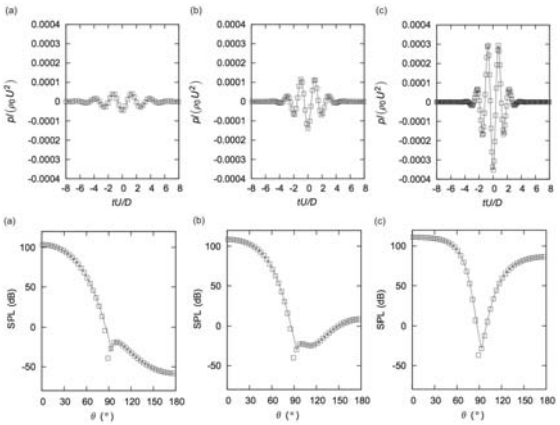

FIGURE 2.11: FF pressure trends; from Dr. Cavalieri simulation code. (Ref. [34])

The author concludes his analysis reporting that his WP model with time averaged envelopes and time jittering characteristics can be effectively used to study one of the **salient features of this type of sources** i.e. the **time-jittering behavior**.

Although accurate calculations of acoustic sound fields can be made nowadays using powerful DNS simulations, it is not yet clear which specific feature of a turbulent jet drives the **production of sound** and, as a direct consequence, how jet turbulence can be manipulated in order to **reduce the emitted noise**, especially in the far field, it is still a challenge.

A brief recap of the studied WP model key-features, as intended by the author:

- **spatial modulation**
- **temporal modulation and intermittency** (i.e. jittering)
- **superdirectivity**
- $St_{avg} = 0.3 \div 0.4$

The proposed source model represents a combination of two previous studied ones, namely the Crow's Ref. [19] and Sandham's Ref. [18] models: it is built like a **convected instability wave** with both **space** and **time modulations**. This simple scheme analyzed tries to represent the jet as a **one dimensional antenna** and helps to determine a fairly accurate prediction of the sound transmitted by the compact source especially in the Far field.

It is also thought to be a quite valid representation of the analyzed phenomenon if one compares the successful results of the **convected jittering wave packet *"Ansatz"***

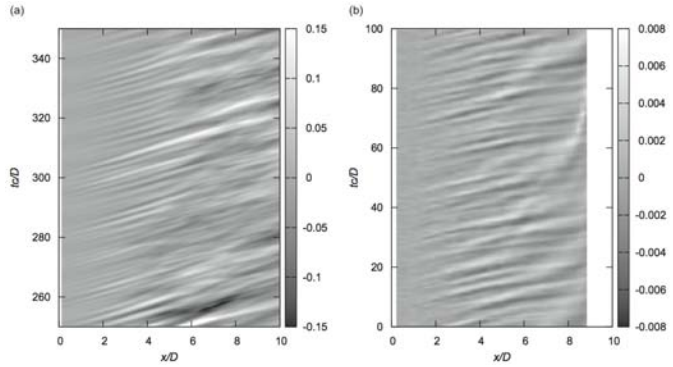

FIGURE 2.12: Jittering WP in numerical and experimental subsonic jet data; azimuthal mean of stream-wise velocity and NF pressure of a coaxial jet. (Ref. [34])

model with data collected from experiments and, above all, numerical simulations. (see again Dr. Cavalieri Ref. [34]).

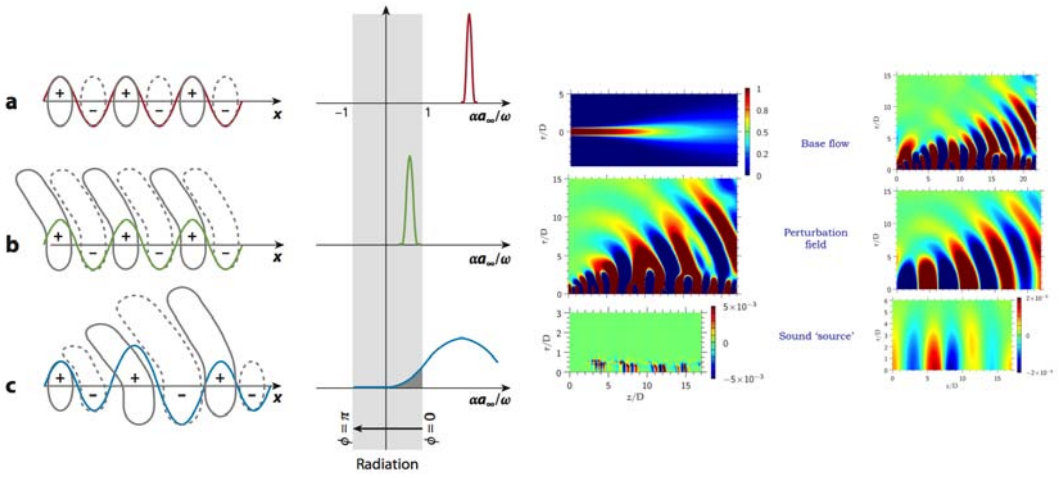

FIGURE 2.13: Left image: spatial and spectral representations of wave packets; (from Ref. [28]). Right image: non linear interaction in laminar, axisymmetric jet driven by two different frequencies (see the source for more information, Ref. [20])

As can be seen on the left image of Figure 2.13 (directly take from Ref. [28]), the three representations are respectively for the (a) **subsonic advection case**, (b) the **silent supersonic advection case, generating Mach waves** and (c) the **subsonic advection case, with spatial modulation, leading to sound leakage**.

It is well written and reported in Ref. [20] that, in the **space-time representation of the WP** - images on the left of Figure 2.13 - **amplitude inhomogeneities** lead to **incomplete cancellation** and associated compressions and rarefactions especially for the radiation mechanisms in the cases of the subsonic WP, namely (a) and (c).

2.2.4 Wave Packet Model for Jet Sound Radiation Influenced by the Presence of a Flat Plate

In order to be able to analyze phenomena like those already cited and described (i.e. **reflexion** of sound waves by boundaries and especially those related to **diffraction** and **edge-scattering**) that are mainly due to the presence of a body-obstacle in the proximity of the jet (such as, for instance, a semi-infinite or a finite plate), a physically and mathematically more advanced theory have to be developed.

Dr. A. Cavalieri has developed such a theory in Ref. [34] that has given life to a **simplified analytical and numerical wave packet model** that should prove to be remarkably indicated in order to justify these aforementioned effects, due to the **presence of the wing** in the near field of the scattered sound.

In his theory, Dr. A. Cavalieri obtains an expression for the sound field reported in Equation 2.58, by using a **tailored Green's function** of the type $G(\mathbf{x}, \mathbf{y}, \omega)$:

$$p(\mathbf{x}, \omega) = \frac{1}{4\pi} \int_V \frac{\partial^2 T_{ij}(\mathbf{y}, \omega)}{\partial y_i \partial y_j} G(\mathbf{x}, \mathbf{y}, \omega)\, d\mathbf{y} \tag{2.58}$$

Given the fact that, as already noted in the previous paragraphs, the **free-field solution** (i.e. without *scattering* and *diffracting effects*) is obtained by replacing in Equation 2.58 the tailored Green's function $G(\mathbf{x}, \mathbf{y}, \omega)$ with its **free-field Green's function** counterpart, namely $G_0(\mathbf{x}, \mathbf{y}, \omega)$.

The *simplified source model* used in this theory is always of the type of a **wave packet**, but this time with the characteristics of **non-compactness** and **super-directivity**. It has the following analytical form:

$$T_{xx}(x, r, m, \omega) = 2\rho_0\, \bar{u}_x(r)\, \hat{u}_x(r, m, \omega)\, e^{-ik_H x} \cdot e^{-(x/L)^2} \tag{2.59}$$

where

- $\bar{u}_x(r)$ is the **mean velocity profile** at $x = D$
- $\hat{u}_x(r, m, \omega)$ is the **velocity fluctuations profile** (modeled as *linear instability waves* of frequency ω and azimuthal mode m, with base flow the mean velocity profile)
- k_H is the **axial wavenumber** (determined by linear stability results)
- L is the **Gaussian envelope parameter**

Part II

Stage Detailed Report

Chapter 3

Stage Project Work Overview

3.1 Introduction

In this chapter is reported and described, as directly taken from the **"Stage Report"**, the work that I have done during my *Erasmus stage experience* at the **CEAT laboratory** in Poitiers, France.

3.2 Abstract of the Stage Report

After the first two months of bibliography and study of mainly aeroacoustics subjects, wave packet theories and some advanced numerical models developed here at the laboratory by other researchers and doctors like Dr. P. Jordan and Dr. A. Cavalieri, I concluded the theoretical background and formation with the acquisition of some **signal processing fundamentals and operative techniques** used in the laboratory, for *data treatment*, *numerical analysis* and *microphone's signals post-processing*.

During the following months, I had the opportunity to focus for a while on a more practical activity, such as helping in the **setup and restoration of the facility** where I was supposed to perform some acoustic measurements later on: the famous subsonic wind tunnel of CEAT called *Bruit & Vent* and its updated annexed anechoic chamber, used for aeroacoustics measurements and data acquisition.

The work consisted in helping the chief engineer head of the facility, Dr. J. Delville, a post-doc student, Dr. J. C. Laurentie and some others research engineers, post docs and trained technicians, in the **cleaning and setup of the anechoic chamber** and especially in taking part to some late February 2013 **tests and velocity measurements**,

in the re-qualified facility, that was brought from a subsonic regime of $M_{max} \approx 0.6$ to a transonic one of $M_{max} \approx 0.9 \div 1.0$.

During this second phase of the stage, that started back in January 2013, I performed a lot of manual tasks such as the **set up and the testing of a near field antenna** for later use in experiments; the **calibration of two pressure probes** needed for jet velocity-field measurements & validations; I also participated in the **preparation, the setup and the wiring of aeroacoustic instrumentation** such as near/far fields microphones and last but not least, the **precise mounting of one pitot tube**. I also attended and helped a little bit during the **mounting of the new displacement system** in the test room, its **calibration** and **accurate positioning & alignment procedures**; some **preliminary operations of jet centering & alignment** and even at a few **preliminary test runs**, that took place in the renewed and upgraded facility.

In the last period of the stage, namely from late January 2013 to the end of March 2013, I switched back to some **numerical modeling/computation** and **fortran/Matlab programming**, in order to conclude the work previously began in the first phase of the stage concerning the acknowledgment of WP theories for aeroacoustic problems modeling and **simulations of WP scattering**, using the fortran mono-dimensional model written by Dr. A. Cavalieri.

In the following paragraphs are reported some of the achievements and goals that have been reached during this long stage experience in a top quality research laboratory, known around the EU for the following facilities and very specific fields of study:

- **turbulence** and **noise advanced measurements and reduction strategies**
- **turbulence control and optimization techniques**
- **free-jets** and **coaxial jets** testing facilities
- **subsonic**, **transonic** and **supersonic** wind-tunnel
- **anechoic chamber** for precise aeroacoustic measurements and studies
- **rocket motor** vertical testing facility

3.3 General Overview of the Stage Experience

The six-months stage that I conducted has taken place at the CEAT laboratory, a well known and renowned facility shared by 'The University of Poitiers', the 'ENSMA' and the 'CNRS'. During this period of time I personally met a lot of highly trained and

specialized members of all the three institutions mentioned above; people that belongs mainly to the following fields of study: "Aerodynamics", "Aeroacoustics", "Turbulence Modeling and Control" either applied or numerical/computational, who work in both post-University and advanced research fields.

The stage last 6 months from the **beginning of October 2012** until the **end of March 2013** and I have been conducting my Thesis Project under the main supervision of Dr. P. Jordan and with the help of a lot of other great people who work at the facility (Master's and PhD's students, technicians, engineers with various specializations, Ph.Ds researchers, professors, assistants etc...).

My overall knowledge of the subject was very poor and limited at the beginning; nowadays I have acquired a **better understanding of what Aeroacoustics is**, both from a **theoretical** point of view and from the point of view of the **applications** concerned, **test facilities**, **instrumentation used** etc...

Despite the fact that due to some **unfortunate problems encountered** in this period (unreadiness of the wind tunnel and some security issues) I couldn't personally perform more tests and experimental analysis on the field, has it had been agreed in the beginning with my supervisor but, a part from these little technical problems, I really enjoyed the staying at the lab and discovered at CEAT what are the main types of research and experiments that the **TAMCO** team is conducting.

3.4 Stage Objectives and Achievements

3.4.1 General Objectives

At the beginning of the stage, the objectives were the following:

1. Learn and understand what does the TAMCO group do at CEAT/LEA laboratory.
2. Conduct a brief but intense study and overview of both the disciplines of **aeroacoustics** & **signal processing** and understand the main concepts behind the problems that the first subject does treat: both from the *physical* point of view and from a more *mathematical/analytical* one.
3. Get acknowledged and more confident with phenomena related to **"jet-noise"** in general and their implications.
4. Grasp a better understanding of how and where **aeroacoustics measurements and tests** are done (with the focus on jet-noise problem and its main applications and studies conducted at the laboratory).

5. Learn the main guidelines and the overall study and investigation methodologies that are followed in a **highly qualified research laboratory such as CEAT**.

6. Discover what are the **main test facilities of the laboratory** (wind tunnels, anechoic chamber etc.) the **types of measurements** that the lab. can perform (*LDV, PIV, microphones arrays and antennae*) and the instrumentation in use (e.g. for the case of aeroacoustics: *condensing microphones, linear and azimuthal antennae for both NF and FF measurements, analog-digital cards & instrumentation for signal acquisition and data processing, etc.*)

3.4.2 Thesis-Related Objectives

From a more practical point of view and for what would have also concerned my **thesis project** more directly, the following targets had been emphasized at the beginning of the stage and achieved before the end of the whole period:

1. Get acquainted and confident with aerodynamics/aeroacoustics **data acquisition process**, some **post-processing** data treatment and **numerical manipulation strategies**

    - Learn the **basic functioning of the used instrumentation**: the main acquisition systems (**ETEP**), microphones arrays and other sensors (like pitot tube and its calibrating procedure).
    - Learn some **fundamentals of data acquisition software** and ad-hoc written routines for aeroacoustic computations; (types of expected signals, ways to acquire and treat them, etc...)

2. Learn the **basics of data post processing** of acquired signals and how to perform further laboratory-like analysis.

    - **DSP applied to aeroacoustics** (*Fourier analysis*, *spectra analysis* in general, *correlations*, *coherence analysis*)

3. Learn some basics of *Fortran*, a scientific **programming language**, *gnu-scripting language* and some powerful analysis-graphing tools like *gnuplot*. All tools used in the world of research and useful for obtaining highly customizable simulation environments, with or or without graphical user interfaces and hi-fidelity customizable plots for research papers and tech articles).

3.4.3 Practical Achievements

A part from the more "intellectual" and theoretical phases of the stage, where I had to study a whole new, interesting and challenging subject like aeroacoustics, from books and research papers (mostly written by my supervisor Dr. P. Jordan, as well as by many other people of CEAT), my work was divided into two more main phases as already explained in the introduction:

1. a **Numerical part** (see Part II Chapter 6) with numerical simulation and experimental data DSP treatment and post-processing.
2. a **Practical work part** (see Part II Chapter 5) with hands-on experience in the test facility and with experimental instrumentation.

For what concerns the second point, i.e. the **Practical work part**, I had to perform many tasks like the following reported:

- manually work on the field, helping research engineer Dr. J. DelVille and post-doc. Dr. J. C. Laurentie during the **cleaning and tidying operations** of the anechoic chamber of the Bruit & Vent wind tunnel.
- helping with the **setup of the facility** for the first tests of re-qualification after its update to transonic regime; instrumentation displacement system mounting and alignment, jet centering operations, re-insulation of the whole chamber, calibration of pressure probes transducers, setup and wiring of the microphones for the new acquisition system
- **working** on the labeling system for the 18 microphones of the 3-ringed NF antenna for the new jet-noise experiments
- **helping** with the setup and mounting of the NF azimuthal antenna, plus wiring of this device to the acquisition system and microphones integrity check operations.

While for what concerns the first point, i.e. the **Numerical part**, I had to

- do some tasks of **code writing**; I wrote a Matlab code - that has to be yet finely tuned and debugged - which can help me or the test engineer on the field, in order to do a quick analysis of collected microphones data (by running the code and inputting some known data or parameters, such as number of used microphones, basic test variables etc...)

- do the **validation** of the written code by running it on some past experiments data, in order to compare my results with the ones from other author's;
- run some **post-processing analysis** of microphones data form previous experiments and do some DSP elaborations, like *spectral* and *coherence analysis* of measured signals.
- work on *Dr. A. Cavalieri's Fortran code* on both his versions: *temporal version* and *spectral* one, in order to **understand wave packets theory** and their **modeling** from the theoretical/numerical point of view.

Chapter 4

CEAT Laboratory & used Facilities

4.1 Brief Introduction

The CEAT, namely the "Centre d' Études Aérodynamiques et Termiques", is a big research site situated in France, at the following address: 43, route de l'aérodrome, 86036 Poitiers Cedex, France, (near the city airport), at the suburbs of Poitiers, a beautiful city, located in the mid-west of the country.

The site comprehends many laboratories and facilities that are used for both, **state and industrial research purposes**; for over 50 years, in fact, the CEAT laboratory has been servicing the research departments of both, the **Univerity of Poitiers** and the **ISAE-ENSMA** (i.e. the "École Nationale Superiéure de Mecanique et d'Aérotechnique") that is one of the most important schools of engineering in France, from the point of view of aerospace and AS industrial connections.

The laboratory is a great international and multicultural center, for research and experimental resources and it is part of the famous French **P' Institute (PPRIME)** - that is a **CNRS** (*"Centre national de la recherche scientifique"*) associated laboratory (lab N. 3346) -, which bases its researches and studies in the following **fields of advanced engineering**:

- **Aerodynamics** (both of *compressible* and *incompressible* media)
- **Aeroacoustics**
- **Hydraulics**

- **Combustion**
- **Material sciences**

The CEAT is an cutting-edge and well suited place for conducting research at University level and at a much higher level as well.

It gathers all kinds of professionals, who work in the previously mentioned fields, altogether: professors, Ph.D's doctors, researchers (from CNRS, UFR, SFA, IUT, as well as from both the main Schools of Engineering "les écoles d'ingénieurs", namely the ENSMA, the ENSIP of Poitiers).

It is also a great place of *"know-how transfer"* and collaboration between the greatest French organization of the national research such as, for instance, **ONERA**, **CNES**, **CEMAGREF** (and many more), and with the major companies of **aeronautics, transports and environmental engineering** such as **EADS**, **SNECMA**, **AIRBUS**, **DASSAULT**, **SAFRAN**, **PSA**, **RENAULT** etc...

4.2 Used Facility Description

The building, in which the most of the practical work of this thesis project took place, is the "Soufflerie anechoïque" i.e. the **Anechoic-chambered Subsonic wind tunnel** named *"Bruit & Vent"* (literally "Noise and Wind"), located approximately at the center of the perimeter of the whole facility.

FIGURE 4.1: Exterior of the facility: subsonic wind tunnel "Bruit & Vent" and particular of the new installed hi-power compressor.

This wind tunnel is a renewed facility, dedicated to the study aerodynamics problems and mainly those related to subsonic jets and aeroacoustics: one of the major problem of **industrial concern** is the growing need of understanding the **origin of sound in high speed flows**, for the reasons stated in the previous chapters, so here, at CEAT, it is possible to perform such **aeroacoustic tests and measurements** with the aid of the highly trained and qualified personnel of the aeroacoustic team also known as the

TAMCO group (i.e. the group of **Turbulence analysis modeling and control**), led by the chief in research Dr. P. Jordan.

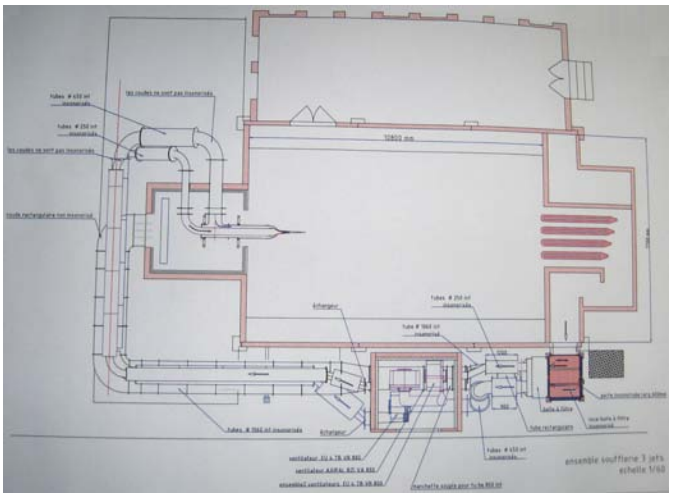

FIGURE 4.2: Plant of the building of the "Bruit & Vent" wind tunnel.

The possibility of measurements in this facility is very broad: it goes from **acoustic measurements** with *microphones arrays and antennae* (for both the Near field (NF) and the far field (FF)) to the more **aerodynamic** ones such as *velocity measurements* done with the aid of sophisticated *LDV* and *PIV* coupled systems, *pitot tubes, hot wires* and many other devices.

Industrial collaborations as well as University and CNRS ones, have permitted the growth of this facility as the "pulsating hearth" of the CEAT. Nowadays many experiments use the advanced features and possibilities of test that this great facility offers, like those reported in the following list:

- subsonic or transonic ranges of simulations;
- **jet noise studies** and investigations;
- **simple** or **coaxial** jets;
- **cold** or **warm** jets;
- jet noise **control and mitigation solutions** studies;
- **microjets systems** development and testing;
- **chevrons** testing;

Projects are developed and maintained in collaboration with some of the major aerospace industries of the whole European Union such as those previously mentioned in Paragraph 4.1.

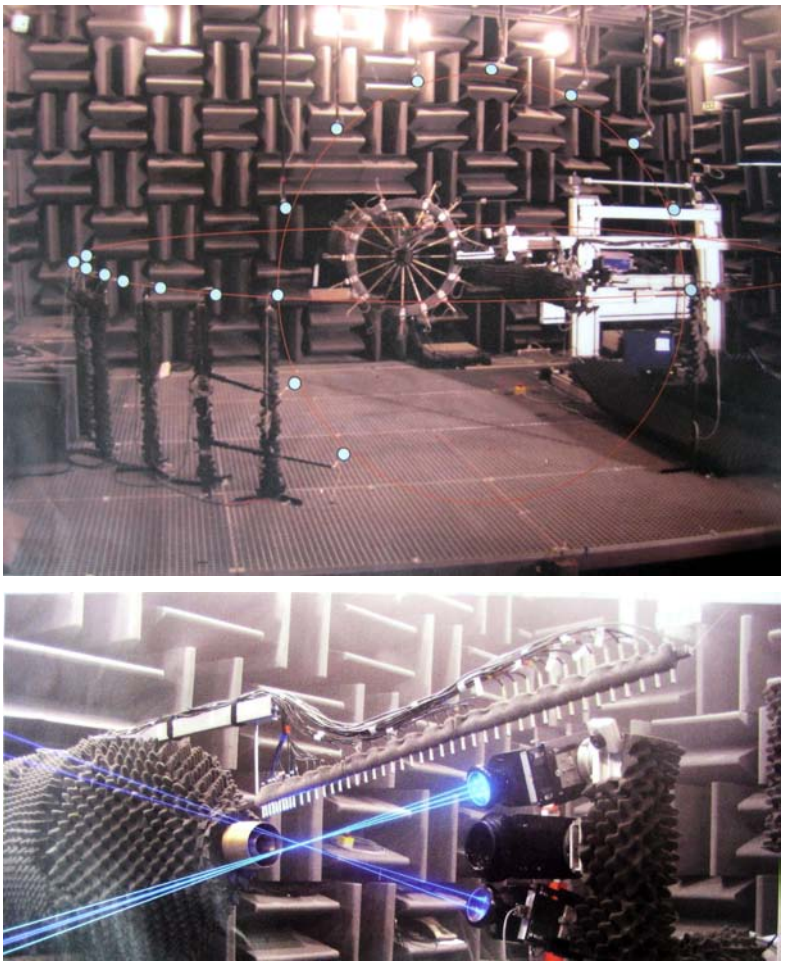

FIGURE 4.3: Interior of the subsonic wind tunnel "Bruit & Vent": particular of the anechoic chamber during aeroacoustic measurements with arrays and antennae of microphones *(upper image)* and a functioning LDV system *(lower image)*.

4.3 Specifications of the "Bruit & Vent": Anechoic-Chambered Subsonic/Transonic Wind Tunnel

Below are briefly reported some **technical data**, **specifications** and **information** of the used facility; namely are reported in Table 4.1 the physical characteristics of the jets in use, - visible in Figure 4.5 during a n early phase of the mounting process after the facility update - while in Table 4.2 are reported the overall dimensions of the **anechoic chamber** used for aeroacoustic measurements, that is located at jet's exit of the wind tunnel and is a well equipped and expensive facility for **accurate testing** and **measurements**.

In Figure 4.4 it is possible to see some of the previously mentioned instrumentation, namely in the upper figure an experimental setup for aeroacoustic measurements with a NF azimuthally-ringed-antenna and in the background a bar of microphones; while

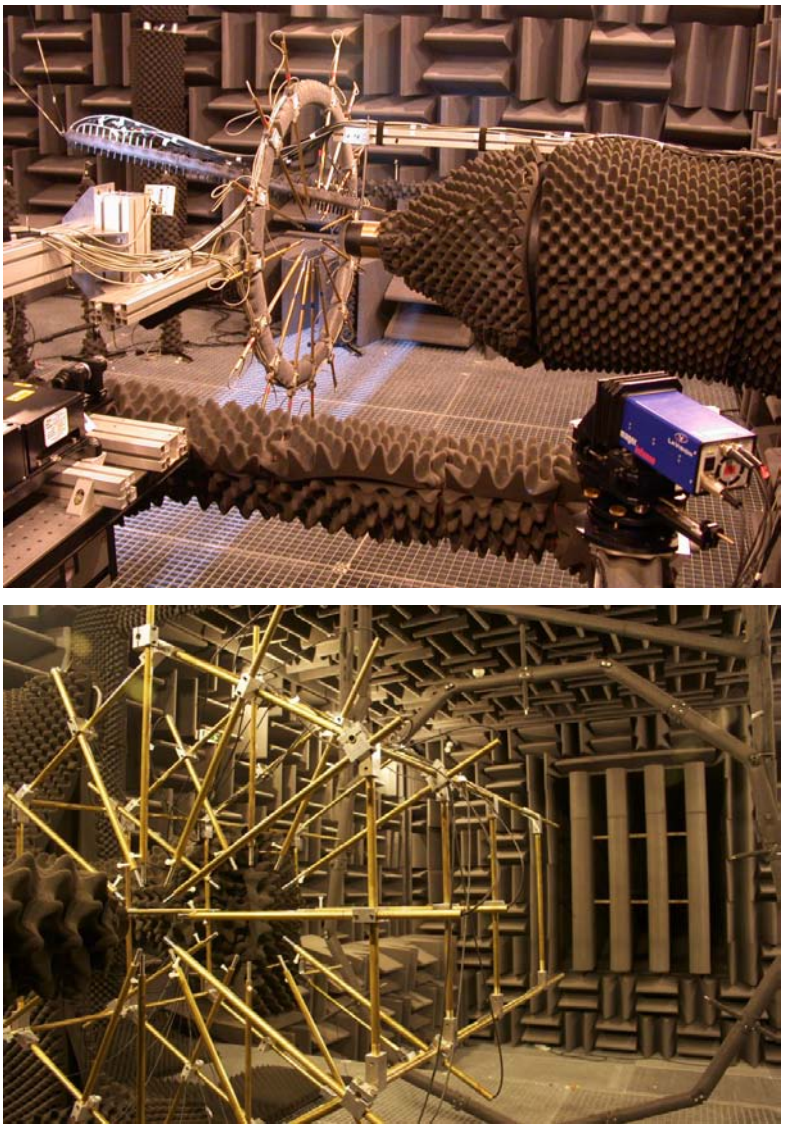

FIGURE 4.4: Interior of the anechoic chamber during aeroacoustic testing.

in the lower figure, a setup with the 3-ringed NF antenna and in the background, the black-foamed-insulated FF antenna.

	Speed $[m/s]$	**Diameter** $[mm]$	**Power** $[kW]$
central jet	200	50	22
secondary jet	150	100	15
	Speed $[m/s]$	**Section** $[m^2]$	**Power** $[kW]$
jet entrainment	10	1	2

TABLE 4.1: B&V technical data: nominal jets characteristics.

In Figure 4.6 it is possible to see the terminal of the jet's nozzle with the **turbulence tripping device** (i.e. the small, black, rough thin strip inside the nozzle, used for promoting turbulence transition).

FIGURE 4.5: Closeup of jet exit during mounting and setup (terminal nozzle is absent).

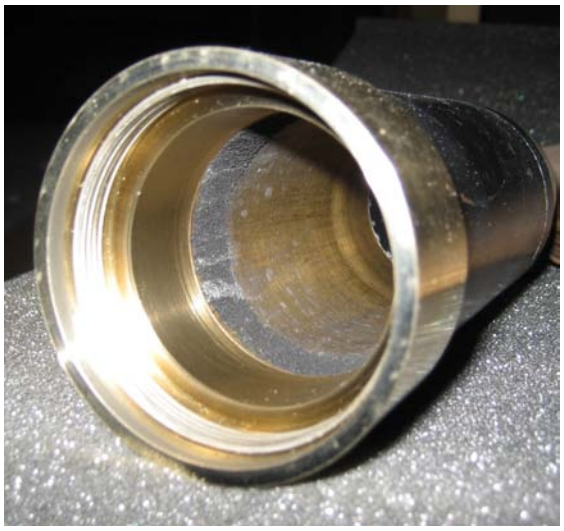

FIGURE 4.6: Particular of the terminal jet's nozzle.

Dimension	**Value** $[m]$
Length	9.4
Width	6.3
Height	4.6

TABLE 4.2: B&V technical data: dimensions after acoustic chamber preparation.

Other technical information about the facility are listed below:

- Presence of a **recirculating double flux**
- **Velocity** and **temperature regulations**
- Possibility of **continuous functioning**
- Anechoic chamber **effective volume**: 270 $[m^3]$

- Height of **acoustic foam wedges**: 70 $[cm]$
- **Low frequency Cut-off** : 200 Hz
- **Max Temperature**: 230 $^{\circ}$ $[C]$
- **Actual Max Mach number reachable**: $M_{max} = 0.9 \div 1.0$
- **Targeted Max Mach number** with next updates: $M_{max} = 1.4$

Chapter 5

Practical Work

5.1 Introduction

In this chapter are briefly reported the **practical tasks** that I completed during the six-months period of stage at CEAT; this work has been carried out in order to prepare the whole renewed facility for the testing campaigns of year 2013 and followings.

First of all, the whole anechoic chamber that had previously been dismantled has been **cleaned and reconfigured**, with all the insulating foam carefully repositioned; next step was the **mounting of the displacement system** and its precise alignment (see Paragraph 5.2): this system is needed in order to be able to mount on it various instrumentation that is used to perform **velocity measurements**, in and around the jet (e.g. *pitot tube* probe, *LDV*, *PIV*; see Figure 4.3 for the mounted view of the system and some carried instrumentation). Next step was the **set up of the jet** itself (see Paragraph 5.3); insulation, mounting and fine laser-alignment with all the reference frames in the chamber, used for measurement purposes. The last step of this first list of tasks was the **accurate mounting of the pitot tube** probe on the displacement system and alignment with the jet (always in Paragraph 5.3).

Some more practical tasks before the first run of the newly reconfigured transonic facility were the **calibration of the two pressure probes** (one total pressure probe and one differential pressure probe) used for velocity measurements (see Paragraph 5.4).

For what concerns the aeroacoustics point of view, the list of tasks carried out comprehend the **mounting, setup and preliminary testing** for accurate signal response of the **near-field 3-ringed azimuthal array of microphones**, called in this paper the ***"NF antenna"*** composed of a *primary - bigger structure* - and a *secondary - smaller*

structure - that will be placed in very close proximity of the jet's nozzle in order to perform **accurate aeroacoustic near field measurements** (reported in Paragraph 5.5).

5.2 Displacement System Mounting, Setup and Centering

All the operations of mounting of the displacement system took about one week.
In Figure 5.1 are reported the photos of the final setup of the system in mounted configuration.

The system is a structure made of *aluminum trusses* and *three motors* that permit the displacement of these trusses - on which the measuring instrumentation will be mounted - in the *three dimensional space*. Once mounted and fixed to the ground, this sophisticated **3 *dof.* displacement system** has been firstly **centered** with regards to the jet and then finely aligned - with the aid of a *laser theodolite* - to all the *reference frames* of the testing chamber (i.e. the absolute wall-floor reference frame, the jet-axis reference frame etc.). The whole system has been then *wired and grounded*.

Engineers **remotely and numerically control** the displacement of the system by using ad-hoc-written software and Labview user interfaces: this will permit to move all the mounted instrumentation (pitot tubes, LDV, PIV etc.) in the surrounding space around the jet and, if needed, as in the case of **velocity in-jet profiles measurements** with the pitot tube that enters also in the jet itself.

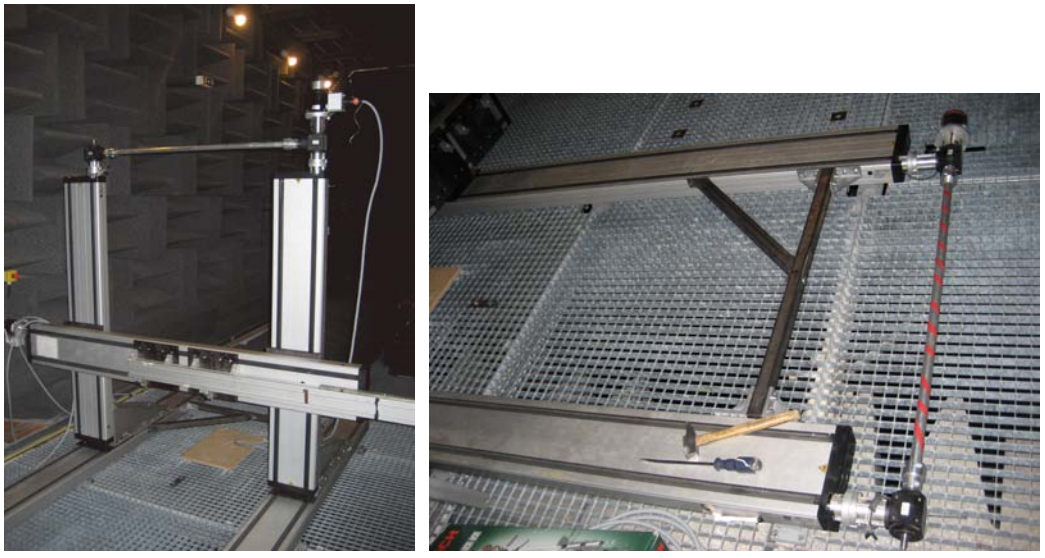

FIGURE 5.1: Displacement system mounting operations.

5.3 Jet Centering Procedure and Pitot Tube Mounting

The pitot tube device assembly and mounting operations took about two days. In Figure 5.2 are reported the photos of the **final setup of the mounted system** in a configuration positioned near jet's exit, ready for the qualification tests.

Once set up and connected to the right, already calibrated probes and captors, the pitot tube needs to be **centered** with respect to the jet axis in order to be able to **accurately perform measurements** of both, **jet's velocity field** and, more difficult and important, those of the **boundary layer** (or *"couche limite"*).

The procedure for centering the pitot tube with respect to the jet center, consists of a numerically generated set of points that are needed in order to make the system describe *four imaginary crosses* in the space of the jet exit, at four different x-coordinate positions (given that x is the coordinate along the jet axis). Once the four crosses are generated and the system has moved in the space describing these figures, the **respective offsets** from the correspondent coordinate axis are computed and taken into account for the subsequent commands to give to the displacement system.

The accurate procedure produced the following Table 5.1 of offsets that were lately corrected by chief research engineer Dr. J. Delville, in order to **perfectly center the jet** and the pitot tube, towards jet's center of reference.

x position	**y(x) offset**	**z(x) offset**
10	0.7	0.8
150	1.1	-1.0
250	2.0	-1.8
750	6.8	-2.2

TABLE 5.1: Chart of measured offsets as obtained from the jet centering procedure.

Once concluded all the centering procedures, a new test grid of points - again numerically generated - has been given as an input command to the displacement system in order to **recheck the quality of the centering**: indeed, the pitot tube would describe in its final configuration, a very **thick and fine mesh of points** in order to take really **accurate measurements of the velocity field** of the jet.

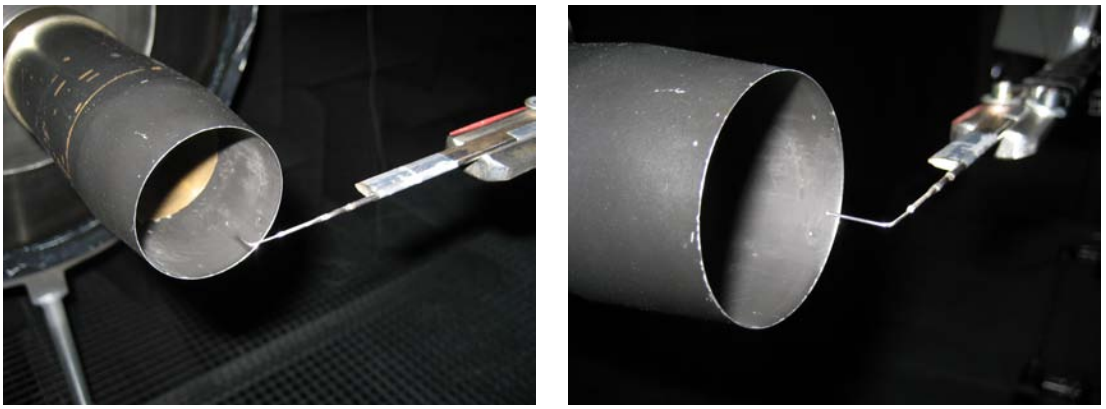

FIGURE 5.2: Pitot tube positioning, centering and final setup layout.

5.4 Pressure Transducers Calibration

During the phase of pressure probes calibration, acquired data has been used in order to compute the **transducers calibration coefficients** (i.e. the value of the *slope of the lines* resulting from data fit from the graphs) as shown in Figure 5.4.

- absolute pressure probe with the following range[1]: (0 - 2 bar)
- and of the differential probe within the following range[2]: (0 - 0.3 bar)

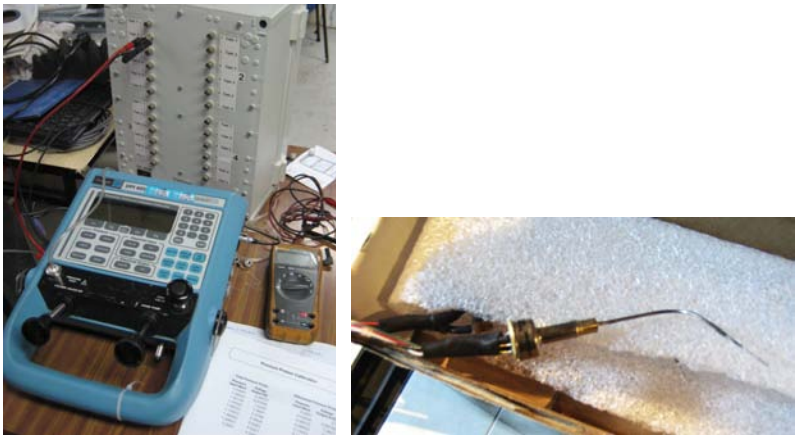

FIGURE 5.3: Probes calibration procedure: used instrumentation and pitot tube.

Values acquired from the calibration instrumentation showed in Figure 5.3 have been reported in the Table 5.2.

[1] White box reference connection: p+ (ABS) $0 \div 2$ $[B]$ row 1 position 1
[2] White box reference connection: p+ (DIFF) ± 0.3 $[B]$ row 2 position 3

Measurements trends show the **linearity of the response** of both tested probes. (Figure 5.4)

Total pressure probe		**Relative pressure probe**	
Pressure input $[bar]$	Voltage output $[V]$	Pressure input $[bar]$	Voltage output $[V]$
1.2097	0.474	0.1500	4.8938
1.5090	2.0056	0.20232	6.5980
1.6422	2.6921	0.28362	9.2540

TABLE 5.2: Calibration data of both used probes (*total* and *relative* pressure probes).

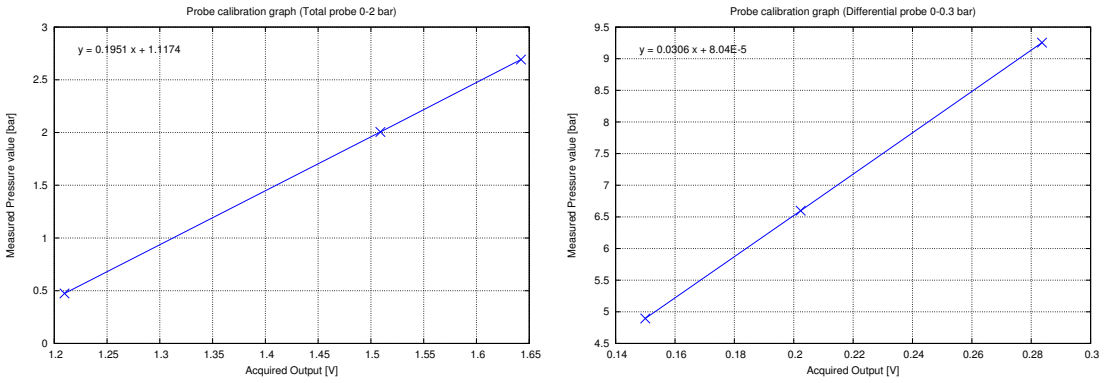

FIGURE 5.4: Total pressure probe and differential pressure probe calibration graphs.

The evaluation of the coefficients of calibration has been made using a **simple linear fit** and results are listed in Table 5.3:

probe type	**calibration coefficient**
total pressure	0.1951
differential pressure	0.0306

TABLE 5.3: Calibration coefficients of the two used probes.

5.5 Near-Field Antenna Setup, Wiring and Mounting

The work of setup and cabling of the near field antenna, took about three weeks; this antenna is used during aeroacoustics experiments in the Bruit & Vent facility. The near field antenna is a device that permits, with its high density of microphones equally spaced around its circumference and distributed over 3 levels (*"rings"*), the **accurate analysis of the acoustic field** near the jet exit and the calculation and **decomposition** of this

near field into **azimuthal modes**, in order to permit to discern and describe which are the higher energetic modes of jet turbulence.

The tasks completed in this phase were the following:

1. Redefinition and recreation of a **new labeling system** for the 18 microphones on the main piece of the system.
2. Antenna's main structure **microphones check**[3]
3. **Setup of the labels** on all the exposed cables and microphones.
4. **Rebuild** from scratch the **secondary structure** of the near field antenna.
5. Antenna's secondary piece **microphones check**[3] (checking signal and correct response of all its 12 microphones).
6. **Recheck** of all microphones for **correct functioning** (*pistonphone* and *signal scope*)[4]
7. **Creation of a joint system** in order to *link together the two structures* - principal and secondary - of the whole antenna setup.

In Figure 5.5 are reported two pictures of the final double-piece mounted configuration of the NF antenna.

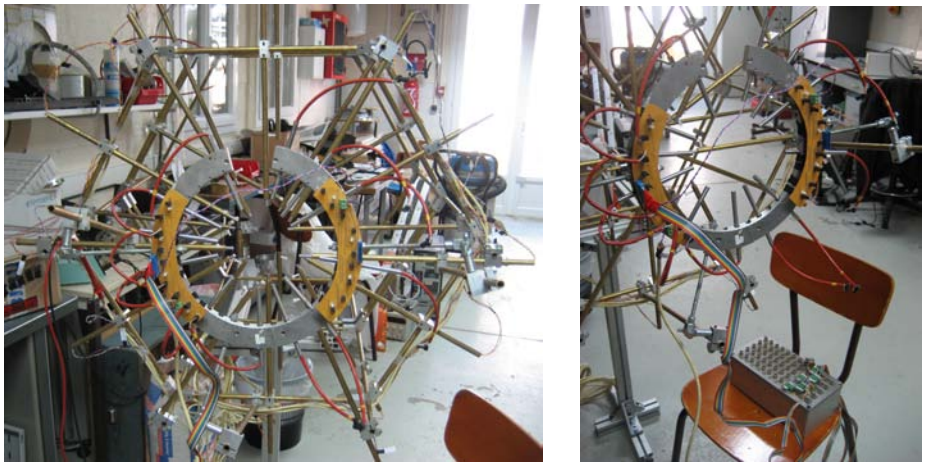

FIGURE 5.5: Final setup of the near field antenna.

[3] (cabling, connectors, electronics, acquisition box, and microphones)

[4] The signal has been captured and evaluated with the ETEP acquisition system, an analog/digital transducer and hardware device that permits the assessment of the parameters of the waveform of the microphone signals. Acquisition parameters are: $2 \cdot 10^5[kHz]$ at $2.5V$ DC (direct current)

5.5.1 NF Antenna: Configuration Details

The near field antenna is a sophisticated system used to perform aeroacoustic measurements; it is composed by two main pieces: a bigger structure (called here *"primary antenna structure"* (or **PAS**)) and a smaller one (called here *"secondary antenna structure"* (or **SAS**)) that are assembled together and are used as a measuring system for the near acoustic field of the jet. Configuration parameters are briefly listed below.

- **PAS specifications:**

  A hexagonal-section-frame, made up of copper tubes that serve as microphones supports. All the microphones are wired and connected to a box of electronics (that needs to be placed under the wind tunnel floor); it has long cables and connectors that runs down the whole length of the antenna. (Figure 5.6) and the following characteristics:

  - **overall assembly length**[5] $\approx 1.35\ [m]$
  - **frame effective length** $\approx 95\ [cm]$
  - hexagonal section with 6 **edges** of $\approx 38\ [cm]$ each
  - total **number of microphones** is 18 ; distributed in 3 levels (6 mics. per level)

FIGURE 5.6: Near field antenna PAS setup and wiring operations.

[5] with both PAS and SAS positioned.

- **SAS specifications:**

  It is a smaller ring-shaped piece that has to be placed in *front of the PAS*, it is needed to **finely characterize the very near acoustic field** (i.e. just the very first centimeters outside the jet). SAS configuration can be seen in the subsequent sketches and figures (Figures 5.7, 5.8 and 5.9). On the upper surface of the ring two PCB (printed circuit boards - aka. electronic cards -) are glued onto the metal and provide **power and signal acquisition functions** for all the microphones that are connected to them. It has to be noted that, the **optimal angle** for placing the maximum number of microphones and then **maximizing the angular resolution** of the system[6] is $\Delta\theta = 40°$. This has been computed taking into account the fact that the antenna has an *angular sector cut* in the border, that give rise to this **minimum-spacing angle**.

  By the way, the chosen final antenna layout is dictated by the fact that the acquisition system must get as many inputs as the number of tracks from the controlling box (i.e. *6 tracks per input at most*) so, since on the PAS have been placed only **6 microphones** per ring, in the SAS have to be placed only 6 microphones, as well.

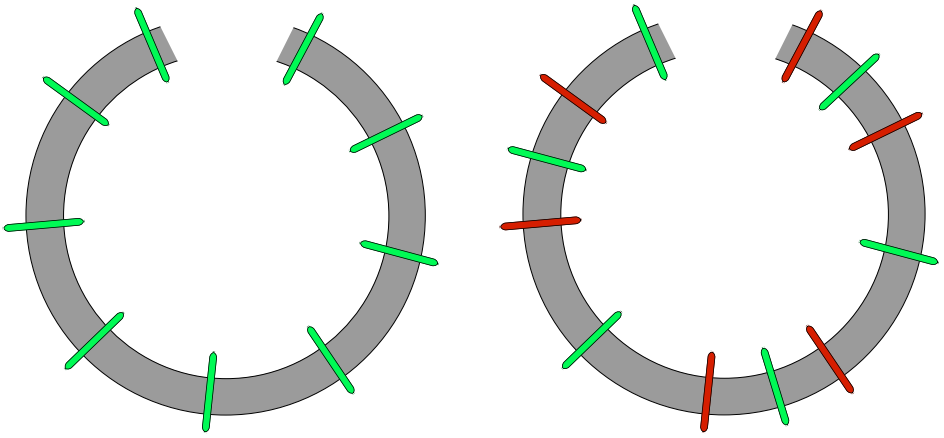

FIGURE 5.7: Sketches of two possible configurations of the SAS.

This second subsystem presents the following characteristics:

- **internal diameter**: 20 $[cm]$
- **external diameter**: 26 $[cm]$
- **width**: 3 $[cm]$
- **thickness**: 1.2 $[cm]$
- **total number of microphone holes**: 33

[6] this should be also the best configuration for azimuthal decomposition till fourth mode.(see the first antenna configuration sketch 1 of Figure 5.7).

- **total number of installed microphones**: 12
- **optimal number of microphones equally spaced**: 9 (+ *3 backup mics.*)
- **optimal angle for maximum angular field resolution** for the 9 mics. installation: $\Delta\theta = 40^\circ$
- **required number of microphones** for the experiment: 6
- **optimal angle for needed configuration** (6 mics. installation): $\Delta\theta = 60^\circ$
- **number of PCBs** on the antenna: 2
- **maximum number of connectable microphones** per each PCB: 9

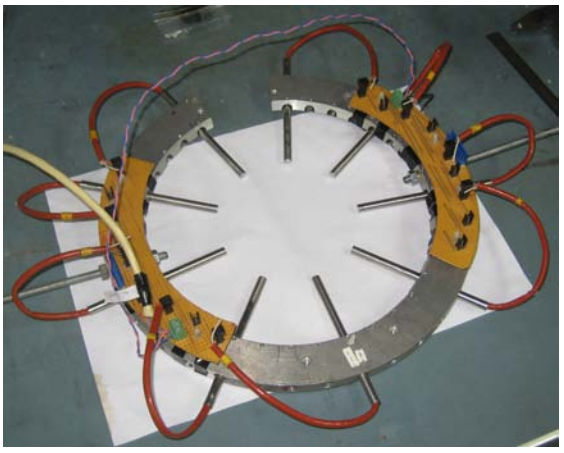

FIGURE 5.8: Image of the first configuration layout of the SAS.

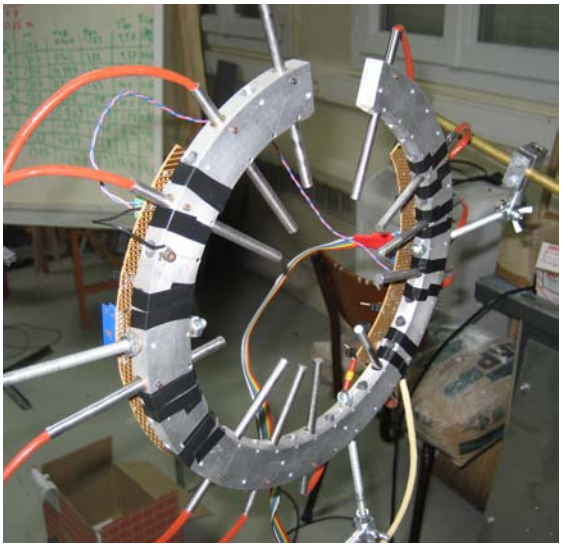

FIGURE 5.9: Second configuration layout of the SAS in mounted position.

- **Microphones :**

  Microphones[7] have been checked with the reference sine wave form generated by the *pistonphone*[8] at 94 dB for the calibration procedure and the acquired signal has been checked for conformity to the attended sine wave, in order to assess **functioning problems** or **electronic ones** (either from the microphones or the PCBs or the connector themselves). The ETEP parameters used for the calibration test were a $2 \cdot 10^5$ $[kHz]$ acquisition frequency and a 2.5 $[V]$ DC alimentation, in order to remove the AC output at 50 $[Hz]$ that was seen to be modulated in the sine wave of the actual calibration signal. Both the antenna and the acquisition system (*connection box* and all the *electronic cards* too) must have grounded plugs, microphones jacks and connectors for shielding purposes.

FIGURE 5.10: Close-up look of used microphones: assembled configuration, mounted configuration and original PCB capsule.

Characteristic	**value**
max current alim.	400 $[\mu A]$
diameter	5.8 $[mm]$
heigth	3 $[mm]$
dimensions	5.8×3 $[mm]$
impedance exit	1.6 $[k\Omega]$
SNR	38 $[dBA]$
accuracy	-63 $[dB]$
T_{max} operat.	$+60\,^{\circ}[C]$
T_{min} operat.	$-10\,^{\circ}[C]$
std. funct. voltage	3 $[V]$ DC
mounting type	PCB

TABLE 5.4: Chart of microphones characteristics.

[7] of the type 1/4 $[in]$ electret microphones
[8] pistonphone model: BT 4231 sound calibrator with 2 levels: 94 & 114 $[dB]$ SPL @1000 $[Hz]$

In Figure 5.10 are showed a close up image of the microphones, as used in the antenna (i.e. within the 10 $[cm]$ case) and in their original PCB raw-component state (some images have been taken from producer's reference website).

Microphones specifications and parameters are listed below and in Table 5.4:

- **case diameter** 6 $[mm]$
- **case length** 10 $[cm]$
- **maximum bandpass** 10 $[kHz]$

Chapter 6

Numerical Work

6.1 Introduction

In this section are summarized the steps that I have followed in order to do the **post processing campaign** of previously taken aeroacoustics measurements, as part of my Thesis Project.

The material presented here is based on the work made by other researchers and doctors who have been working at CEAT like Dr. A.V.G. Cavalieri[1], whose work on jet noise and wave packets modeling has been cited many times throughout this thesis paper.

6.2 Jeronimo Experiment Data Post Processing

The Project is mainly based on two previous experiments and data acquisition/post processing campaigns conducted between 2010 and 2012 by Dr. A. Cavalieri who had previously worked on the subject for his PhD. thesis paper (Ref. [12]).

These cited experiments are related to the **Jeronimo project** (see Appendix A and Appendix B for more details) and the main article on which the following presented work is based on, is the one in Ref. [33], namely about the ***"Scattering of wave packets by a flat plate in the vicinity of a turbulent jet"***.

Sketch in Figure 6.1 and the picture in Figure 6.2 show the configuration of the experiment in which a plate has been put near a single stream, round, subsonic turbulent jet of $D_j = 50\,[mm]$, that would mimic the presence of the wing, near an underwing-installed HBPR engine.

[1] André Valdetaro Gomes Cavalieri, Docteur de L'Université De Poitiers.

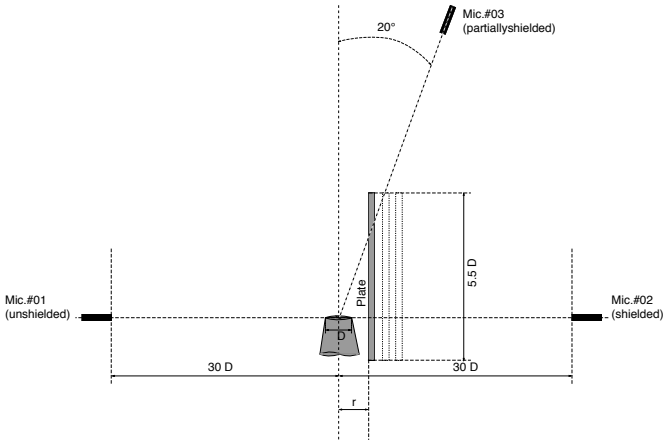

FIGURE 6.1: Sketch of the Jeronimo experiment: CEAT experimental configuration.

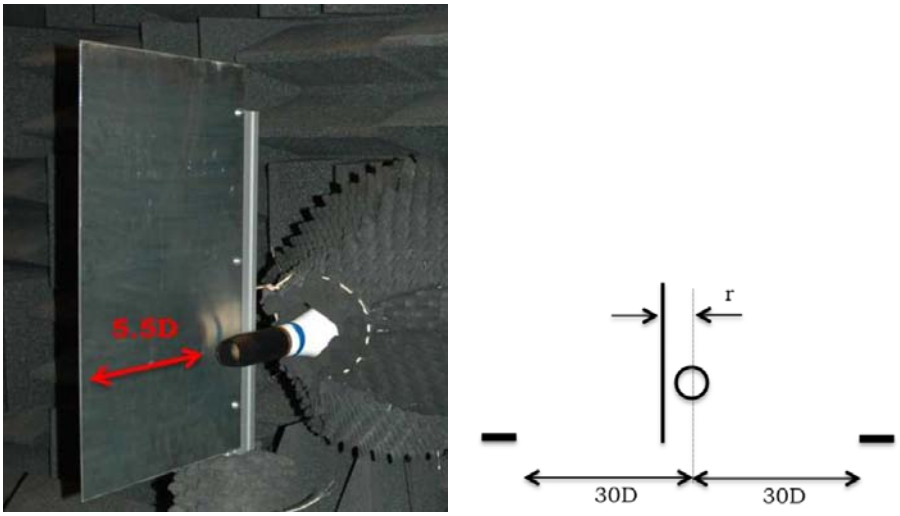

FIGURE 6.2: Original photo and sketch of the CEAT Jeronimo experiment test campaign, taken from article (Ref. [33]): the plate is in the mounted position near the jet exit at distance r.

Three microphones have been used and placed in the positions shown in the sketch of Figure 6.1, in order to perform acoustic measurements of the **scattered sound field** and in order to both inform and validate theoretical models concerning with the **effects of diffraction** and **interaction of a/c structures** - mainly the wings - on the **noise produced by propulsive jets**.

The experiment showed how **installation effects** of the propulsive jet can lead to the spreading of **hydrodynamic jet fluctuations**, through **reflection** and **diffraction** phenomena, typical of sound waves and produce a **scattered sound field that is more intense**, *even ten times louder in some cases*, than the **equivalent uninstalled configuration** of the same jet engine.

6.2.1 Data Treatment Procedure

Aeroacoustics measurements data were directly acquired from the author of the previously mentioned article, from both the following experiments:

- **Subsonic free-jet** experiment
- **Subsonic jet with a near plate** (to study reflection/diffraction phenomena)

The given test bundle of data, was comprehensive of measurements for **various Mach numbers** and **various position of the plate**, and it contained data collected by all the *three microphones* placed in the field around the jet.

The work done and reported here is mainly based on a **parameter variational analysis** of the following variables:

1. **Microphone ID** (mic.#01, mic.#02, mic.#03)
2. **Mach number $\mathbf{M_j}$** (in the following range: $M_j = [0.35 \div 0.60]$)
3. **Plate-jet relative distance $\mathbf{r/D_j}$** (namely: $r/D_j = [1.0, 1.5, 2.0]$)

The accurate procedure followed to analyze and *post-process* given data is reported..

Acquired voltage signals of all the microphones have been imported and analyzed with the help of both *Matlab*© environment and *Fortran*© compiler suite.

Data comes from the set of the three microphones, positioned as in the sketch of the experiment reported in Figure 6.1, namely at ($+90°$, $-90°$, $+20°$) from the jet centerline.

Starting from **voltage data** (Figure 6.3) **pressure** has then been computed and plotted in Figure 6.4, considering as a **reference pressure value** $P_{ref} = 2 \cdot 10^{-5}$ $[Pa]$.

After the **calibration of the microphones** has been taken into account, Figure 6.5, **calibration coefficients** for these have been calculated and obtained values are reported in Table 6.1.

Finally, data has been thoroughly analyzed in order to retrieve some useful informations that are reported in subsequent paragraphs.

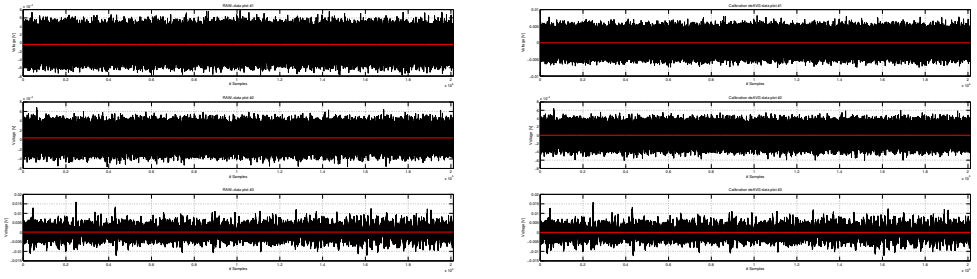

FIGURE 6.3: Raw and de-averaged voltage data graphs for the three microphones.

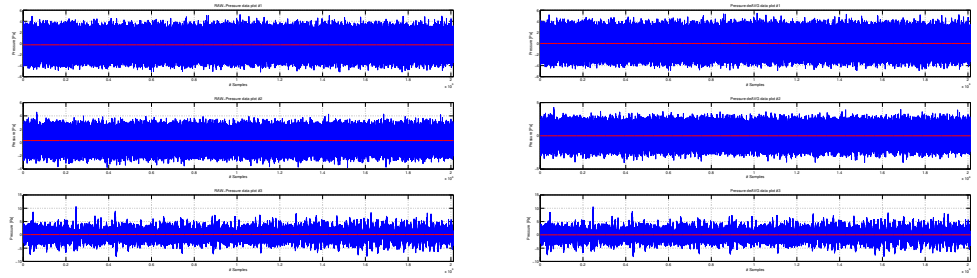

FIGURE 6.4: Raw and de-averaged pressure data graphs for the three microphones.

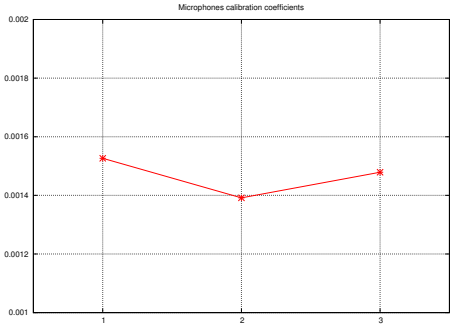

FIGURE 6.5: Computed calibration coefficients for the three used microphones.

Microphone	Calib Coeff.
01	1.527e-04
02	1.392e-04
03	1.479e-04

TABLE 6.1: Chart of calibration coefficients for the three used microphones.

6.3 Spectra Analysis and Plots Comparison

6.3.1 Forewords

In this paragraph are presented some operations of post-processing of Dr. A. Cavalieri measurements.

Due to the lack of microphone's direct output data files of the *free-jet cases* (see author's previous experiment on subsonic jets) **I decided to use the already available computed spectra**, that have been given to me by the author himself, in order to have the possibility later on, **to compare the freejet case with the diffraction one** (i.e. in the jet/plate configuration); another consideration that I made before deciding not to recompute the spectra with a **higher frequency resolution** is the fact that for *subsonic jets* at given *low Mach numbers* and at the given frequency range of the experiment, a very high frequency resolution in the range $St = [0 \div 0.5]$ only brings a lot of *"signal noise"* in the spectrum and does not really add any more useful information.

In order to treat the data more deeply and accurately though, one should get the original *bin files* from microphone measurements for the *free-jet case* already mentioned and, more importantly, for the whole range of Mach numbers (i.e. $M = [0.35 \div 0.60]$ with $\Delta M = 0.05$)

Another approach lately suggested by Dr. R. Maury would be the one that follows the *"non-dimensionalization of the spectra* by the factor $\delta f = f_s/NFFT$.

For the sake of clarity, both mentioned and computed spectra for all the three microphones of the experiment, are reported in the following paragraph and have been **thoroughly compared** with Dr. Cavalieri original results, in order to **avoid computational errors**.

6.3.2 Spectra Comparison Plots for All Microphones

The first set of plots deals with the **spectrum analysis of the pressure signals** for the three microphones considered in the experiment.

Here are reported respectively in Figures 6.6, 6.7 and 6.8 the plots of the calculated **sound spectra** for the *relative test case*, for *each microphone*, at a *variable Mach number* and for each of the three main considered plate/jet positions.

Each row represent the spectra at a different value of the Mach number ($M = 0.4$, $M = 0.5$, $M = 0.6$). First, second and third plots are relative to a specific plate position vs. jet axis (namely: $r/D = 1.0$, $r/D = 1.5$, $r/D = 2.0$).

In the following figures, the current value of the parameter NNFT (number of points of the FFT) used for spectra computation is $\mathbf{NFFT = 2^{10} = 1024}$

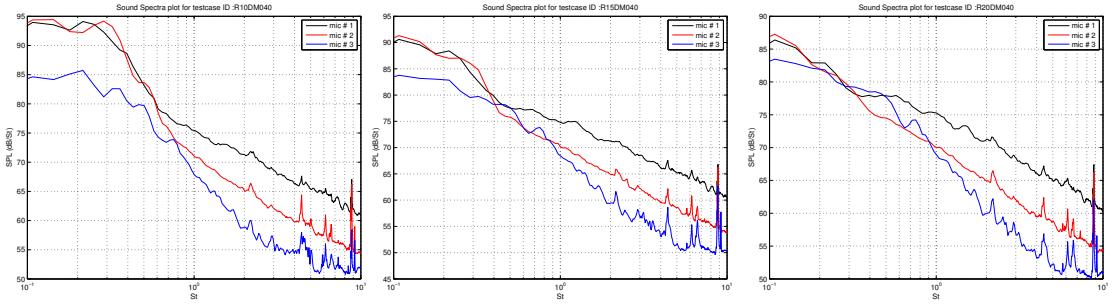

FIGURE 6.6: Sound spectra plot at $\mathbf{M = 0.40}$ for $r/D = 1.0,\ 1.5,\ 2.0$

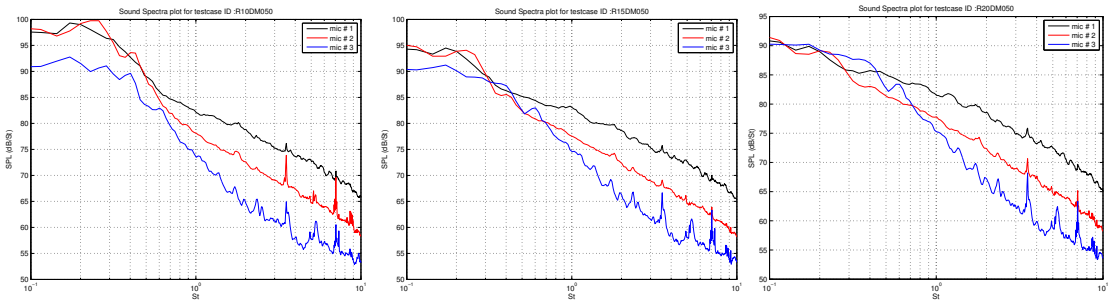

FIGURE 6.7: Sound spectra plot at $\mathbf{M = 0.50}$ for $r/D = 1.0,\ 1.5,\ 2.0$

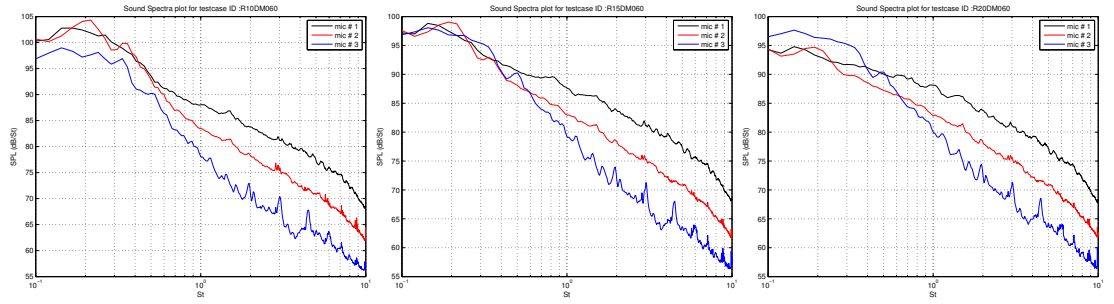

FIGURE 6.8: Sound spectra plot at $\mathbf{M = 0.60}$ for $r/D = 1.0,\ 1.5,\ 2.0$

These plots have been made in order to validate the *Matlab*© code written from scratch and in order to compare its results with those given in Ref. [**33**].

As later suggested by other doctors in the office, the spectra have been recomputed with a higher value of the NFFT parameter. For this second run of the code, the current value is $\mathbf{NFFT = 2^{14} = 16384}$ and graphical results are reported in Figures 6.9, 6.10 and 6.11.

As one can observe by comparing Figures 6.6, 6.7 and 6.8 with their higher-resolution counterparts in Figures 6.9, 6.10 and 6.11, it is easy to observe how **more defined features of the spectra** are visible at **lower frequencies** when one increments the FFT resolution but, at the same time, **more noise** is brought in, in the **mid-hi frequency bands**.

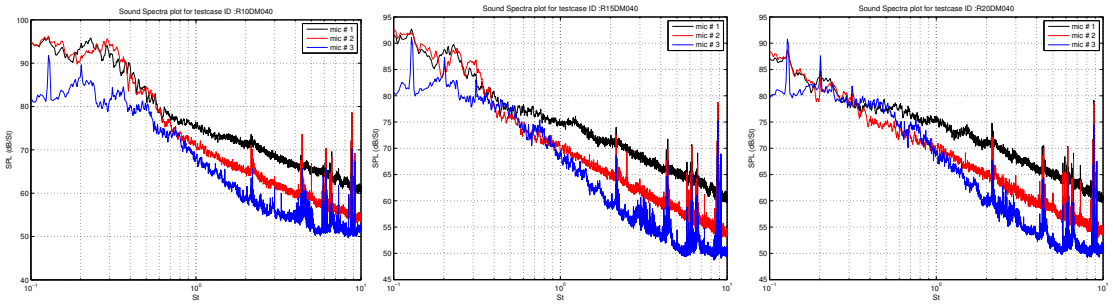

FIGURE 6.9: Sound spectra plot at $\mathbf{M = 0.40}$ for $r/D = 1.0, 1.5, 2.0$

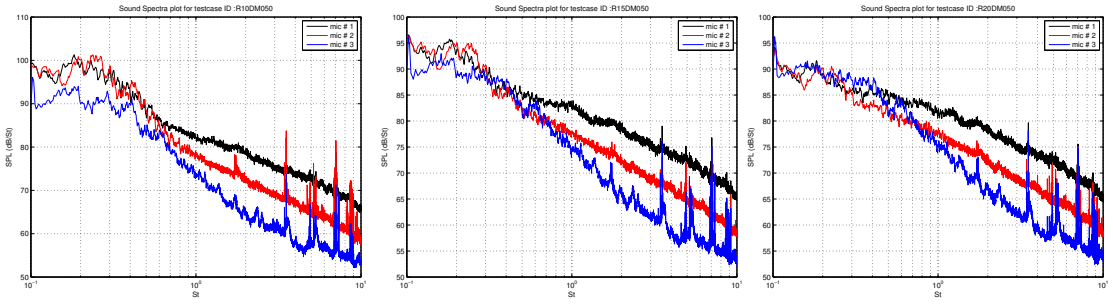

FIGURE 6.10: Sound spectra plot at $\mathbf{M = 0.50}$ for $r/D = 1.0, 1.5, 2.0$

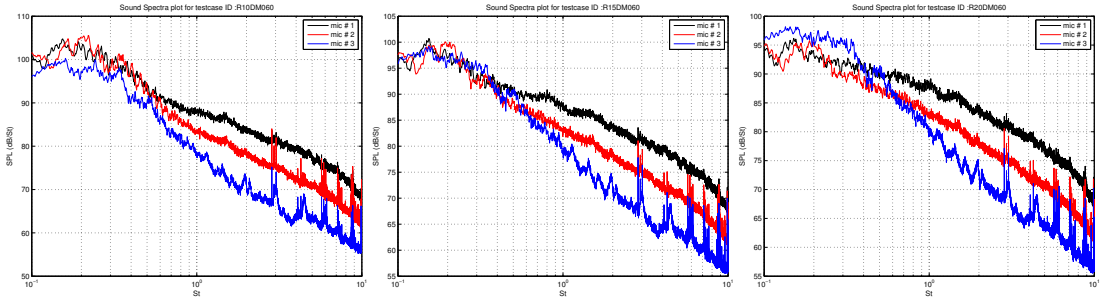

FIGURE 6.11: Sound spectra plot at $\mathbf{M = 0.60}$ for $r/D = 1.0, 1.5, 2.0$

6.3.3 Lateral Microphones (+90/-90 deg.) Comparison Plots

Some other **spectra comparison plots** have been made afterwards; the results are shown in Figures 6.12 and 6.13. These graphs have been computed considering only the **two diametrically opposed microphones** (i.e. those respectively at $\theta = -90°$and $\theta = 90°$ always taking as *zero-reference the jet axis*). These microphones have been re-named, in fact, for sake of clarity, as in previous articles respectively ***"unshielded"*** and ***"shielded"*** microphones and have been plotted with *solid* and *dashed lines*, respectively.

Each plot shows with different colors the *variability of the curves* with the **increasing Mach number parameter** and, in both rows, the three plots refer, as usual, to the **three different plate positions** versus the jet axis.

In Figure 6.12, spectra are calculated as SPL $[dB/St]$ and plotted versus St (i.e. the Strouhal number) while in Figure 6.13, they are recomputed and **rescaled** as function of He (namely the Helmholtz number), in order to clarify at which particular frequency they present **alignment** and possibly the same *"local spectrum shape"*, (local peak features, local valleys etc.).

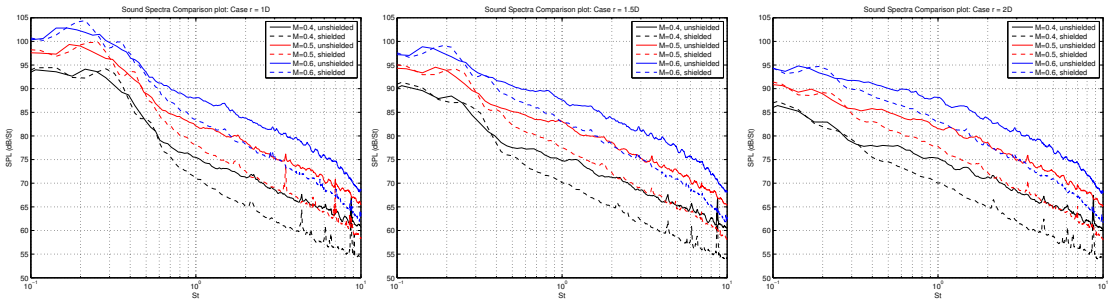

FIGURE 6.12: Sound spectra comparison plot (vs. **St**); ***shielded*** and ***unshielded*** mics.; parametric Mach number and various plate positions ($r/D = 1.0,\ 1.5,\ 2.0$)

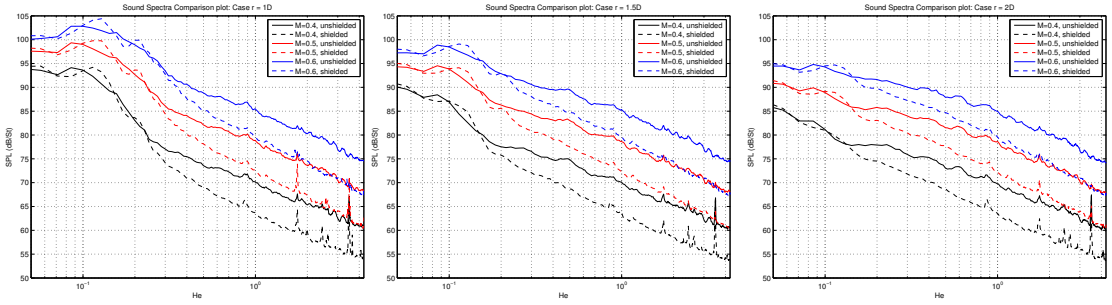

FIGURE 6.13: Sound spectra comparison plot (vs. **He**); ***shielded*** and ***unshielded*** mics.; parametric Mach number and various plate positions ($r/D = 1.0,\ 1.5,\ 2.0$)

Also these plots have been used to **validate** the written *Matlab*© code, because their original version was already included in Ref. [**33**] and available for comparison.

6.3.4 Freejet-Diffraction First Comparison: r/D Dependencies

Plots of Figures 6.14, 6.15 and 6.16 show the comparison between the **spectra of each microphone** - plotted against St number - and the **spectra of the relative free-jet case**, for parametrical values of the plate position (r/D).

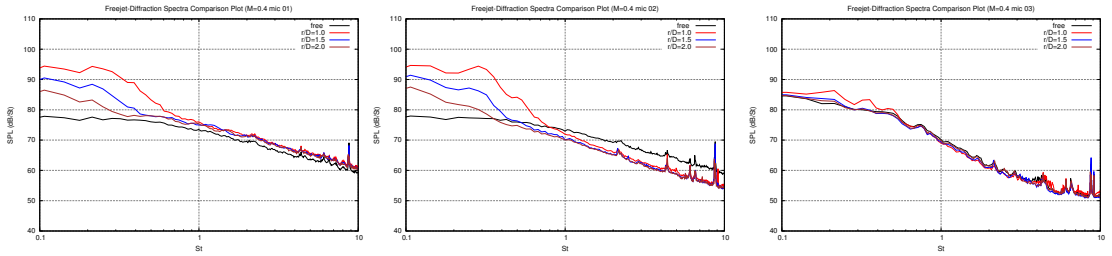

FIGURE 6.14: Spectra (vs. **St**) comparison plots for all mics.; parametric plate position (r/D) and fixed Mach Number ($\mathbf{M = 0.4}$)

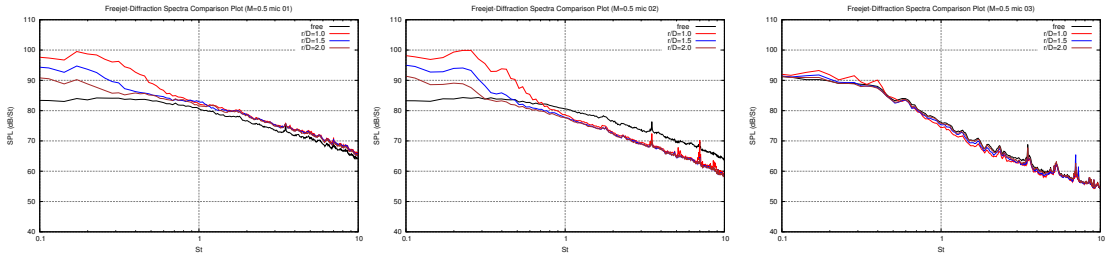

FIGURE 6.15: Spectra (vs. **St**) comparison plots for all mics.; parametric plate position (r/D) and fixed Mach Number ($\mathbf{M = 0.5}$)

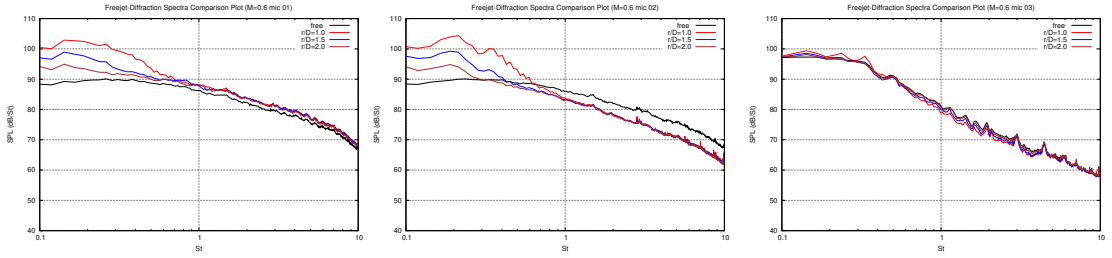

FIGURE 6.16: Spectra (vs. **St**) comparison plots for all mics.; parametric plate position (r/D) and fixed Mach Number ($\mathbf{M = 0.6}$)

Observations:

These plots have been made in order to assess, at least qualitatively, the **effects of diffraction phenomena** and how they change when the **jet-plate distance** is changed.

The phenomenon of **jet noise amplification** is visible especially at **lower frequencies**, at least approximately in the range $St = [0.1 \div 0.6]$ for mic.#01(unshielded) and mic.#02 (shielded) . Each row corresponds to a different Mach number value and they all show three plots: one for each considered microphone, respectively.

It has also to be noted that:

- mic.#02 (shielded) *always* presents **amplification at lower frequencies** followed by **attenuation at higher** ones;
- mic.#01 *always* shows **amplification: bigger at bigger frequencies**, if one compares the jet-plate case with the free-jet one.
- mic.#03 shows **very little amplification in some specific frequency bands**; (it is possible to check with the aid of He plots if these are related/aligned).

In Figures 6.17, 6.18, 6.19 the spectra comparison for r/D dependencies has been re-considered and the plots have been here **rescaled** and replotted against He number, as it has already been done for the spectra plots of previous paragraph's analysis.

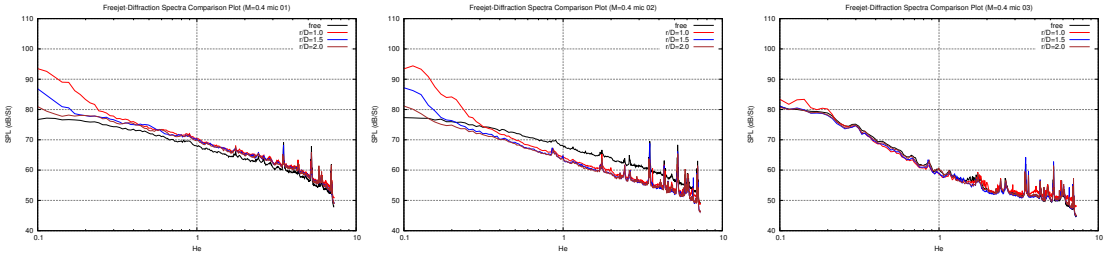

FIGURE 6.17: Spectra (vs. **He**) comparison plots for all mics.; parametric plate position (r/D) and fixed Mach Number ($\mathbf{M = 0.4}$)

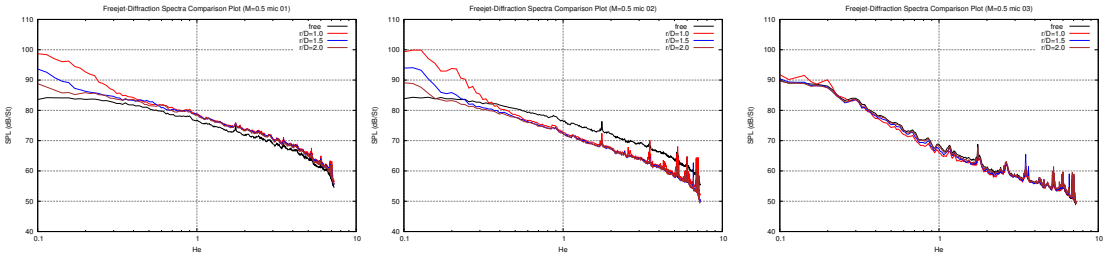

FIGURE 6.18: Spectra (vs. **He**) comparison plots for all mics.; parametric plate position (r/D) and fixed Mach Number ($\mathbf{M = 0.5}$)

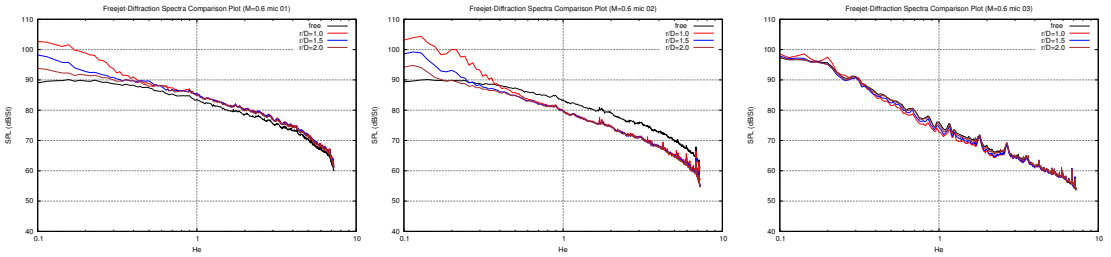

FIGURE 6.19: Spectra (vs. **He**) comparison plots for all mics.; parametric plate position (r/D) and fixed Mach Number ($\mathbf{M = 0.6}$)

6.3.5 Freejet-Diffraction Second Comparison: M Dependencies

If the relative distance between the jet axis and the plate is maintained fixed, respectively at each considered plate/jet position studied, it is possible to obtain the curves in Figures 6.20, 6.21, 6.22, where the comparison between the **free-jet case** with the **amplified** one (i.e. the one which takes into account the *diffraction* and *scattering* effects due to the plate) is now plotted for **parametrical values of the Mach number**. In each row of the cited figures, left, central and right graphs correspond respectively to each one of the considered microphones ($\theta = 90°$ *shielded*, $\theta = -90°$ *unshielded* and $\theta = 20°$ *partially shielded*).

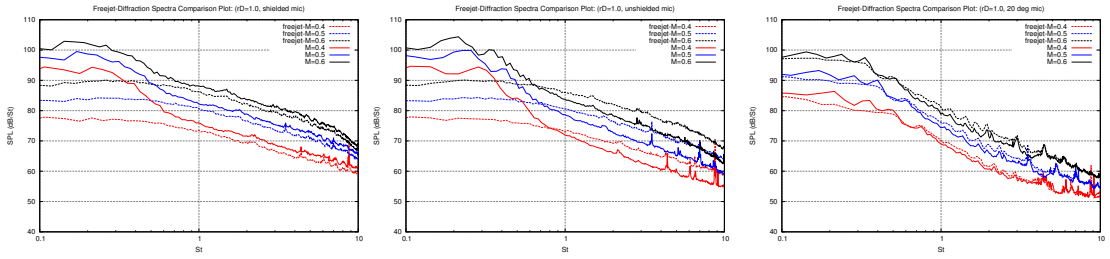

FIGURE 6.20: Freejet/Diffraction-case Spectra (vs. **St**) comparison for each microphone and parametric Mach number. Jet-Plate distance is $\mathbf{r/D = 1.0}$

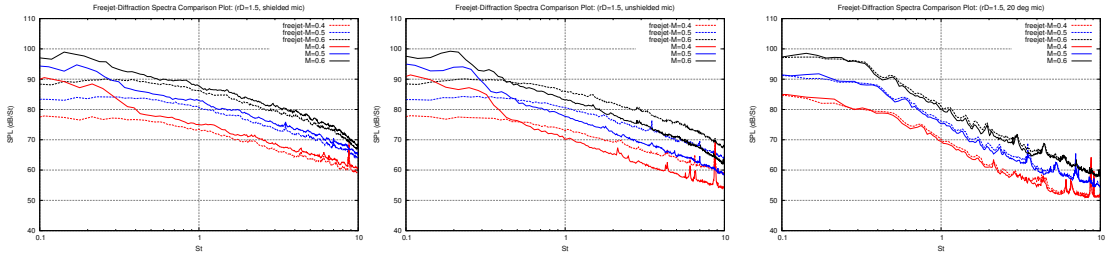

FIGURE 6.21: Freejet/Diffraction-case Spectra (vs. **St**) comparison for each microphone and parametric Mach number. Jet-Plate distance is $\mathbf{r/D = 1.5}$

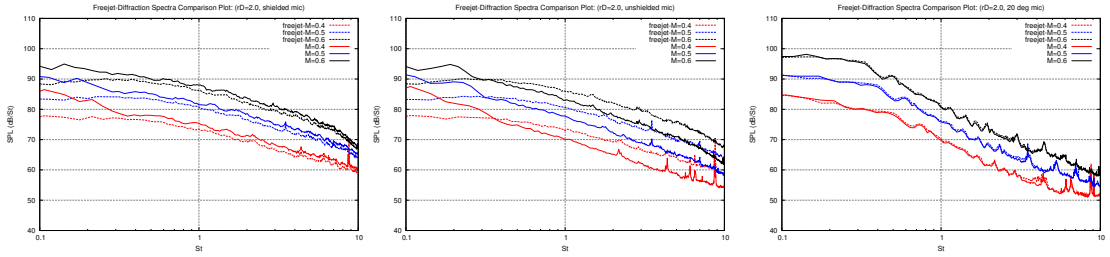

FIGURE 6.22: Freejet/Diffraction-case Spectra (vs. **St**) comparison for each microphone and parametric Mach number. Jet-Plate distance is $\mathbf{r/D = 2.0}$

Again, as in the graphs of the previously reported case, the first set of plots made, considers the SPL $[dB/St]$ plotted versus St number, while the second set of plots has been rescaled and plotted towards He number (compare Figures 6.20, 6.21, 6.22 and Figures 6.23, 6.24, 6.25 respectively).

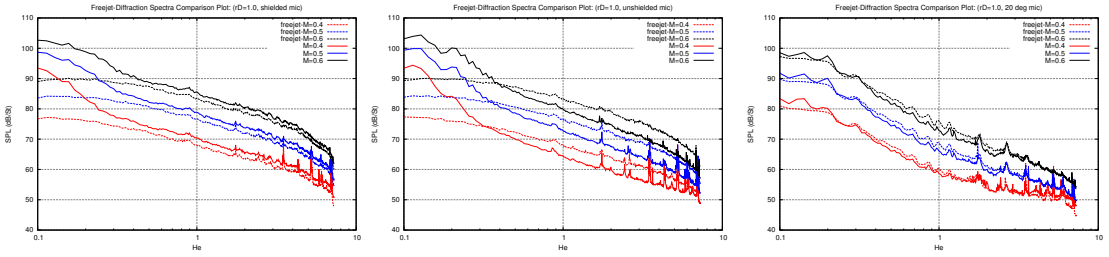

FIGURE 6.23: Freejet/Diffraction-case Spectra (vs. **He**) comparison for each microphone and parametric Mach number. Jet-Plate distance is $\mathbf{r/D = 1.0}$

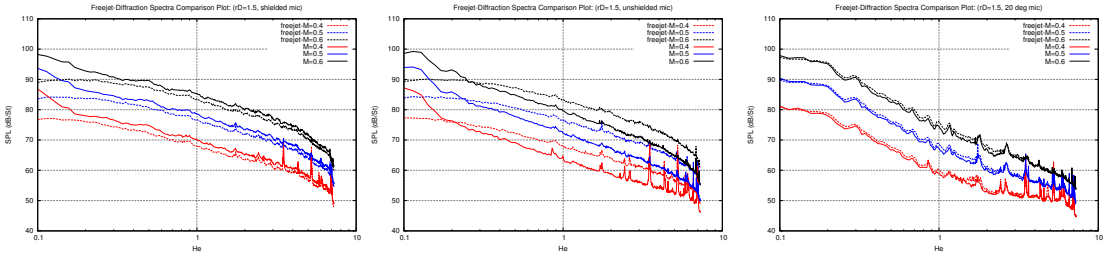

FIGURE 6.24: Freejet/Diffraction-case Spectra (vs. **He**) comparison for each microphone and parametric Mach number. Jet-Plate distance is $\mathbf{r/D = 1.5}$

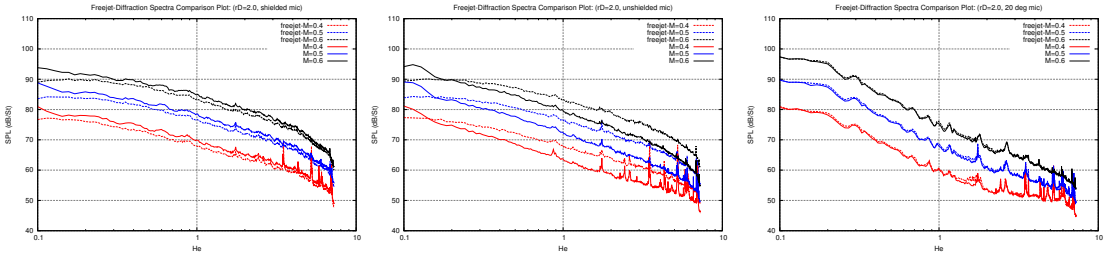

FIGURE 6.25: Freejet/Diffraction-case Spectra (vs. **He**) comparison for each microphone and parametric Mach number. Jet-Plate distance is $\mathbf{r/D = 2.0}$

6.3.6 Spectra comparison plots (full tested Mach range: $M = (0.35..0.60)$)

In the next page are reported all the plots for the full range of tested Mach numbers. These can give useful information when assessing the **variability of the spectra** for a given fixed plate position.

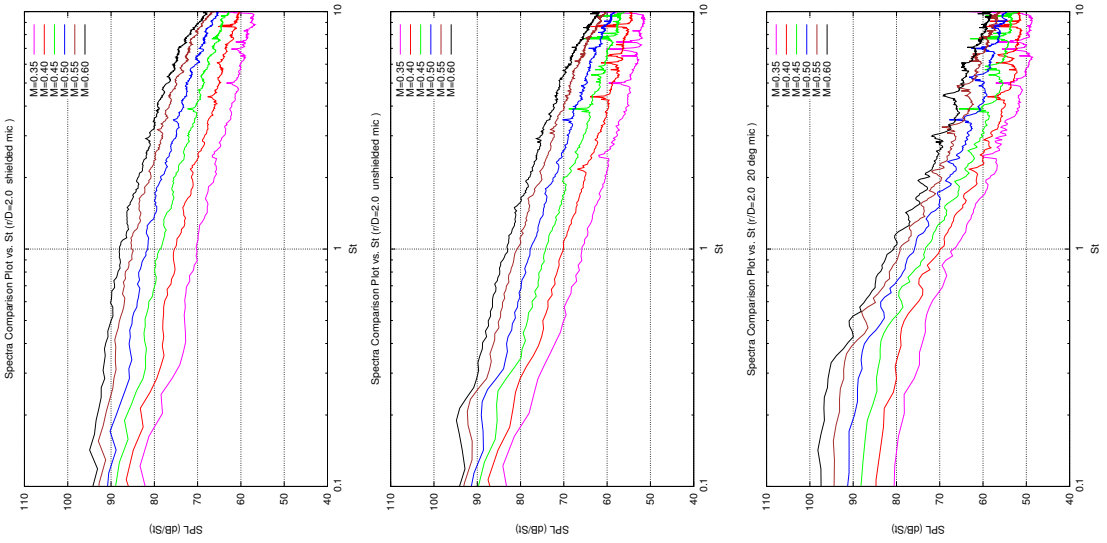

FIGURE 6.26: Spectra comparison plot for parametrical Mach number $(0.35 \div 0.60)$ for each microphone in the relative position jet-plate of $\mathbf{r/D = 2.0}$

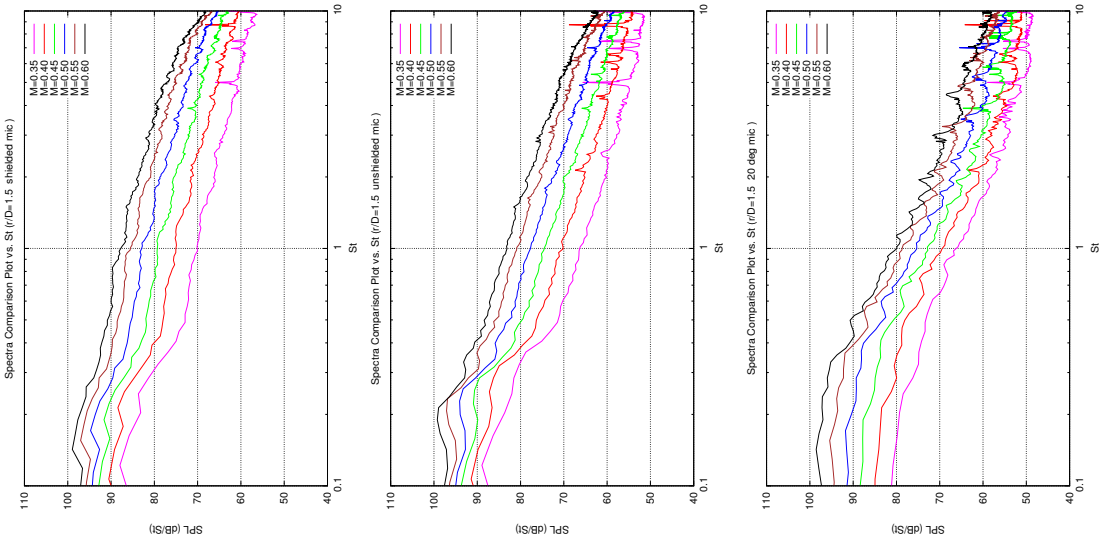

FIGURE 6.27: Spectra comparison plot for parametrical Mach number $(0.35 \div 0.60)$ for each microphone in the relative position jet-plate of $\mathbf{r/D = 1.5}$

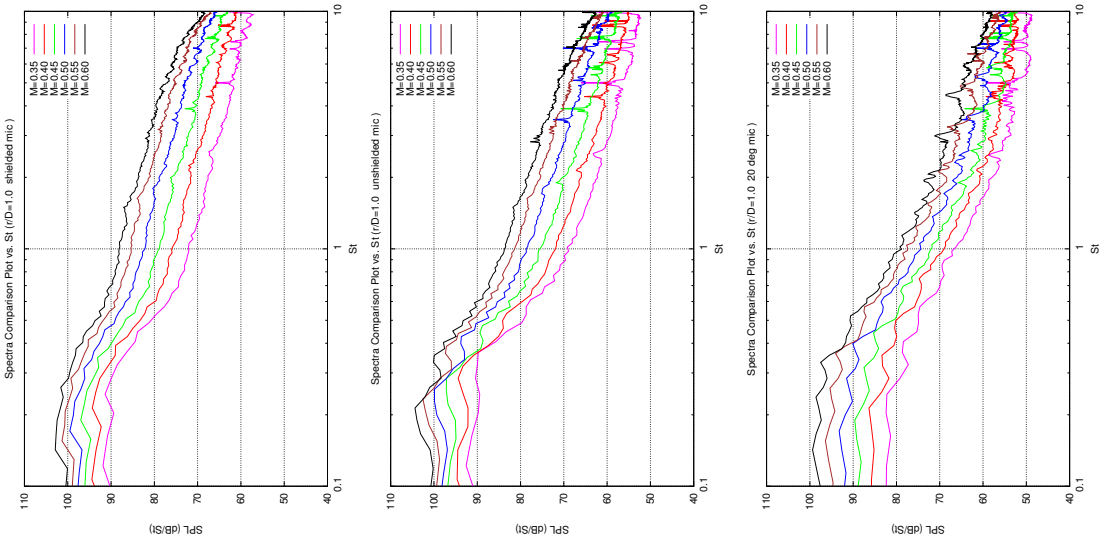

FIGURE 6.28: Spectra comparison plot for parametrical Mach number $(0.35 \div 0.60)$ for each microphone in the relative position jet-plate of $\mathbf{r/D = 1.0}$

6.4 Observations on Spectra Comparison Plots

In this paragraph Figures 6.26, 6.27 and 6.28 have been qualitatively analyzed, and the spectra of all the three microphones have been compared, for the whole range of Mach numbers for which there were sufficient available data (i.e. $M = [0.35 \div 0.60]$ with a step of $\Delta M = 0.05$). Graphs have been superimposed for the various analysis cases, at different r/D positions, in order to take a look at the **effects of the plate displacement**.

The observations reported hereunder could lead to useful considerations about the **interference of the refracted/reflected fields** with the one directly emitted by the main source. The following observations have been made with the help of the commercial software *Photoshop*© by super-positioning the previous considered images and analyzing them altogether, in the same graph, for the same microphone case considered.

6.4.1 Shielded Microphone He-Spectra Comparison

1. **Comparison between r/D = 1.0 and r/D = 1.5**:
   - for $M = 0.40 \div 0.60$ and at $He \approx 0.45$ **diminishing** spectra ($He = [0.10 \div 0.45]$)
   - for $M = 0.35$ and at $He \approx 0.50$ **diminishing** spectra ($He = [0.10 \div 0.50]$)
   - for $He > 1$ spectra **perfectly overlaps for every Mach number** evaluated ($M = 0.35 \div 0.60$)
   - for $M = 0.35$ the spectrum is still **lower** than that at $r/D = 10$ and presents also an **attenuation** for $He > 0.45$
   - there seems to appear an **attenuation structure** for each Mach number evaluated, located in the range: $He = [0.55\,;0.75]$
   - there seems to appear an **amplification structure** for each Mach number evaluated, located in the range: $He = [0.45\,;0.55]$
2. **Comparison between r/D = 1.5 and r/D = 2.0**:
   - there is a **perfect spectra overlap** for $He > 0.8$
   - for $M = 0.35 \div 0.55$ there is a **first attenuation structure** for the range: $He = [0.35\,;0.45]$ while for $M = 0.6$ there is **no evidence** of this feature
   - there is evidence of a **second attenuation structure** for all Mach values studied and within the approximate range: $He = [0.42\,;0.55]$

- there is an **amplification structure** visible for each Mach value in the following He range: $He = [0.55\,;0.70]$

3. **Comparison between r/D = 1.0 and r/D = 2.0**:

   - there is a **perfect match/overlap** between the spectra of the following Mach case $M = 0.45 \div 0.60$) for $He > 1$, while there is still **some attenuation** for Mach values of $M = 0.35$ and $M = 0.40$

6.4.2 Unshielded Microphone He-Spectra Comparison

1. **Comparison between r/D = 1.0 and r/D = 1.5**:

   - for $M = [0.45, 0.55, 0.60]$, at $He > 0.9$ there is **overlapping** between similar spectra profiles
   - for $M = [0.35, 0.40, 0.50]$, at $He > 0.9$ there is **attenuation** for the $r/D = 1.5$ profile.
   - for $He = (0.1 \div 0.9)$ there is a **bigger attenuation** for all Mach numbers

2. **Comparison between r/D = 1.5 and r/D = 2.0**:

   - for $He > 0.5$ spectra **overlaps for all Mach numbers** spectra
   - for $He < 0.5$ there is an **attenuation for all Mach numbers** spectra
   - for $He < 0.25$ there is **bigger attenuation for all Mach numbers** spectra

3. **Comparison between r/D = 1.0 and r/D = 2.0**:

   - for $M = [0.55, 0.60]$, at $He > 1.0$ spectra **overlaps well**
   - for $M = [0.35, 0.40, 0.45, 0.50]$, at $He > 1.0$ spectra show **decreasing attenuation as Mach number increases**
   - for $He < 0.8$ there is a **bigger attenuation for all Mach numbers** spectra

6.4.3 20 deg. Microphone He-Spectra Comparison

1. **Comparison between r/D = 1.0 and r/D = 1.5**:

   - for $He < 0.35$ there is **attenuation for every Mach number** but it seems to be **greater** for the following values: $M = [0.35, 0.40]$
   - for $He = [0.35 \div 1.5]$ and for $M = [0.35, 0.40, 0.45]$ there seems to be a **little amplification** (with **lower values** of $\Delta dB/St$ for $M = 0.35$ and $M = 0.40$)

- for $He = [0.35 \div 2.5]$ and for $M = [0.50, 0.55, 0.60]$ there seems to be a **little amplification** (with **higher values** of $\Delta dB/St$ for $M = 0.45$ and $M = 0.60$)

2. **Comparison between r/D = 1.5 and r/D = 2.0**:

   - for $He < 0.2$ there is a **very low attenuation** for the range $Ma = [0.45 \div 0.60]$ and especially for **higher Mach numbers**
   - for $He = [0.2 \div 1.2]$ approximately, and $M = [0.35, 0.40, 0.45]$ there is a **low amplification**
   - for $He > 2$ the same **little amplification** is for $M > 0.45$
   - for $He = [1.2 \div 1.8]$ approximately, there is **attenuation** in the spectra for $M = [0.35, 0.40]$

3. **Comparison between r/D = 1.0 and r/D = 2.0**:

   - there is a **visible attenuation** for $He < 0.3$
   - there is an **increasing amplification with increasing Mach number**
   - there is an **attenuation zone** for $He = [1.2 \div 1.8]$ approximately and $M = 0.35$ and in the broader range $He = [1.2 \div 8]$ for $M = 0.40$

6.5 Coherence plots

In this paragraph are presented some plots of the **coherence** between the various microphone signals and the usual **parameter variational analysis** is made in order to assess, at least qualitatively, the effects of both, **Mach number variation** and the **jet-plate relative position change**.

6.5.1 First Coherence plots set: M dependencies

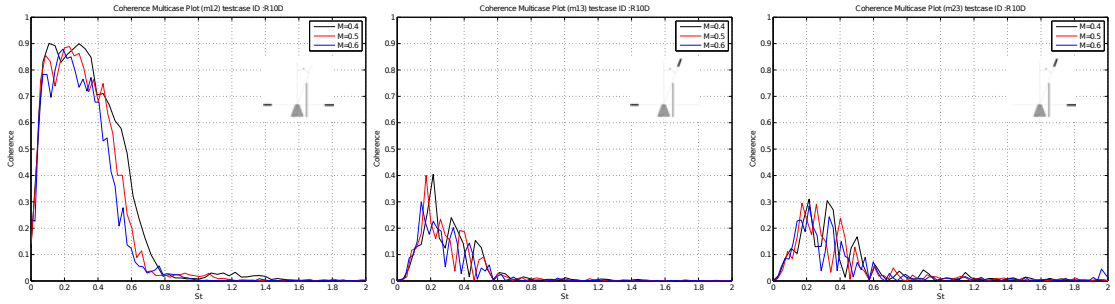

FIGURE 6.29: Coherence comparison plots (vs. **St**) between all mics. for parametric Mach number and for plate positions $\boldsymbol{r/D = 1.0}$

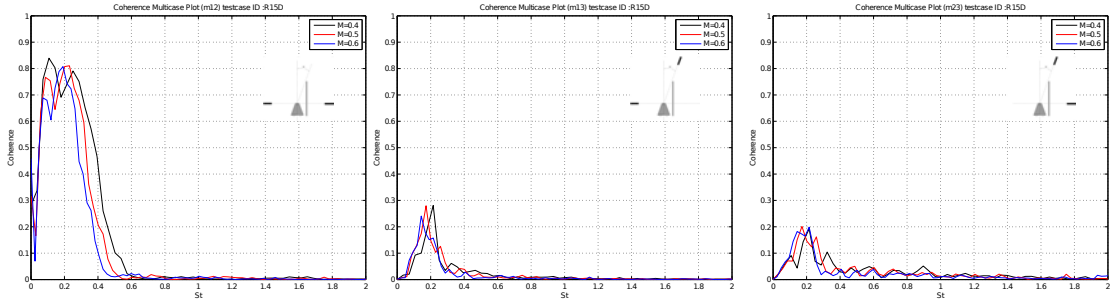

FIGURE 6.30: Coherence comparison plots (vs. **St**) between all mics. for parametric Mach number and for plate positions $\boldsymbol{r/D = 1.5}$

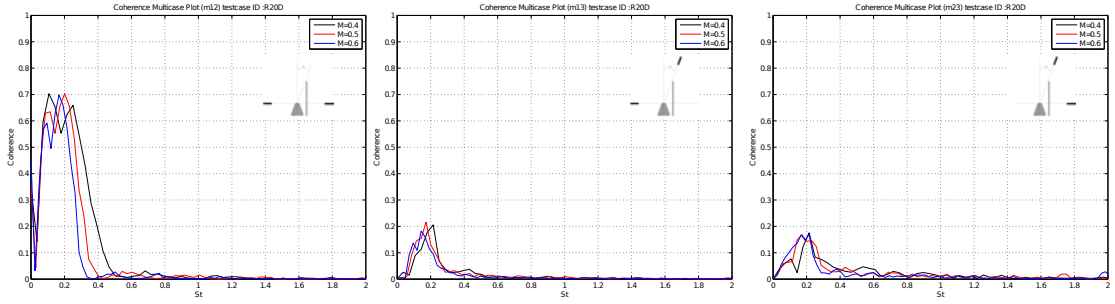

FIGURE 6.31: Coherence comparison plots (vs. **St**) between all mics. for parametric Mach number and for plate positions $\boldsymbol{r/D = 2.0}$

Here, the first coherence plot of each row of Figure 6.29, 6.30 and 6.31 has been used as usual to **evaluate and test** the *Matlab*© code that I wrote, by directly comparing these obtained graphs with the ones in Ref. [**33**].

New plots for the coherence, respectively between mics.#1-#3 and mics.#2-#3, have been made here and added to those reported in the cited article by the author (i.e. those for the coherence between mics.#1-#2). These plots are then all considered for the variation of all the three available *jet-plate relative position* and for *parametrical values of the Mach number*, as well.

In Figure 6.32 are reported the *possible microphones combinations* considered in the coherence computations; these three cases are named for shortness **Cohe12**, **Cohe13** and **Cohe23**.

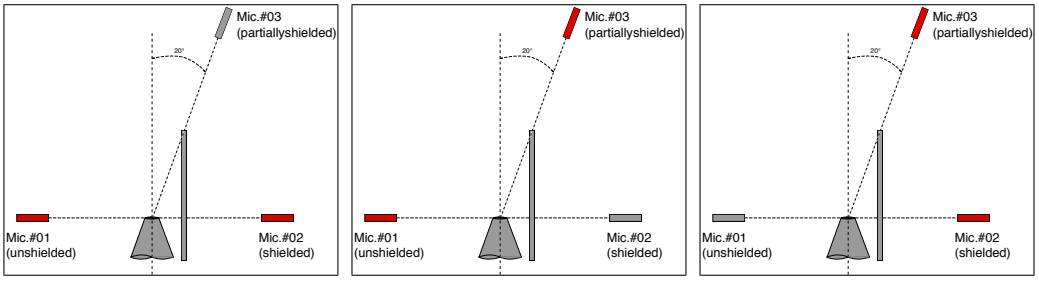

FIGURE 6.32: Combinations of microphones considered for the coherence calculations.

Observations:

As can be seen from Figures 6.29 through 6.31, it is possible to note an **overall decrease** in the coherence between microphone signals if the plate distance r/D is increased, passing from the lowest to the highest value respectively, for each combination of microphones. These are for the three coherence cases, respectively:

- **Cohe12**: $\gamma^2 \approx 0.9$ to $\gamma^2 \approx 0.8$ and then to $\gamma^2 \approx 0.7$
- **Cohe13**: $\gamma^2 \approx 0.4$ to $\gamma^2 \approx 0.3$ and then to $\gamma^2 \approx 0.2$
- **Cohe23**: $\gamma^2 \approx 0.3$ to $\gamma^2 \approx 0.2$ and then to $\gamma^2 \approx 0.15$

Not only the values of the **coherence decrease with increasing r/D** but also the **St range of interested frequencies seems to diminish respectively for the three cases**.

In fact, taking $\gamma^2 = 0$ as a reference value, the *high-coherency frequency band* can be seen to diminish, respectively for the three cases:

- **Cohe12**: from $St = [0.0 \div 0.8]$ to $St = [0.0 \div 0.6]$, then again to $St = [0.0 \div 0.5]$
- **Cohe13**: from $St = [0.0 \div 0.6]$ to $St = [0.0 \div 0.4]$, then again to $St = [0.0 \div 0.3]$
- **Cohe23**: from $St = [0.0 \div 0.5]$ to $St = [0.0 \div 0.3]$, then again to $St = [0.0 \div 0.2]$

Also the $St = 0.2$ **high coherency peak** seems to be quite a *constant feature* for the cases **Cohe13** and **Cohe23**, while for the case **Cohe12** there seem to be **two high coherency peaks** at $St = 0.1$ & $St = 0.3$, rather than only one at $St = 0.2$.

6.5.2 Second Coherence plots set: r/D dependencies

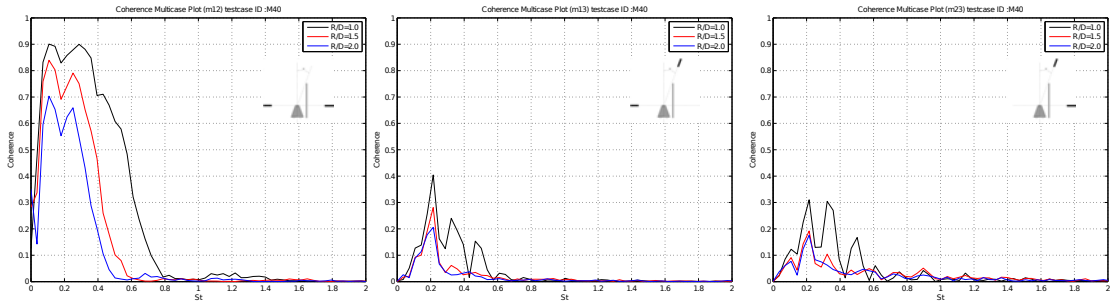

FIGURE 6.33: Coherence comparison plots (vs. **St**) between all mics. for parametric plate positions and fixed Mach number **($M = 0.4$)**

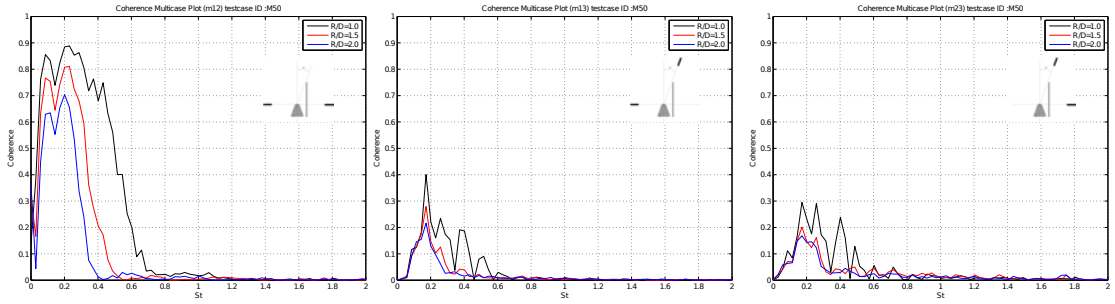

FIGURE 6.34: Coherence comparison plots (vs. **St**) between all mics. for parametric plate positions and fixed Mach number **($M = 0.5$)**

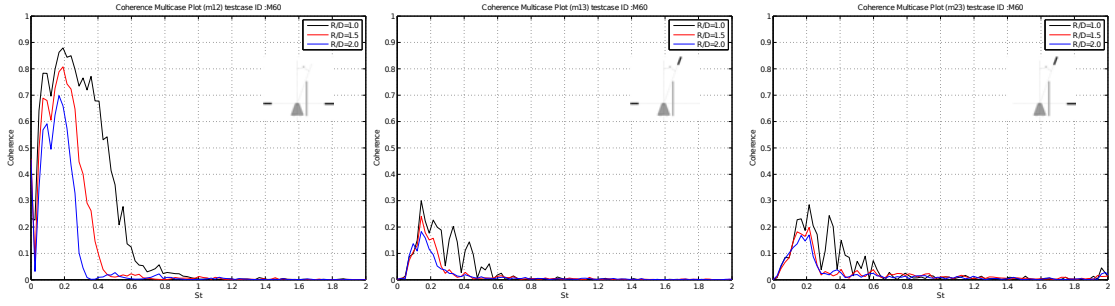

FIGURE 6.35: Coherence comparison plots (vs. **St**) between all mics. for parametric plate positions and fixed Mach number **($M = 0.6$)**

Observations:

It can be seen from the plots above that for the following three cases:

- **Cohe12**: to an **increase of the plate distance** from the jet, corresponds a **decrease in the coherence value (amplitude peak)** for all the three studied Mach numbers, as well as to a **narrowing of the band of frequencies of interest**.
- **Cohe13**: coherence **curves are quite overlapped** especially the ones for $r/D = [1.5\,;\,2.0]$ while the curve for $r/D = 1.0$ present **more peaked features** in the range $St = [0.2 \div 0.6]$; the **max coherency peak** at $St = 0.2$ seems to **diminish sensibly** passing from the $M = [0.4\,;\,0.5]$ case to the last value of the Mach number, with a **little shift** towards $St = 0.1$ for the last two cases of Mach. **No narrowing of the band of frequencies of interest** seems to occur.
- **Cohe23**: again, coherence **curves are quite overlapped** especially the ones for $r/D = [1.5\,;\,2.0]$ while the curve for $r/D = 1.0$ present **more peaked features** in the range $St = [0.2 \div 0.4]$. Also in this case there is a **little shift** towards $St = 0.1$ for the case $r/D = 1.0$ **max coherency peak**, that tend though to settle back again in the last Mach value case.

6.5.3 Third Coherence plots set

This last set of graphs is just a recap to see in one single plot all the values of γ^2 for all the three combinations of microphones (**Cohe12**, **Cohe13**, **Cohe23**).

Refer to Figure 6.32 for a quick legend of the coherence case considered).

- Each *row* reports a **given and fixed value** of the parameter $\mathbf{r/D}$.
- Each *column* reports a **given and fixed value** of the Mach number **M**.

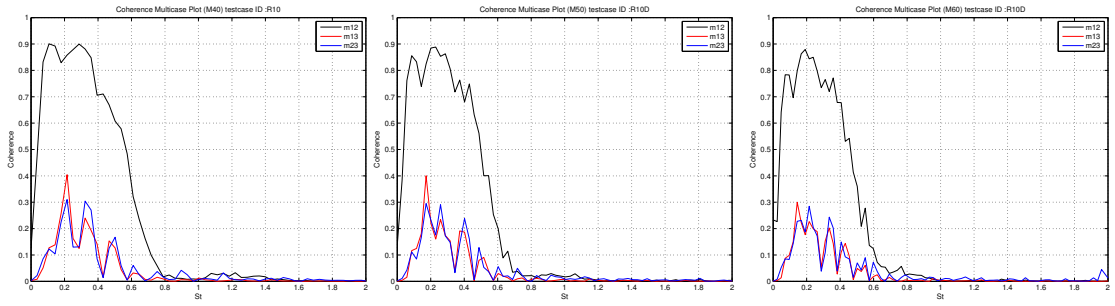

FIGURE 6.36: Coherence comparison plots (vs. St) for fixed plate position $\boldsymbol{r/D = 1.0}$ parametric (i, j) mics. combination and variable Mach number

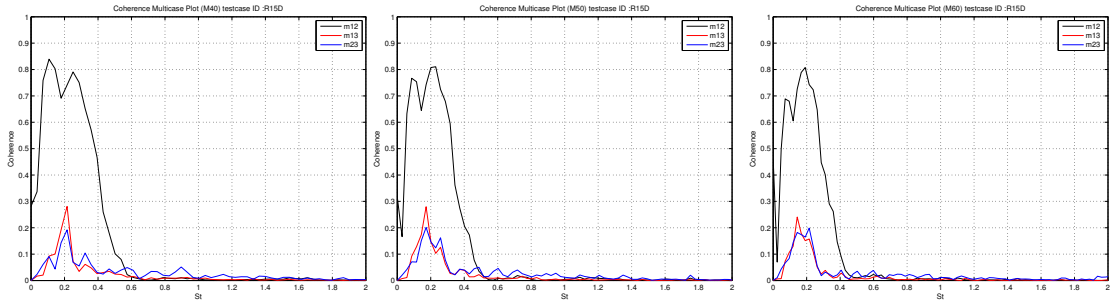

FIGURE 6.37: Coherence comparison plots (vs. St) for fixed plate position $\boldsymbol{r/D = 1.5}$ parametric (i, j) mics. combination and variable Mach number

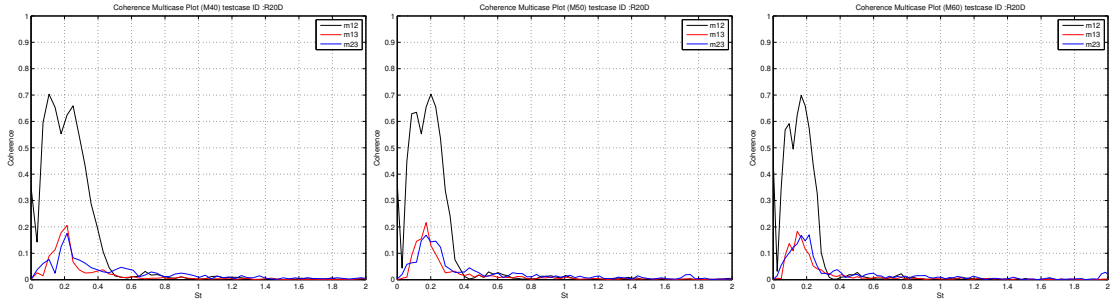

FIGURE 6.38: Coherence comparison plots (vs. St) for fixed plate position $\boldsymbol{r/D = 2.0}$ parametric (i, j) mics. combination and variable Mach number

6.6 Velocity Trend Plots

This paragraph deals with **velocity trend laws identification**;

Post-processed data trends have been sought in order to **inform and validate current theories of aerodynamic noise** - that consider *reflexion, refraction, diffraction and scattering phenomena due to the presence of solid boundaries* - based on the original Lighthill's **acoustics analogy** and on its later extended forms, as reported in Chapter 2.

Here are presented some **preliminary results** for the **velocity exponent trends**, as analyzed.

In Figures 6.39, 6.40 and 6.41 are shown the plots used for the SPL **data fit analysis** for each microphone at $St = 0.2$ and at different values of r/D; while in the subsequent Figures 6.42 through 6.44, are reported the plots used for the **velocity exponent trend identification**.

Always in Figures 6.42, 6.43 and 6.44 a **graphic comparison** has been made between *experimental data points* and the *fitted curves*, respectively calculated for $\mathbf{u^6}$ and $\mathbf{u^8}$.

The main results are those for $\mathbf{St = 0.2}$ reported in the first set of mentioned figures, but for completeness purposes, also the other calculated plots are reported in the subsequent figures, (respectively for $\mathbf{St = 0.1}$, $\mathbf{St = 0.3}$ and $\mathbf{St = 0.4}$, though these last data sets have yet to be further analyzed).

In Table 6.2 are summarized the **calculated velocity exponents** for the three cases r/D and for each microphone considered.

	$St = 0.2$		
Microphone	$r/D = 1.0$	$r/D = 1.5$	$r/D = 2.0$
shielded $(+90)^\circ$	5.31997	5.93729	6.31156
unshielded $(-90)^\circ$	6.3863	6.93304	7.30791
20 $^\circ$	6.17606	7.44916	7.72558

TABLE 6.2: Velocity exponents discovered by the trends of fitted experimental data.

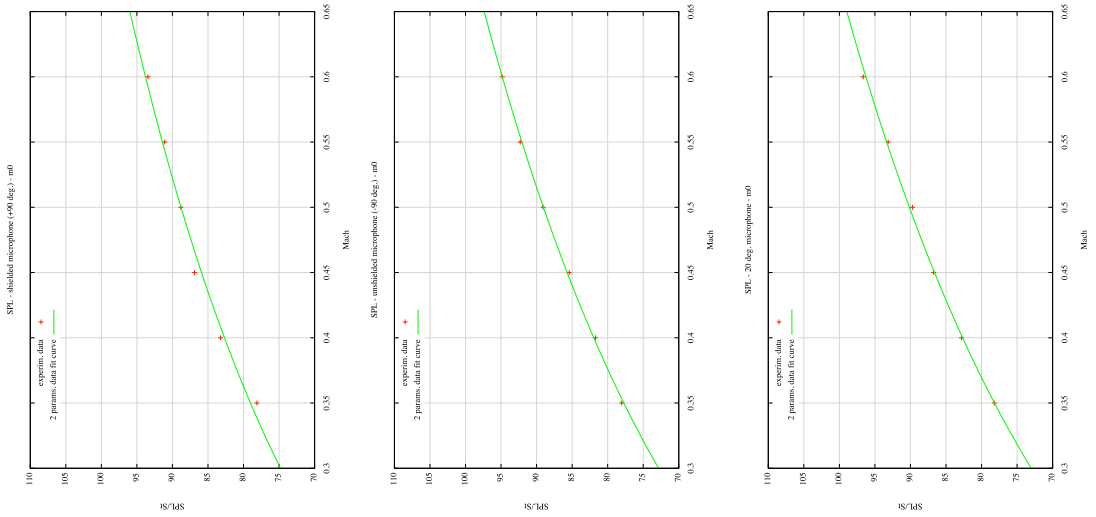

FIGURE 6.39: SPL experimental data & 2-parameters fit plots ($\mathbf{r/D = 2.0}$, $\mathbf{St = 0.2}$)

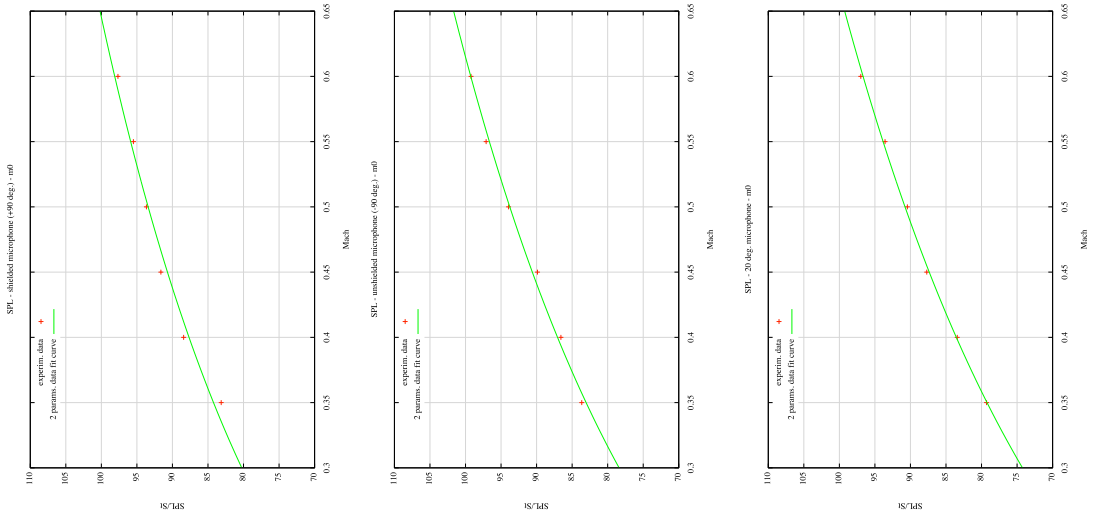

FIGURE 6.40: SPL experimental data & 2-parameters fit plots ($\mathbf{r/D = 1.5}$, $\mathbf{St = 0.2}$)

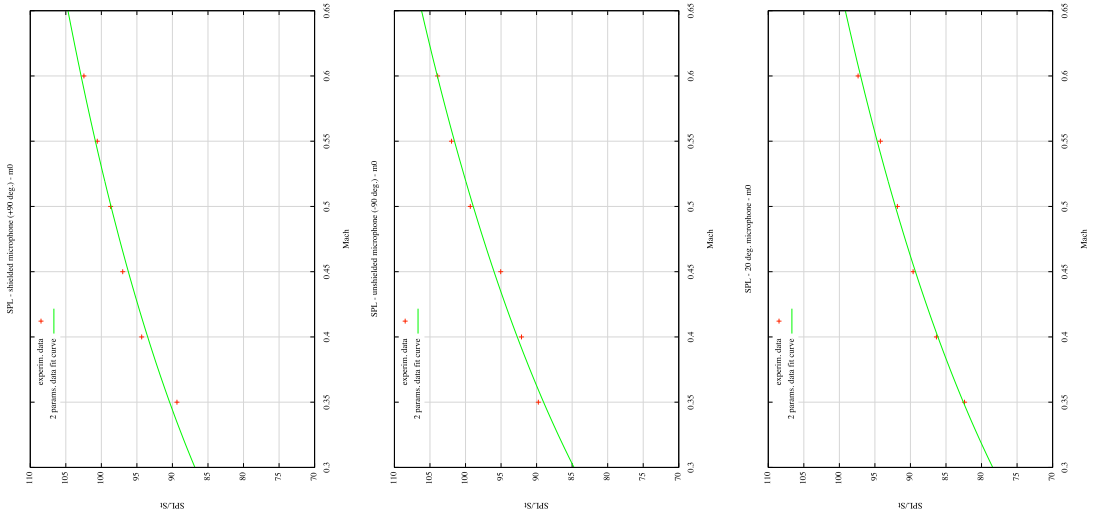

FIGURE 6.41: SPL experimental data & 2-parameters fit plots ($\mathbf{r/D = 1.0}$, $\mathbf{St = 0.2}$)

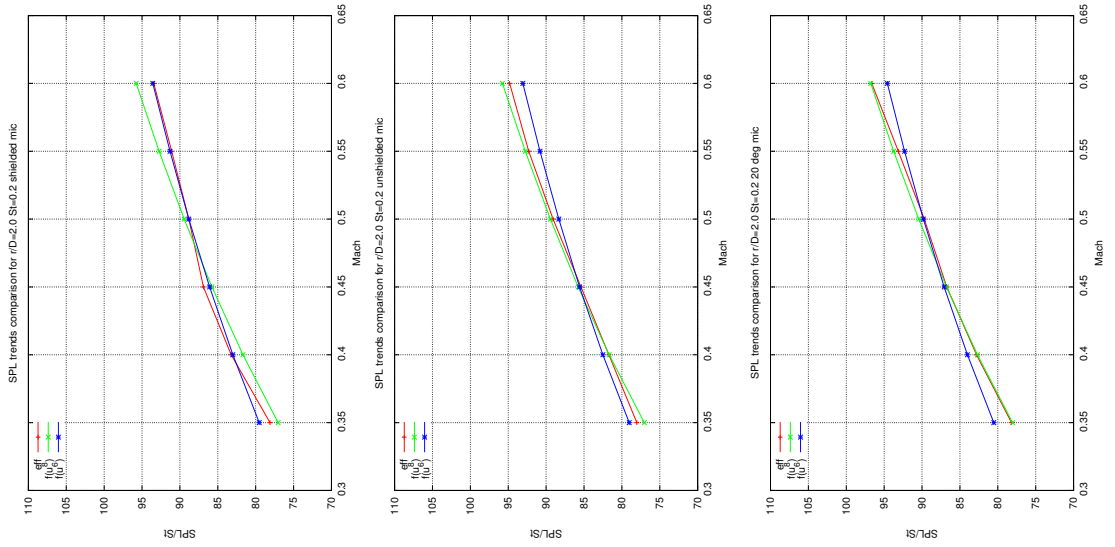

FIGURE 6.42: SPL trend identification & comparison plots ($\mathbf{r/D = 2.0}$, $\mathbf{St = 0.2}$)

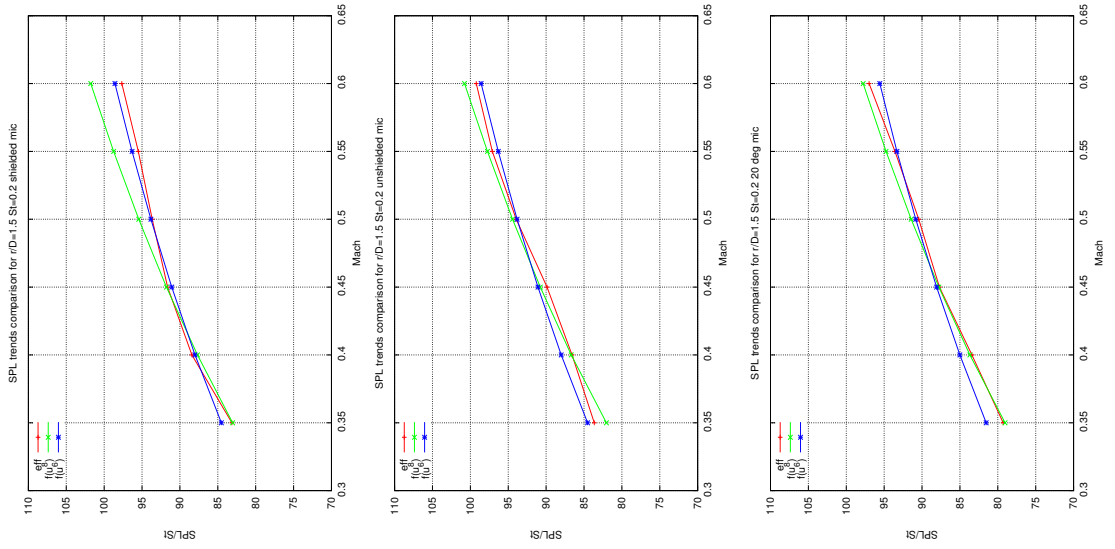

FIGURE 6.43: SPL trend identification & comparison plots ($\mathbf{r/D = 1.5}$, $\mathbf{St = 0.2}$)

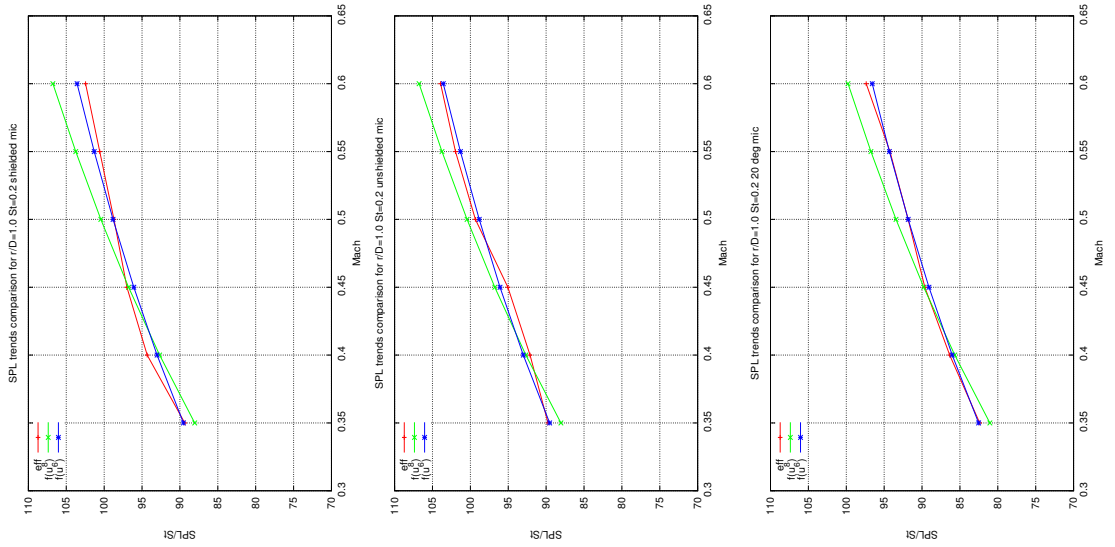

FIGURE 6.44: SPL trend identification & comparison plots ($\mathbf{r/D = 1.0}$, $\mathbf{St = 0.2}$)

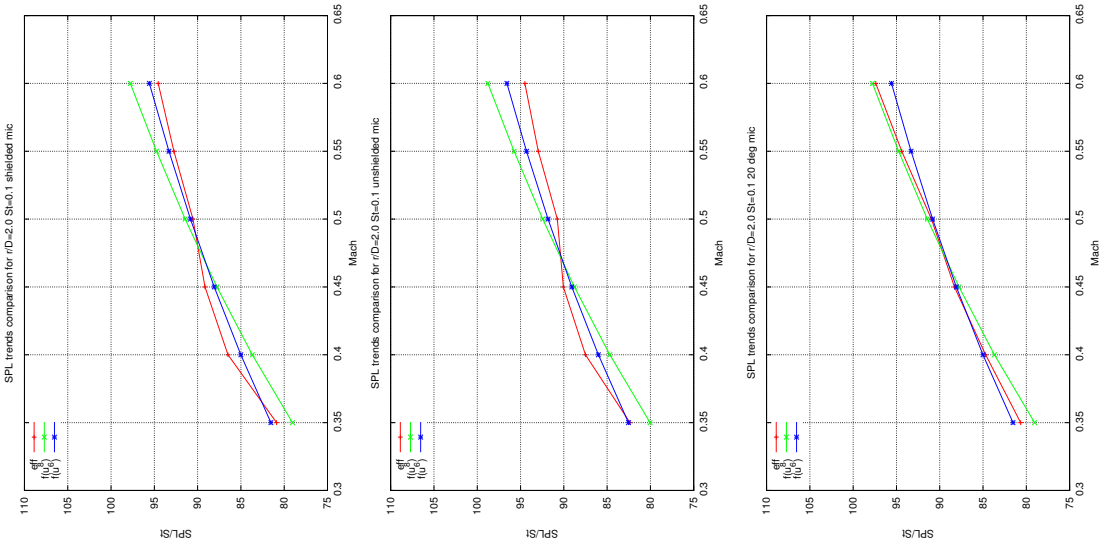

FIGURE 6.45: SPL trend identification & comparison plots ($\mathbf{r/D = 2.0}$, $\mathbf{St = 0.1}$)

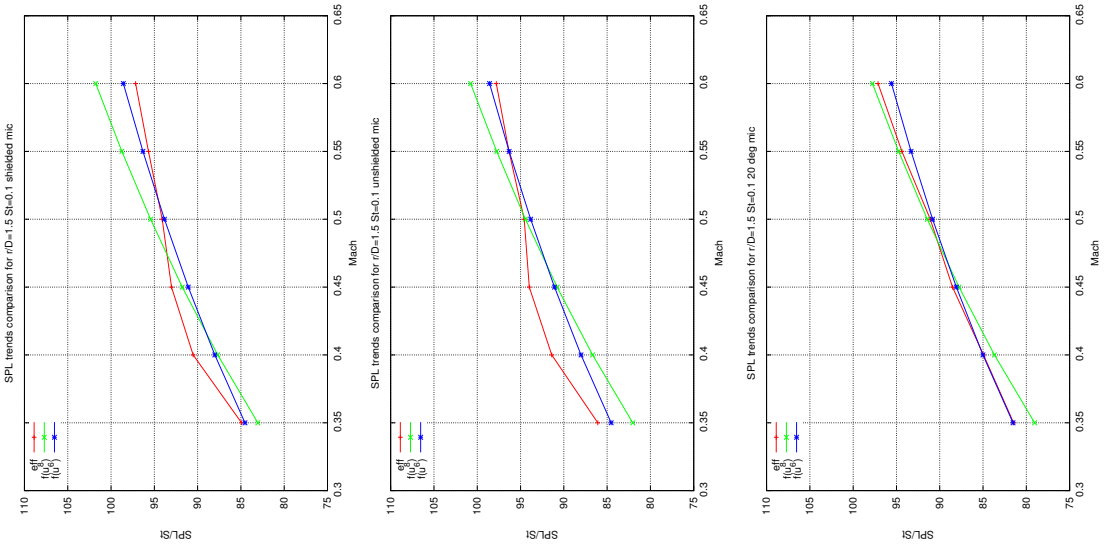

FIGURE 6.46: SPL trend identification & comparison plots ($\mathbf{r/D = 1.5}$, $\mathbf{St = 0.1}$)

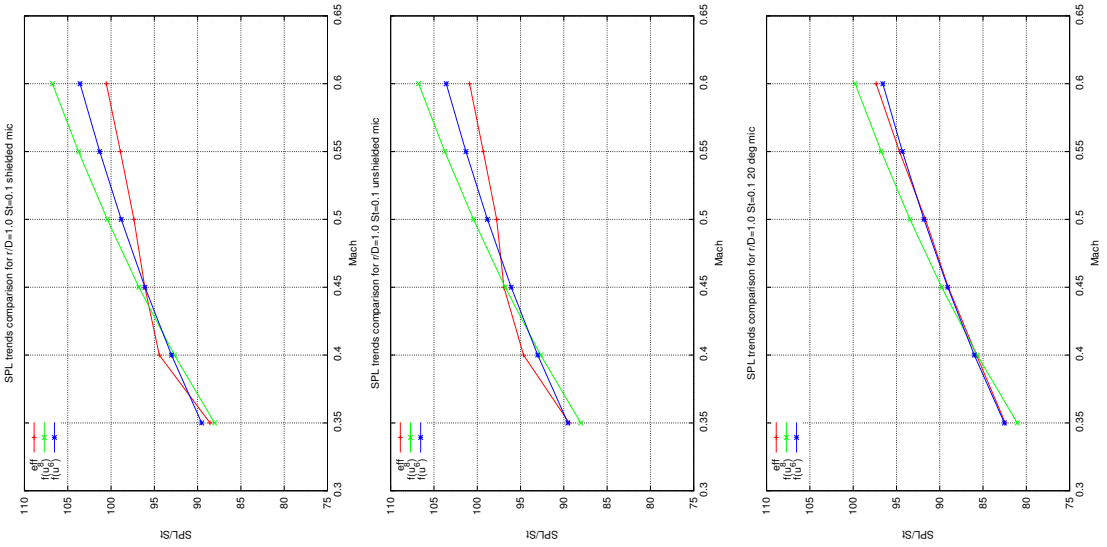

FIGURE 6.47: SPL trend identification & comparison plots ($\mathbf{r/D = 1.0}$, $\mathbf{St = 0.1}$)

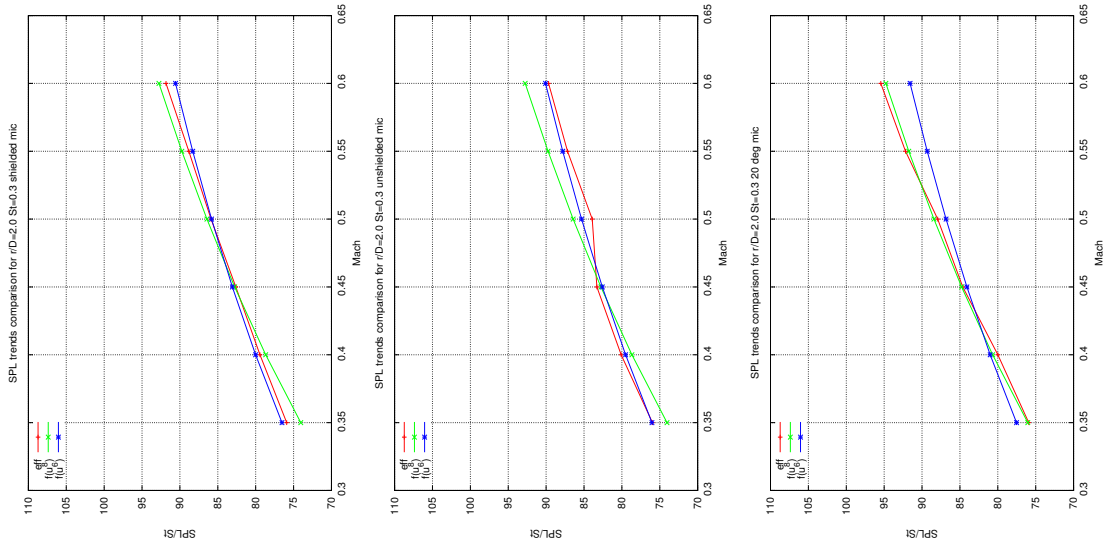

FIGURE 6.48: SPL trend identification & comparison plots ($\mathbf{r/D = 2.0}$, $\mathbf{St = 0.3}$)

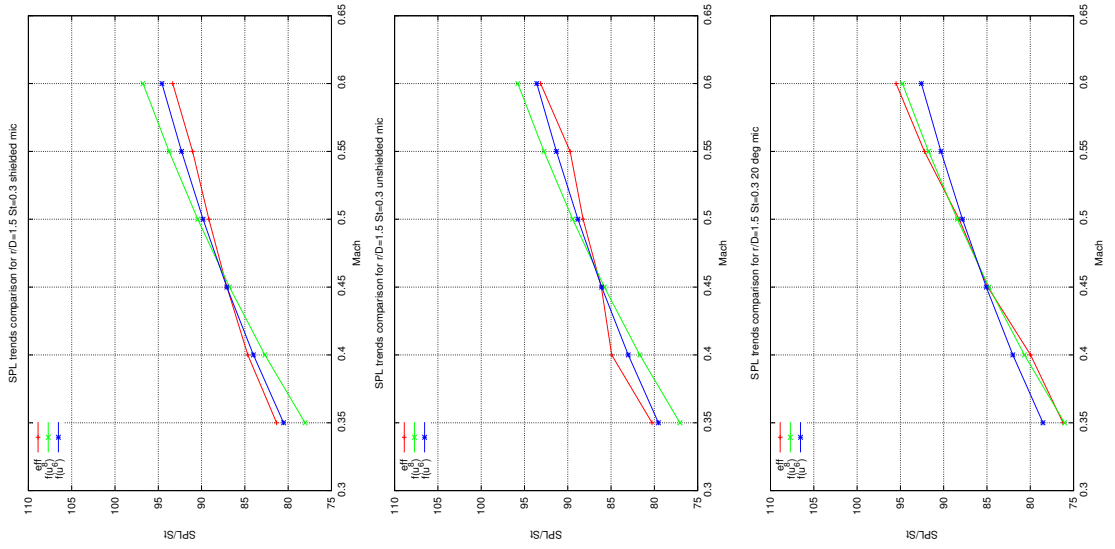

FIGURE 6.49: SPL trend identification & comparison plots ($\mathbf{r/D = 1.5}$, $\mathbf{St = 0.3}$)

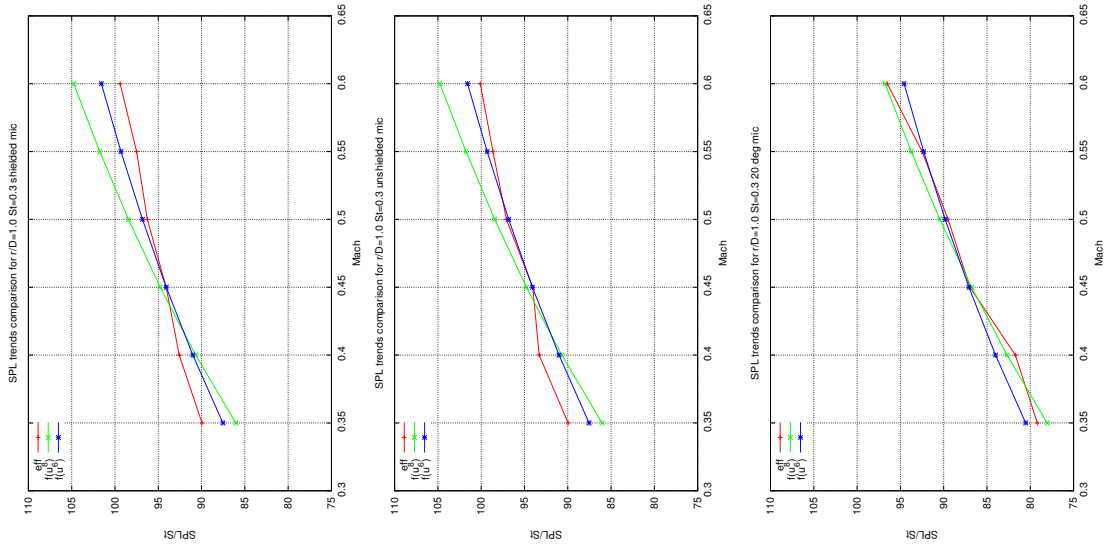

FIGURE 6.50: SPL trend identification & comparison plots ($\mathbf{r/D = 1.0}$, $\mathbf{St = 0.3}$)

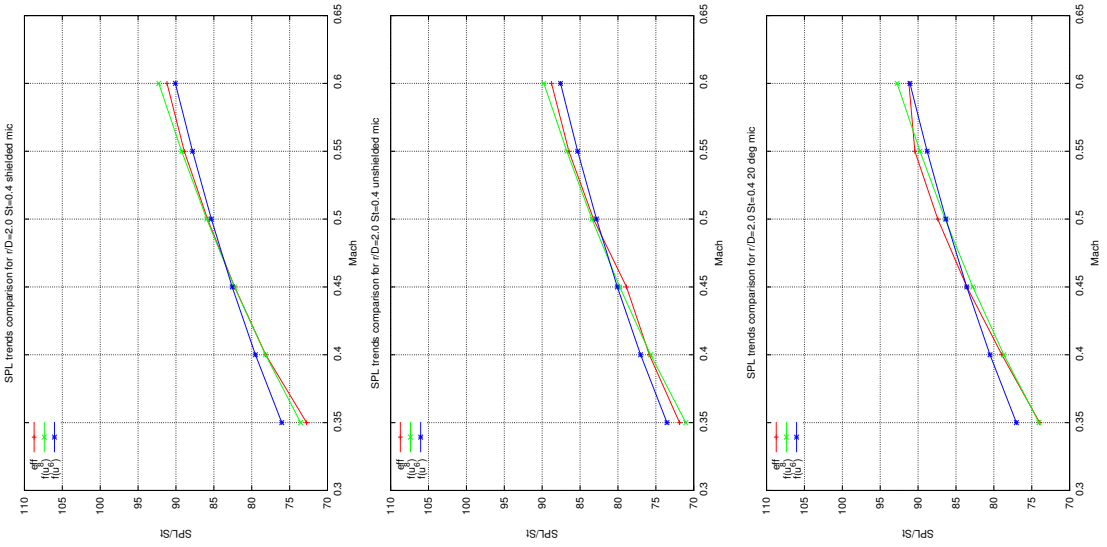

FIGURE 6.51: SPL trend identification & comparison plots ($\mathbf{r/D = 2.0}$, $\mathbf{St = 0.4}$)

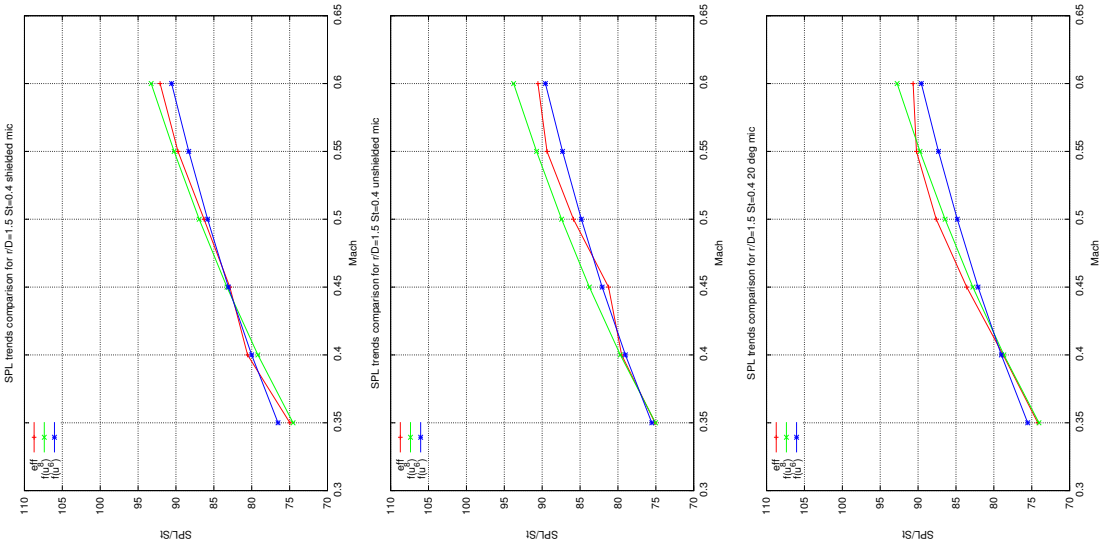

FIGURE 6.52: SPL trend identification & comparison plots ($\mathbf{r/D = 1.5}$, $\mathbf{St = 0.4}$)

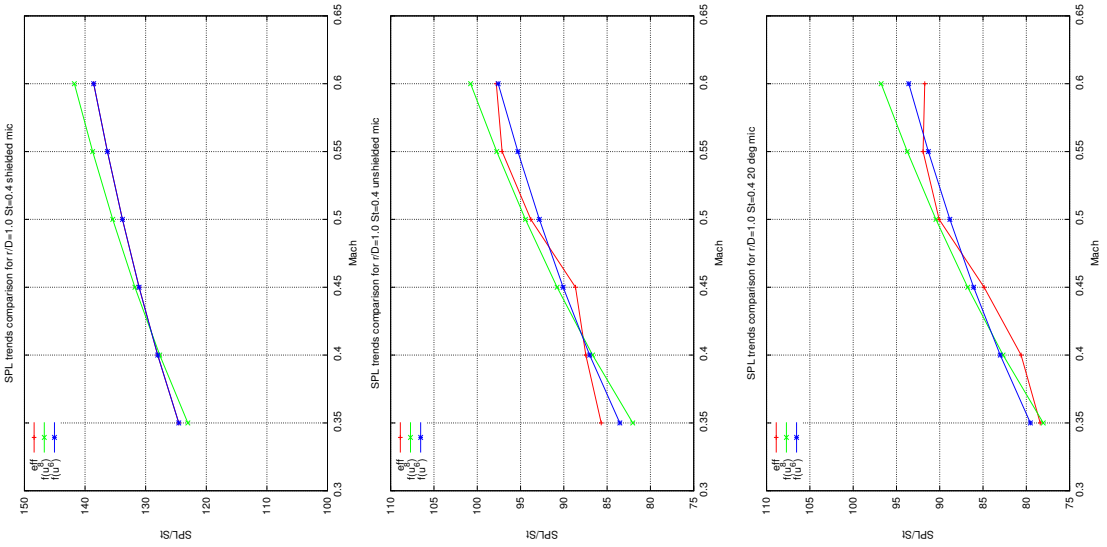

FIGURE 6.53: SPL trend identification & comparison plots ($\mathbf{r/D = 1.0}$, $\mathbf{St = 0.4}$)

6.7 Tweaking & Tuning of the Wave Packets Model Code

In this last section is reported the work done in order to try to model with the wave packets *Fortran*© code written by Dr. A. Cavalieri, the phenomena encountered in the experiments (i.e. the **aeroacoustic scattering and amplification of the jet-noise when a plate that mimics an idealized wing structure is placed in close proximity of the jet exit nozzle**; this is due to what it is supposed to be its primary cause, **sound reflexion and diffraction phenomena**).

6.7.1 Code Sensitivity Analysis: Used Parameter

In order to get acquainted with the code, some variations have been made to the parameters of the original code and noted the output from the model.

The calculation code uses a **modified *Green's function*** (i.e. *specifically tailored for the geometry in use*) in order to take into consideration the presence of the scattering plane in the near field, positioned in close proximity of the jet's exit.

Tweaked, used and modified parameters are the following reported[2]:

- **Reference pressure** : $P_{ref} = 2 \cdot 10^5\ [Pa]$
- **Jet diameter** : $D = 0.05\ [m]$
- **Azimuthal mode** considered [3] : $m = 0$
- **Mach number** : $M = 0.4,\ M = 0.5,\ M = 0.6$
- **Strouhal number** : $St = 0.2$
- **Jet-plate distance** : $r/D = [1.0,\ 1.5,\ 2.0]$
- **Velocity ratio** : $U_c/U = 0.97$
- **number of radial "observers"** : 80
- **number of angular "observers"** : 30
- **"observers" spacing**, $\Delta\theta$: 0.5
- **wave packet configuration**[4]: $K_H L = 6$

[2] Refer to Dr. A. Cavalieri articles Ref. [34] and Ref. [33] and his proprietary code for more insight.
[3] In the absence of azimuthal decomposition data for the sound field of the considered experiment, it has been chosen the axisimmetrical mode ($m = 0$) as the one that gives higher energetic contribute.
[4] This value has been chosen to runs simulations with **non-compact wave packet** characteristics and in accordance with Ref. [33]

6.7.2 Code Sensitivity Analysis: Results & Observations

In the following pages are reported and analyzed the output of the simulations in the following forms:

1. **Cartesian directivity plots** of SPL values plotted against θ, (i.e. jet noise directivity angle with respect to the jet axis) and comparison is made between wave packet-model simulation results (plotted with solid lines) and experimental data (plotted with symbols).
2. **Polar directivity plots** of the pressure fluctuation levels.
3. **Pressure field contour plots** for both the *free-jet* case and the one with the *semi-infinite plate*.

Cartesian directivity plots are an easy way to assess the **directivity of the jet noise**; in fact they permit to see at what angles the SPL levels are higher or lower, for each considered case of relative jet-plate position r/D or jet speed M_j.

Polar directivity plots are the plots of **pressure fluctuation levels** (i.e. of $\overline{p'^2}$ defined in Equations 6.1 and 6.2); this quantity is not expressed in dB but rather in units of pressure. These types of plot give a direct visualization in the bi-dimensional space around the jet of the **directivity pattern** of the scattered quantity.

With these last kind of plots it is very easy to note the difference between the **free-jet** case and the ones that present **diffraction** phenomena, due to the presence of the plate positioned nearby, because of both the changes in *shape* and *magnitude* of the "lobes" of the levels of pressure fluctuations.

$$\left(\overline{p'^2}\right) = p_{ref}^2 \cdot 10^{\left(\frac{dB}{20}\right)} \tag{6.1}$$

$$dB = 20 \cdot log_{10}\left(\frac{p'}{p_{ref}}\right)^2 \tag{6.2}$$

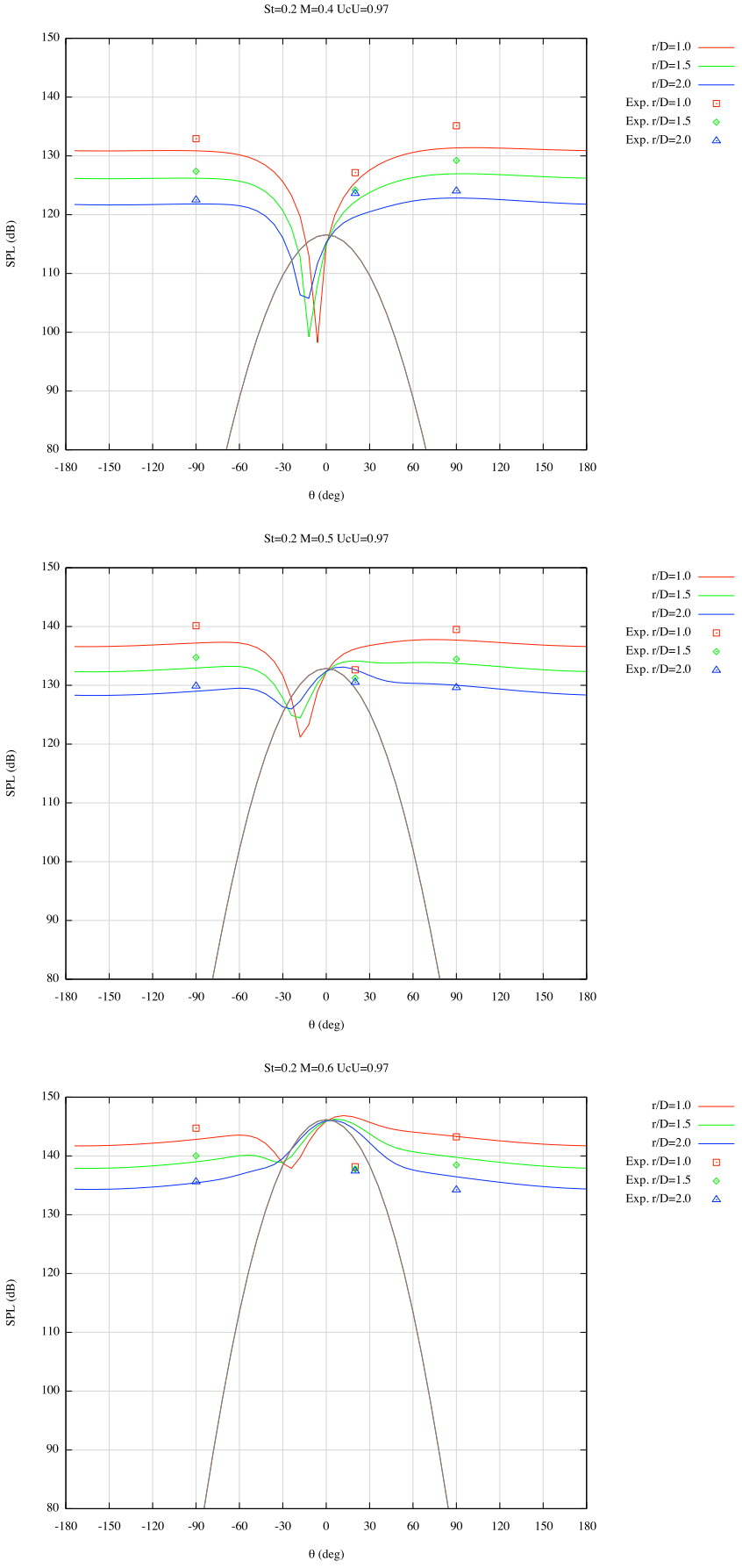

FIGURE 6.54: Cartesian directivity plots; model results and experimental data comparison [$\mathbf{St = 0.2}$, $\mathbf{M = (0.4, 0.5, 0.6)}$, $\mathbf{r/D = (1.0, 1.5, 2.0)}$, $\mathbf{Uc/U = 0.97}$]

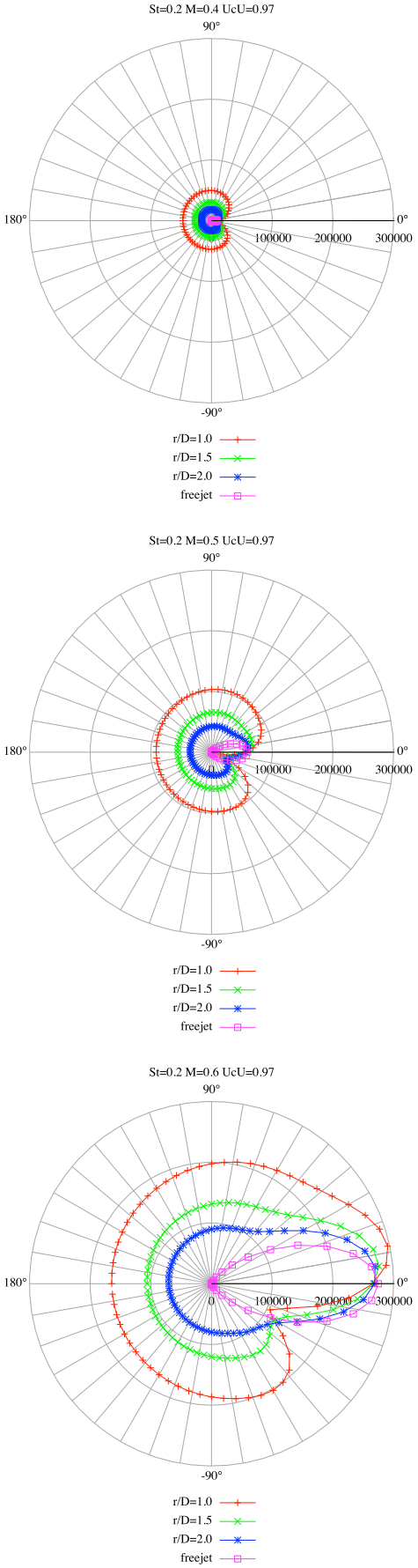

FIGURE 6.55: Polar directivity plots for the pressure fluctuation levels; **results from the model**: **free-jet** and **diffraction** cases.

Observations:

Taking a quick look at Figures 6.54 it is possible to see how the model works (simulation numerical results are plotted in solid lines), in comparison with experimental data (plotted with variable-shape dots).

- In the first graph of Figure 6.54, at $M = 0.4$, the solid curves of the model **underestimate** the experimental data for the two microphones at $\pm 90°$of about $1 \div 3$ $[dB]$ at least, while for the microphone at $20°$ model values are **substantially wrong**.
- In the second graph of Figure 6.54, at $M = 0.5$, the $-90°$ microphone experimental values are **underestimated** approximately as much as the values at $r/D = 1.0$, $r/D = 1.5$ for the $+90°$ microphone, while the value at $r/D = 2.0$ seems to be **correct**; numerical simulation results though, for the microphone at $20°$ seem to be again **all wrong**.
- In the third graph of Figure 6.54, at $M = 0.6$, model results **underestimate** the values for $r/D = 1.0$ and $r/D = 1.5$ for the $-90°$ microphone, while they are in **good agreement** with experimental data at $r/D = 2.0$ for the $-90°$ microphone and the $r/D = 1.0$ case for the $+90°$ microphone. For the last two values of the jet-plate distance though (namely $r/D = 1.5$ and $r/D = 2.0$), the model curves **overestimate** the experimental data for the $+90°$ microphone. Model results are once again **completely wrong** for the $+20°$ microphone as one can see from the figure itself.

It has also to be noted that as in previously mentioned article Ref. [**33**], **comparison** have been made also with the free-jet case that has been simulated by Dr. Cavalieri wave packet model using an **axisymmetric wave packet** with all the parameters fitted for the same jet evaluated, but **without the influence of the plate**.

Analyzing the **pressure field contours** in subsequent figures, obtained for a **wave packet source** as the one shown in Figure 6.56, and comparing the **free-field radiation pattern** with the one obtained by the presence of the **semi-infinite flat plate** positioned at $x < 0$ and respectively at $y = (1.0, 1.5, 2.0\ D)$, it is easy to spot the **differences in the overall pressure distribution**. Moreover, the **effects of the scattering of the of the sound waves far from the jet exit**, are evident by comparing the following graphs:

- Figures 6.57, 6.58, 6.59 for $r/D = 1.0$;

- Figures 6.60, 6.61, 6.62 for $r/D = 1.5$;
- Figures 6.63, 6.64, 6.65 for $r/D = 2.0$.

It is possible to assess the main features of the analyzed and simulated problem, that have already been noticed by the author himself in his paper, Ref. [**33**] and are briefly reported here:

- there is an **expected pressure jump** between the two flat plate sides;
- the radiated sound field, due to scattering is **dispersed in every direction**;
- there is **phase opposition** between the two sides of the plate sideline, as it is possible to tell from the opposite colors of the contour map.

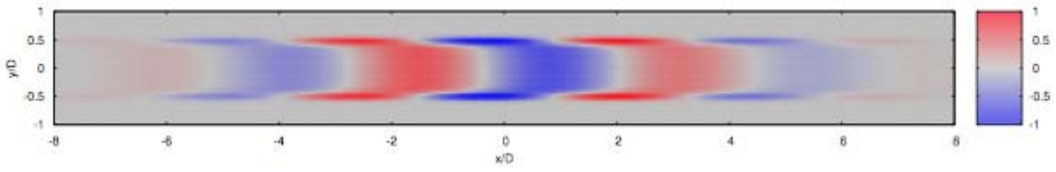

FIGURE 6.56: Wave packet source, shape and its spatial extent.

(This page is intentionally left blank)

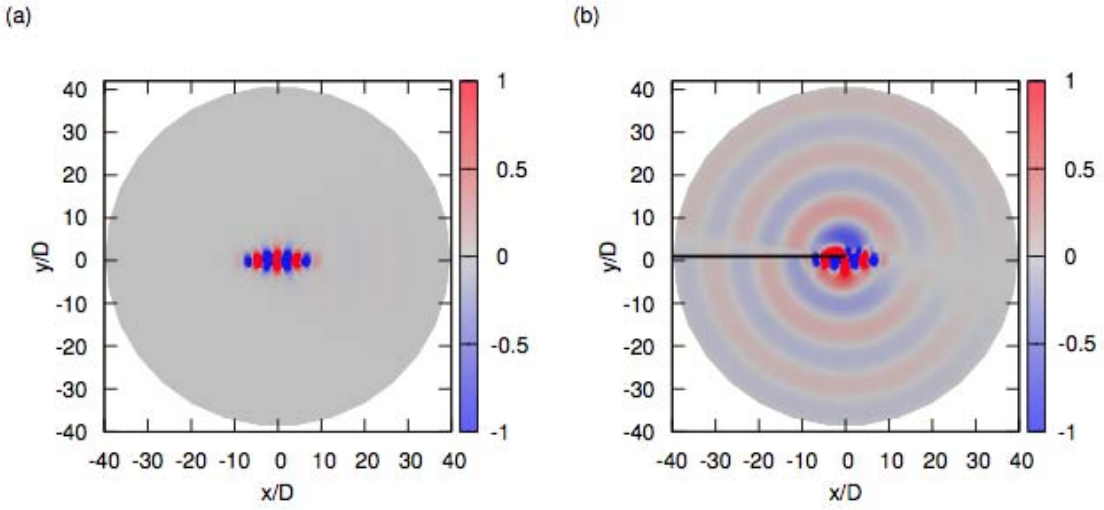

FIGURE 6.57: Pressure fields of a WP source. ($k_H L = 6$, $M = 0.4$, $Uc/U = 0.97\,St = 0.2$) (a) free-field (b) with a semi-infinite flat plate at $x < 0$, $y = 1.0\,D$

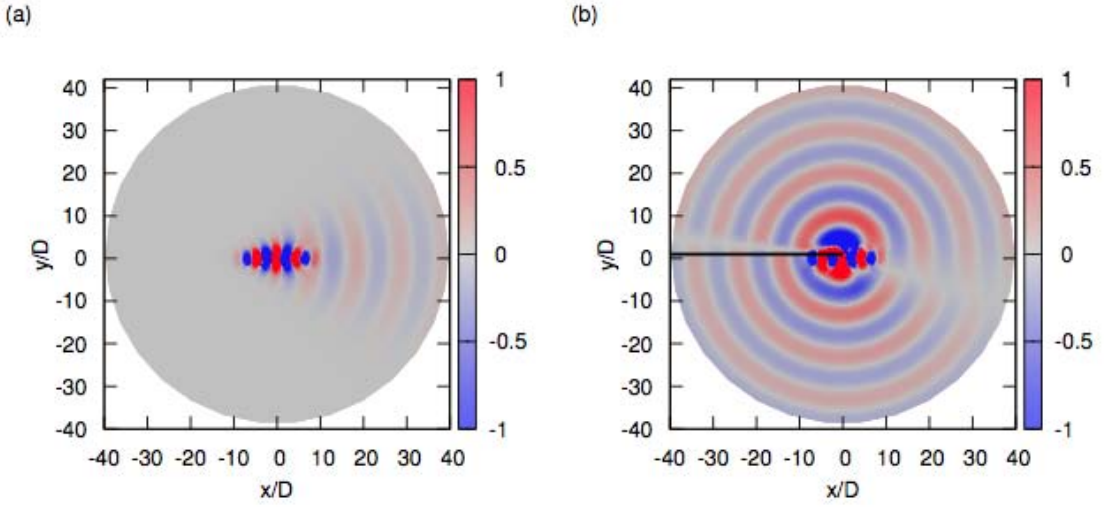

FIGURE 6.58: Pressure fields of a WP source. ($k_H L = 6$, $M = 0.5$, $Uc/U = 0.97\,St = 0.2$) (a) free-field (b) with a semi-infinite flat plate at $x < 0$, $y = 1.0\,D$

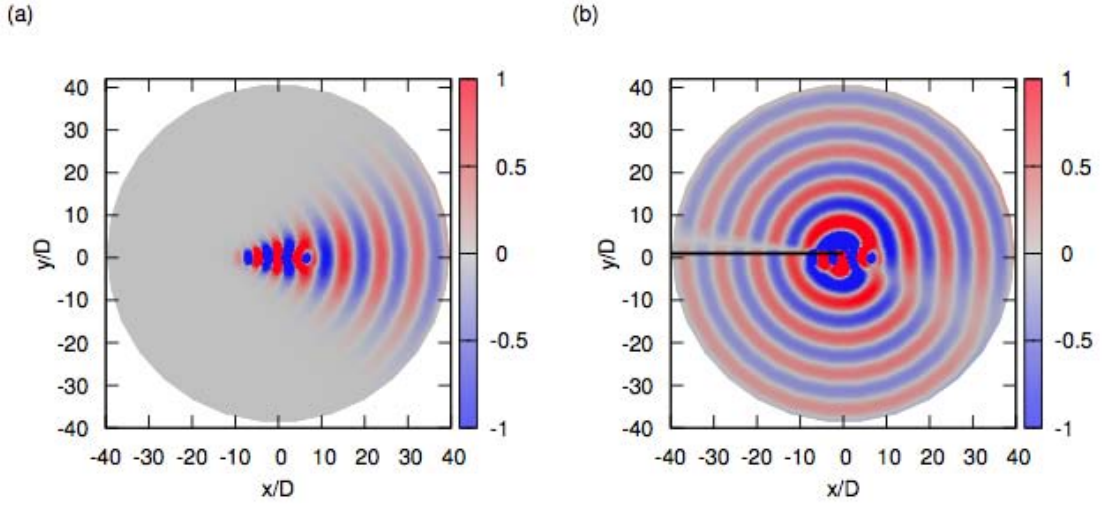

FIGURE 6.59: Pressure fields of a WP source. ($k_H L = 6$, $M = 0.6$, $Uc/U = 0.97\,St = 0.2$) (a) free-field (b) with a semi-infinite flat plate at $x < 0$, $y = 1.0\,D$

(This page is intentionally left blank)

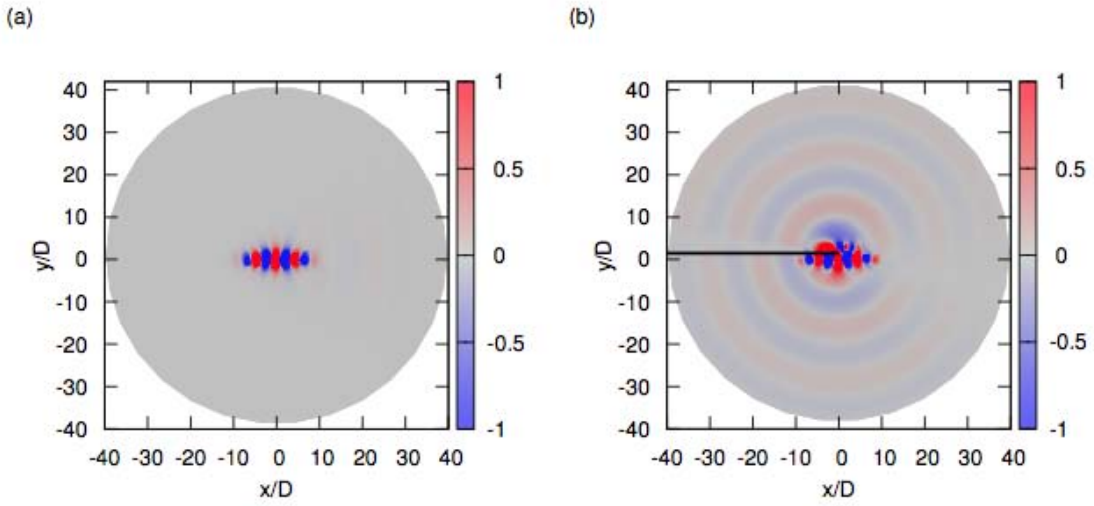

FIGURE 6.60: Pressure fields of a WP source. ($k_H L = 6$, $M = 0.4$, $Uc/U = 0.97\,St = 0.2$) (a) free-field (b) with a semi-infinite flat plate at $x < 0$, $y = 1.5\,D$

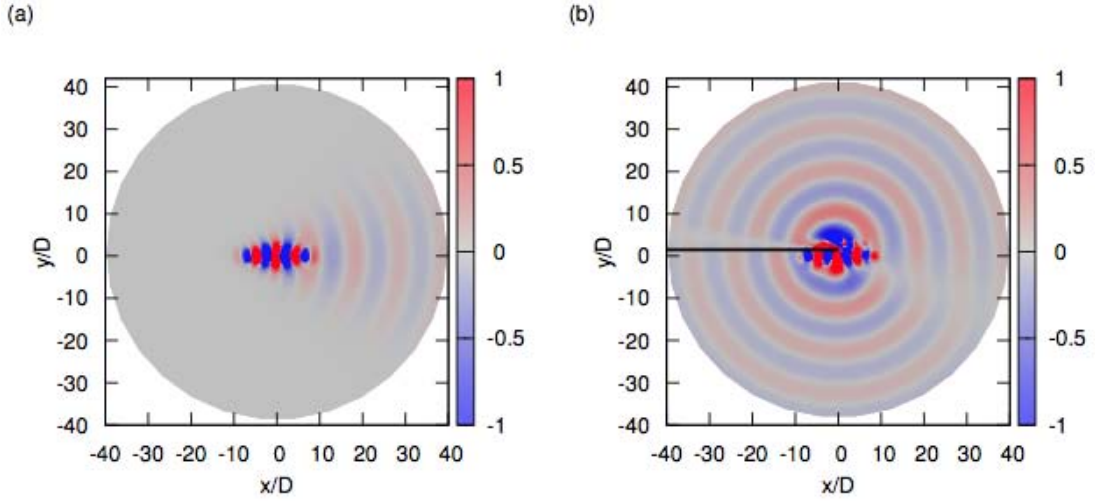

FIGURE 6.61: Pressure fields of a WP source. ($k_H L = 6$, $M = 0.5$, $Uc/U = 0.97\,St = 0.2$) (a) free-field (b) with a semi-infinite flat plate at $x < 0$, $y = 1.5\,D$

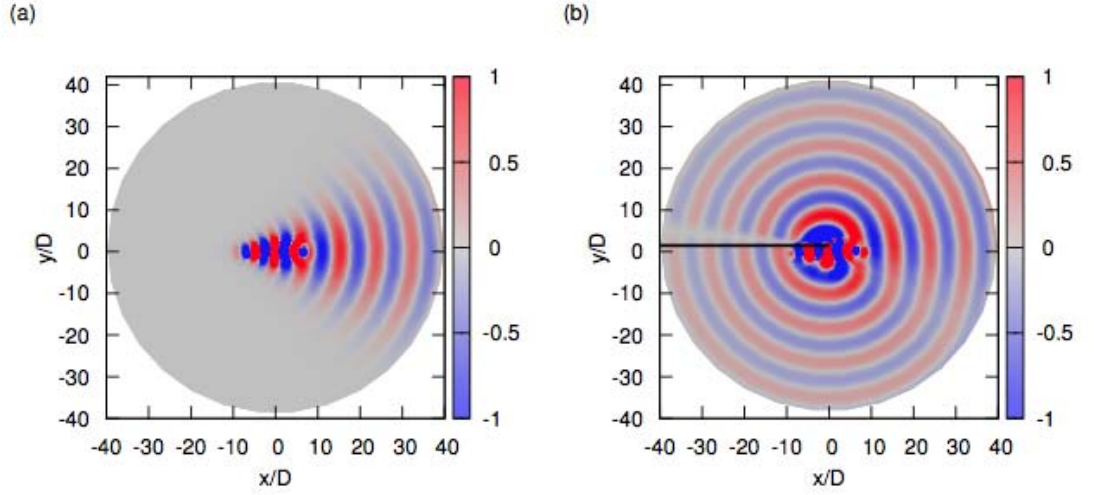

FIGURE 6.62: Pressure fields of a WP source. ($k_H L = 6$, $M = 0.6$, $Uc/U = 0.97\,St = 0.2$) (a) free-field (b) with a semi-infinite flat plate at $x < 0$, $y = 1.5\,D$

(This page is intentionally left blank)

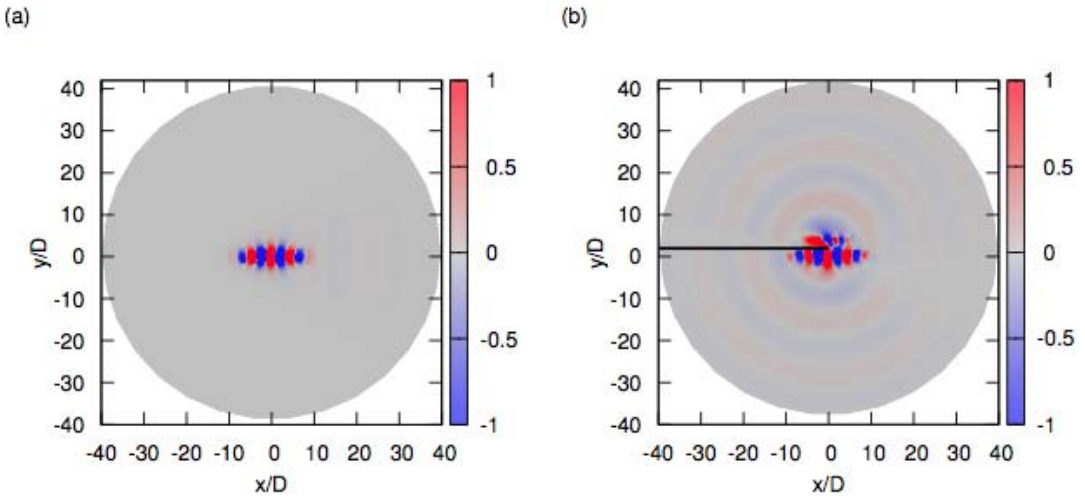

FIGURE 6.63: Pressure fields of a WP source. ($k_H L = 6$, $M = 0.4$, $Uc/U = 0.97$ $St = 0.2$) (a) free-field (b) with a semi-infinite flat plate at $x < 0$, $y = 2.0\,D$

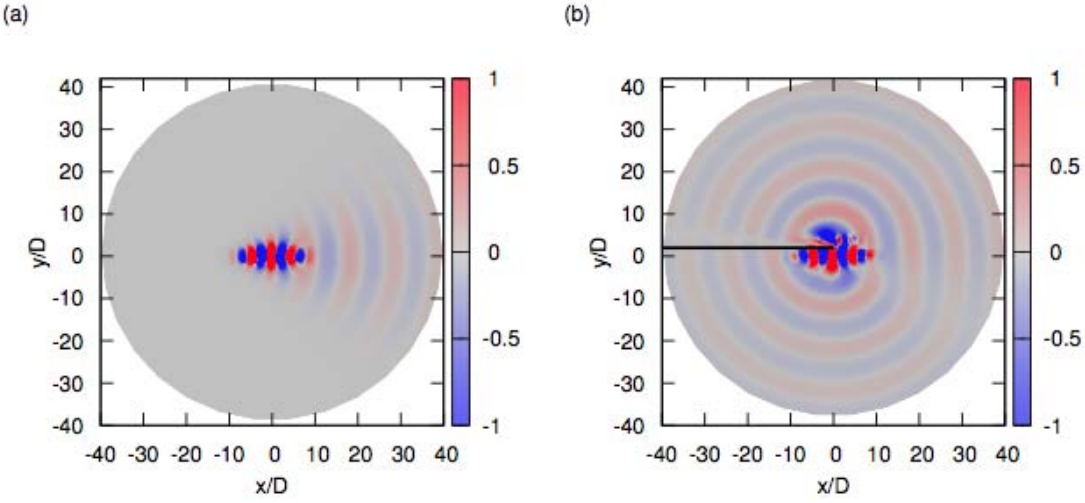

FIGURE 6.64: Pressure fields of a WP source. ($k_H L = 6$, $M = 0.5$, $Uc/U = 0.97$ $St = 0.2$) (a) free-field (b) with a semi-infinite flat plate at $x < 0$, $y = 2.0\,D$

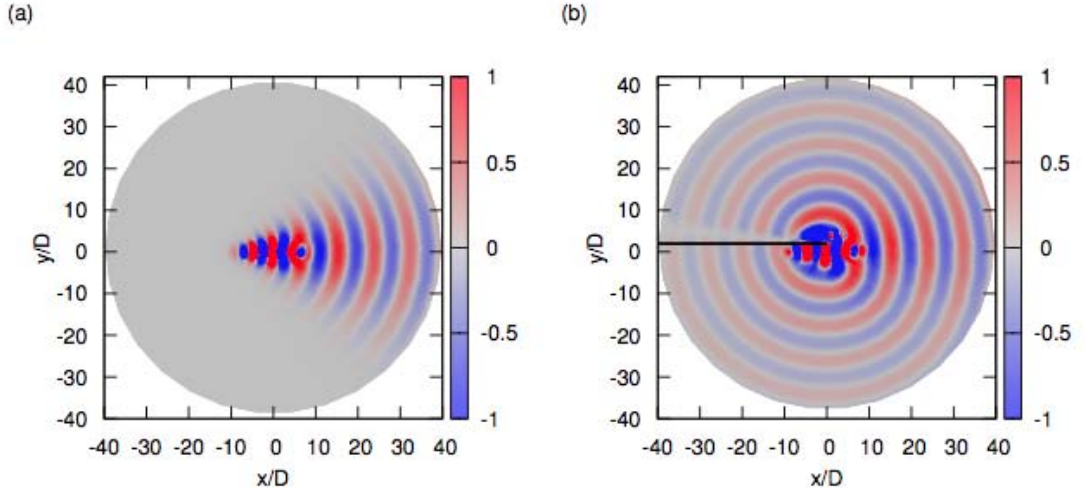

FIGURE 6.65: Pressure fields of a WP source. ($k_H L = 6$, $M = 0.6$, $Uc/U = 0.97$ $St = 0.2$) (a) free-field (b) with a semi-infinite flat plate at $x < 0$, $y = 2.0\,D$

Part III

Conclusions & Future Perspectives

Chapter 7

Conclusions

7.1 Main Considerations

In this thesis paper it has been analyzed one of the phenomena that has great impact and influence on the levels of noise emitted by the new HBPR engines, namely the **effects of surrounding aircraft structures on the noise produced by propulsive jets**.

It has been shown numerically, by post processing experimental data collected during experimental work in a French famous aeroacoustics facility, that the **proximity positioning of a flat plate** - that mimics the wing of an aircraft - **to a simple, subsonic, cylindrical jet** (that mimics the engine's jet exhaust) produce on the generated sound field, effects of **noise amplification**, **reflection**, **diffraction** and **scattering** of the emitted sound waves.

7.2 More General Considerations

Considering what has been introduced in the preliminary chapters, **one of the loudest sources of noise** for these types of studied engines, is in fact the **jet noise**, related to the *mixing* of hot exhaust gases from the motor's exit nozzle, with the cold external atmospheric gases; their produced turbulence is directly related to aerodynamic noise generation, convection and scattering.

It has been also underlined in this thesis project how this **scattered sound is a serious problem of concern**, for both *civil* and *military* aeronautical applications, so **techniques of sound reduction and mitigation** must be studied and employed.

Two of the key-factors that point research studies towards the **reduction of emitted noise**, are firstly the *strict regulation for sound emissions*, constantly updated and made more stringent by the ICAO commission and secondly, the **desperate need for future generation's green aircrafts**.

Following these guidelines, ways for **optimizing noise emissions** must be discovered and evaluated both *numerically* and *experimentally*, in order to achieve the following objectives:

1. **Reduce the noise directly scattered from engines towards the cabin** (with the consequent gain in *"quality of flight"* for both, *passengers* and *crew members*)
2. **Reduce environmental noise** - scattered towards the *surrounding* - mainly during *take off and landing maneuvers* as well as during *on-ground operations* (for both the *safety* of ground personnel and the gain in *"quality of life"* of the inhabitants who live near the airports).

It has been shown also that jet noise depends upon turbulence and has **particular scattering patterns**; its **intensity** is proportional to both the following parameters:

- **jet exit's speed** U_j (*direct proportionality*) - this is why it is a so called *"Mach effect"* - in fact it depends upon a high power (between 5 and 8) of this parameter
- **jet exit's diameter** D_j (*inverse proportionality*).

These dependences are the main reason why actual trends for reducing jet noise, without reducing the thrust, have pointed towards the **increase** of the D_j - hence the production of engines of *bigger dimensions* - rather than the **decrease** of U_j.

From the point of view of the **control and mitigation strategies** of this phenomena and its related effects, it has to be remembered that both, **passive** and **active systems** can be employed nowadays in aeronautical applications like the use of *mechanical chevrons* and *nozzle shaping* techniques (passive mitigation) or by exploiting the power of *microjets systems* for **actively reducing and controlling the noise** (see the advanced studies conducted by the CEAT laboratory).

Moreover, the work presented has shown (as already stated in Paragraph 7.1) how **surfaces** that are placed in relatively close proximity of the jet exit (e.g. wings, wings devices etc..) and thus very near to the main jet noise sources, are crucial for **amplification** or **noise cancellation phenomena**.

Some studied and reported theories, above all the one concerning **wave packet scattering**, can be used in order to perform **approximate calculation of the sound field radiated**, in terms of **topology of the pressure** or **density fields** (see *pressure contours plots*), **directivity** (see *cartesian* and *polar directivity plots*), orders of magnitudes of the **intensity of sound** or **the total emitted power output**, for both *free-jets* and in the case of *presence of boundaries*, in the fluid domain, as it has been done in this case of structure noise diffraction study. For this last situation however, the computational task is harder but can be achieved with the aid of built-ad-hoc mono-dimensional models, based on spectral approaches, that use modified Green's functions tailored for the specific geometry of the studied case (see Dr. P. Jordan and Dr. A. Cavalieri).

7.3 Thesis Main Results

As already underlined many times, throughout this whole thesis paper, some results of the post-processing work that I carried out during my stage at the CEAT laboratory, have already been pointed out by Dr. A. Cavalieri in his article; here I want to discuss, *some others results* that can be possibly regarded as **"new results"** of the newly conducted post-processing campaign that I made, meaning that, pointed in the right direction by Dr. P. Jordan, I gained some insight and confidence with the analysis techniques used and I tried to do some **parameter variational analysis**, in order to **inform and validate previous aeroacoustic theories** and what others had already discovered on this subject.

Starting with the results that were already known and reported in Ref. [33], my analysis confirms what had already been discovered by the Dr. Cavalieri himself in *points 1, 2, 3* of the following list, while **the new part of the analysis that I had made**, was useful to extend previous results and assess other conclusions, reported here in *points 4, 5* and *6*.

1. It is possible to observe **low-frequency amplifications** similar to those observed by Mead & Strange (see Ref. [29]) and others, for both the *shielded* and *unshielded* microphones (mic. #1 and mic. #2) and *for all Mach numbers* in the considered range (i.e. $Ma = [0.35 \div 0.60]$).

2. In the *higher frequencies range*, at about $He > 0.2$ - where the **pressure field incident** on the plate is **purely acoustic** - it is possible to observe the **shielding effects of the wing**.

3. There is a **better scaling of the amplified part of the spectra**, when it is plotted as a function of *Helmholtz number*; these graphs show in fact that this

mechanism of amplification is associated with the ratio between the characteristic length of the problem (namely the *jet diameter* D_j) and the *acoustic wavelength* λ, rather than with some change in the turbulence of the jet. It is also possible to see from this consideration that, while the plate positioned at a *greater distance* picks up only **low frequencies**, when this is positioned *closer to the jet*, also **higher frequencies** are involved.

4. There seems to be a **velocity power law scaling effect on the spectra** (from velocity trend plots of Paragraph 6.6): in fact, while the **high-frequency** part of the spectra scale with a velocity exponent of about 7.5, the **low-frequency** part, scales better with an exponent that varies between 3 and 6, depending on the frequency considered. ***Lower velocity scalings*** *are expected for scattered fields.* From Table 6.2 in fact, it is possible to note and quantify this **scaling effect**: passing from $r/D = 2.0$ to $r/D = 1.0$ the exponent of the velocity law u^x decreases from $x = 7.73$ to $x \approx 6.18$ for the microphone positioned at 20°. Rounding-off it is possible to consider the velocity scaling effect from $\mathbf{u^8}$ to $\mathbf{u^6}$.
   This fact, points out a proportionality to a radiation law that changes from that of a **quadrupole source type** (such as in *direct jet radiation*) to the one of a **dipole source type**, corresponding to the case *with the flat plate in position* and hence, an **enhanced scattered radiation**.

5. When **comparing spectra plots**, the same *"peaks and valleys recurrent patterns"* are due to either **constructive** or **destructive interference features** of the scattered sound field and this is true especially in the nearest jet-plate position case (i.e. $r/D = 1.0$).

6. **New coherence plots** (for the combination cases called in this paper **Cohe13 Cohe23**) showed how the coherence of considered signals still has a *quite high value* (respectively around 0.4 and 0.3) suggesting and indicating a relation between the features of the three signals captured, underlining **reflexion** and **diffraction phenomena**.

7. Always by looking at the coherence plots one can assess the **interference patterns**; this fact can also be checked by looking at **cross-correlation plots**[1] over the whole frequency range: one should expect to find indeed **two higher peaks** in correspondence of the two frequencies of concern.

8. **Strength** VS. **weakness** points of the WP model used: the model operates a **first step estimation** (i.e. it is a first approximation of the complex problem studied and experimentally simulated with the subsonic jets experiments conducted).

[1] Figures of this analysis have not been yet reported in this thesis paper.

Multi-source diffraction influences are not modeled, because of their complexity. Some discrepancies are those found in the directivity plots: in fact, while **the overall trend of directivity seems to be quite predicted** for the **high-angle values** (namely $\pm 90^\circ$) in the lower angles, *where one should be more concerned about variations in this type of directivity patterns* (e.g. the range $\pm 45^\circ$) **experimental data are not well matched by the model** curves of results; this is mainly visible for the 20° microphone of the experiment. (comparisons can be made in plots of Figure 6.54).

Chapter 8

Further Developments

Next steps to take are probably those in the direction of **further investigation of the jet noise scattering-related phenomena** that have been mentioned in project so many times, such as the **amplification effects** produced by the *plate presence near the jet*; the **diffraction** and **scattering effects** of the incident sound waves, etc...

This can be probably done in many ways but, with this last chapter, I would like to discuss *three ways* that can be considered for conducing such further investigation.

1. **The physical approach**: by modifying the *physical experimental setup*. This can be done in various ways like, for instance, the following:

   • by **using more than three microphones** to better qualify in terms of *angular resolution* the *measured pressure field* and possibly in order to be able to make *more comparisons with the results from the WP numerical model.*

   • by **using the built near field azimuthal antenna**, in order to perform *azimuthal decomposition of the field*, to possibly assess which are the mainly involved modes in the diffraction process

   • by **following Airbus scheduled timetable** for the experiment (see Appendix B) and adding the *required features and modifications* (such as, using *coaxial jets*, *real wing planform*, perform *flight effect studies* etc...)

   • by **extending experiment Mach numbers range** of simulation

2. **The mathematical-analytical approach**:

   • by **acting on the analytical and numerical model** of the problem and possibly *correct the results that do not agree with experimental measurements* (like those for the microphone at 20° from the jet axis.)

- by **trying with other azimuthal modes** (i.e. the helical $m = 1$, $m = 2$)
- and for other values of the U_c/U **parameter** of the WP model (some reference values are reported in the article in Ref. [27])
- by **acting on the post processing analysis** (*extended Mach range*, *others St numbers*)

3. **The solution approach**: by **using mitigation strategies** (*passive/active devices* already described) like chevrons or microjets to **research possible solutions to the diffracted jet noise problem**.

Appendix A

The Jeronimo project

A.1 General Overview of the Project

In this first appendix, is summarized with a brief description readapted from the official web source the Jeronimo project and its present status.

JERONIMO - is the name of an European project whose acronym stand for the following:

> *"Jet Noise of High Bypass Ratio Engine: Installation, Advanced Modeling and Mitigation."*

As can be directly read from the internet page of the project[1], the central goal of Jeronimo, is the understanding of the physical mechanisms that lay below the applications of **ultrahigh bypass ratio (UHBR) engines** - with bypass ratios (BPR) larger than 12 - and the related **installed jet noise**, principally focusing on the potential **jet-wing interaction**, especially for underwing jet engine positioning case.

The aim of the project is to *reduce uncertainties in jet noise characterization* of this novel installation configuration, by means of **wind tunnel tests and predictions** and

[1] http://cordis.europa.eu/projects/rcn/103806-en.html

being able to *derive design recommendations* for future UHBR engines, keeping in mind the **new regulation's targets for jet noise reduction**.

In order to achieve these goals and to accurately assess their jet noise characteristic trace, these aforementioned engines have to be largely investigated experimentally, both in **isolated** and **installed** configurations.

By applying advanced and improved measurement techniques, (such as **far-field noise measurements**, **near-field pressure measurements**, in combination with highly sophisticated aerodynamic measurements and test methods, for measuring the **velocity field** of the whole jet, like **LDV** or **PIV** methods) this EU project aims at building a common and consistent *database of experimental results* that will be developed in the major jet noise test facilities, namely the **NTF** and **CEPRA19**[2].

At the same time, existing **CFD-CAA simulation tools** will be exploited, either in their readapted and validated version, or used in their present, state-of-the-art one, while the overall methodology to predict **flight stream effects** and **complex interaction mechanisms** for UHBR engine jet noise will be developed, at medium and full scales.

In order to identify both, overall **physical key-features** and the more specific **fluid-flow-related ones**, a detailed way of conducting experiments will be needed - which will obviously focus on accurate acquisition, processing and post-processing of collected numerical data - for both, **steady** and **unsteady flow** conditions and for **acoustics** too.

A combination between real-life physical experiments and a more analytical/theoretical analysis method, such as, for instance, **flow instability analysis**, **POD**, **azimuthal decomposition** of the radiated acoustic field etc.. will be conjunctionally employed in the research study and evaluation process, while **innovative nozzles geometries** will be designed, regarding the UHBR architecture tested and assessed, in order to **reduce their jet noise signature in the installed configuration**.

Finally, **recommendations** in terms of *mechanical dimensioning and positioning* (e.g. the relative position wing/nozzle) will be provided, while methods & data used to obtain such prescriptions, will be accurately assessed, accordingly, with an overall final evaluation in terms of aircraft noise reductions.

This project intends to use the skills and tools at the state of the art and previously developed during other European programs, as well as those established in national-funded projects.

[2] CEPRA 19 is the **ONERA** aerospace lab's Large-Scale, Anechoic, Wind Tunnel noise research facility

The most suited specialists in Europe will endeavor to:

- **Understand, model and simulate** the physics of UHBR jet installation noise.
- **Propose and validate physics-based principles** toward noise reduction, and associated simulation strategies.
- Validate the means by which the European industry will derive **low-noise guidelines** for its future UHBR engine and aircraft architectures.

A.2 Project Status chart & details:

Detail	Value
Start date	01-11-2012
End date	31-10-2016
Duration	48 months
Project status	Current - active
Program type	7th FWP
Project Reference	314692
Project cost	7.672.723
Project Funding	4.838.815
Programme Acronym	FP7-TRANSPORT
Subprogramme Area	Flight physics
Contract type	Small or medium-scale focused research project
Subject index	Scientific Research

TABLE A.1: Jeronimo Project details.

Project Coordinator: Michael Bauer - EADS Innovation Works (DE)

Project Partners:

- **Airbus** Operations SAS *(FR)*
- **Rolls-Royce** Deutschland LTD & CO KG *(DE)*
- **SNECMA SA** *(FR)*
- Centre Europeen de Recherche et de Formation Avancee en Calcul Scientifique *(FR)*
- **CFD SOFTWARE** - Entwickungs - und Forschungsgesellschaft mbH *(DE)*
- **CNRS:** Centre National de la Recherche Scientifique *(FR)*
- Deutsches Zentrum fuer Luft - und Raumfahrt eV *(DE)*
- Integrated Aerospace Sciences Corporation O.E. *(GR)*
- **ONERA:** Office National d'Etudes et de Recherches Aerosaptiales *(FR)*
- The chancellor, Masters and Scholars of The University of Cambridge UCAM *(UK)*
- Universitá degli Studi Roma Tre *(IT)*
- University of Southampton *(UK)*

Appendix B

Details of CEAT Jeronimo Experiment

B.1 Airbus procedure & schedule

In the following note, found attached to the documentation given me by Dr. A. Cavalieri and Dr. P. Jordan, for data post-processing purposes, it is possible to find more **details about the Jeronimo experiment procedures and timeline**, as expected by Airbus, one of the major contractors.

Notes: JERONIMO, AIRBUS - 18 Oct. 2011 - AIRBUS procedure:

1. **Isolated configuration: jet wind tunnel tests**
2. **Jet plus flight stream configuration**
3. **Installed configuration: wing, pylon plus flight stream**

Possible required intermediate steps :

1. **Isolated configuration jet wind tunnel tests**
2. **Jet plus flight stream configuration**
   (a) **Single jet plus flat plate** : simplest model, theory-convenient, preliminary evaluations.
   (b) **Single jet plus wing (airfoil)**: first step towards applications. (comparison with case 2a.)

(c) **Single jet plus wing (airfoil), plus flight stream**: second step towards applications (comparison with case 2b.)

(d) **Coaxial jet plus wing (airfoil)**: (comparison with case 2b.)

(e) **Coaxial jet plus wing (airfoil), plus flight stream**:
(comparison with case 2d.)

3. **Co-axial jet plus wing (installed configuration, full complexity), plus flight stream:**
(comparison with case 2d.)

Evaluation of physical phenomena & parameters assessment :

- **scattering of hydrodynamics** (by edge and/or surface dipoles)
- **scattering of hydrodynamics by wing** (by edge and or surface dipoles)

  modification of source and Green's function
- **scattering of coaxial hydrodynamics** (by wing)

  modification of coaxial source and Green's function

  modification of source and Green's function

The *PPRIME Institute* would be interested in specifying a subset of pressure (both of surface and free-field) and velocity measurements, for the **QINETIQ** and/or **CEPRA19** tests, and computations, in order to enable comparison of the very simple lab configurations 2a, 2b and 2d, with the more complex scenarios 2c, 2e, and 3.

Appendix C

Derivation of Basic Equations

As can be further analyzed in Ref. [4] Aeroacoustics is mostly concerned with fluids such as water and air, that have very **small viscosity** and **thermal conductivity**. Where disturbances are so weak that their **spatial gradients** are never much larger than the disturbances themselves and these are not allowed to propagate over excessively large distances, the **effects of both, heat conduction and viscosity can be neglected** and the fluid motion can be determined by solving the system of the following equations:

- The **momentum equation** for an inviscid flow (Euler's equation):

$$\rho\left(\frac{\partial \mathbf{v}}{\partial t} + \mathbf{v}\cdot\nabla\mathbf{v}\right) = -\nabla p + \boldsymbol{f} \tag{C.1}$$

- The **continuity equation**:

$$\frac{\partial \rho}{\partial t} + \mathbf{v}\cdot\nabla\rho + \rho\nabla\cdot\mathbf{v} = \rho q \tag{C.2}$$

- The **energy equation** (or *entropy equation*):

$$\frac{\partial S}{\partial t} + \mathbf{v}\cdot\nabla S = 0 \tag{C.3}$$

where ∇ is the vector operator defined below:

$$\nabla = \boldsymbol{i}\frac{\partial}{\partial y_1} + \boldsymbol{j}\frac{\partial}{\partial y_2} + \boldsymbol{k}\frac{\partial}{\partial y_3} \tag{C.4}$$

for a *homo-compositional fluid* in a *thermodynamic state of equilibrium* (i.e. where **relaxation effects can be neglected**) density is a **function of state** and can be expressed as:

$$\rho = \rho\left(p,\, S\right) \tag{C.5}$$

and the following relation holds true for the speed of sound:

$$c^2 = \frac{1}{\left(\frac{\partial \rho}{\partial p}\right)_s} = \left(\frac{\partial p}{\partial \rho}\right)_s \tag{C.6}$$

having defined Eq. (C.6), one can rewrite Eq. (C.2) like the following:

$$\frac{\partial \rho}{\partial t} + \mathbf{v} \cdot \nabla \rho = \frac{1}{c^2}\left(\frac{\partial p}{\partial t} + \mathbf{v} \cdot \nabla p\right) \tag{C.7}$$

for the **steady flow** with **no external forces or mass addition**, it is possible to write the following system of equations:

$$\begin{cases} \rho_0 \mathbf{v}_0 \cdot \nabla \mathbf{v}_0 = -\nabla p_0 \\ \nabla \rho_0 \mathrm{v}_0 = 0 \\ \mathbf{v}_0 \cdot \nabla S_0 = 0 \\ \mathbf{v}_0 \cdot \nabla p_0 = c_0^2 \mathbf{v}_0 \cdot \nabla \rho_0 \end{cases} \tag{C.8}$$

from which velocity pressure and density are determined.

Being interested in **sound** means to consider the **pressure disturbances** that are passing through the atmosphere; an **unsteady disturbance**, *produce changes in velocity, pressure, density and entropy* that can be described by considering, respectively, the following statements:

$$\begin{cases} \mathbf{u} = \mathbf{v} - \mathbf{v}_0 \\ p' = p - p_0 \\ \rho' = \rho - \rho_0 \\ S' = S - S_0 \\ c^{2'} = c^2 - c_0^2 \end{cases} \tag{C.9}$$

with the following perturbation properties: the *time scale* T_p and the *characteristic frequency* of the disturbance f defined below:

$$T_p = \frac{1}{f} \tag{C.10}$$

$$f = \frac{\tilde{C}}{\lambda} \tag{C.11}$$

Because of the *weakness of disturbances*, even in the loudest sounds, it is important to consider only disturbances that satisfy the following conditions:

• **disturbances induced velocity** is smaller, compared to **disturbance propagation speed**:

$$|\mathbf{u}| \ll \tilde{C} = \frac{\lambda}{T_p} \tag{C.12}$$

• **Thermodynamic properties fluctuations** are small, with respect to their **mean background values**.

$$\begin{cases} p' \ll \langle\, p_0 \,\rangle \\ \rho' \ll \langle\, \rho_0 \,\rangle \\ S' \ll \langle\, S_0 \,\rangle \\ c^{2'} \ll \langle\, c_0^2 \,\rangle \end{cases} \tag{C.13}$$

Introducing non-dimensional variables and performing some calculations as can be found in Ref. [4] it is possible to get to the final form of the **system of linearized gas-dynamic equations**:

$$\begin{cases} \rho_0 \left(\dfrac{\partial \mathbf{u}}{\partial t} + \mathbf{v}_0 \cdot \nabla \mathbf{u} + \mathbf{u} \cdot \nabla \mathbf{v}_0 \right) + \rho' \mathbf{v}_0 \cdot \nabla \mathbf{v}_0 = -\nabla p' + \boldsymbol{f} \\ \dfrac{\partial \rho'}{\partial t} + \nabla \cdot \left(\rho_0 \mathbf{u} + \rho' \mathbf{v}_0 \right) = \rho_0 q \\ \dfrac{\partial \boldsymbol{S}'}{\partial t} + \mathbf{v}_0 \cdot \nabla \boldsymbol{S}' + \mathbf{u} \cdot \nabla \boldsymbol{S}_0 = 0 \\ c_0^2 \left(\dfrac{\partial \rho'}{\partial t} + \mathbf{v}_0 \cdot \nabla \rho' + \mathbf{u} \cdot \nabla \rho_0 \right) + c^{2'} \mathbf{v}_0 \cdot \nabla \rho_0 = \dfrac{\partial p'}{\partial t} + \mathbf{v}_0 \cdot \nabla p' + \mathbf{u} \cdot \nabla p_0 \end{cases} \tag{C.14}$$

That holds for any flow region in which **disturbances and their gradients remain small**. Following the approach presented in Goldstein Ref. [4] it can be shown that after

some mathematical simplifications one can get to the famous **wave equation** either written in *terms of pressure fluctuations* or *density fluctuations* but assuming some **hypothesis** listed below:

- the flow field has a **unidirectional**, transversely sheared **mean flow**;
- there could **exist only velocity gradients** and not pressure or density gradients;
- **entropy** doesn't change with time for an observer moving along with the mean flow
- c_0^2 **is constant**, as well as the **mean velocity**U

$$\nabla^2 p' - \frac{1}{c_0^2}\frac{D_0^2}{Dt^2}p' = \nabla \cdot \boldsymbol{f} - \rho_0 \frac{D_0 q}{Dt} \equiv -\gamma \tag{C.15}$$

$$\nabla^2 \rho' - \frac{1}{c_0^2}\frac{D_0^2}{Dt^2}\rho' = \frac{1}{c_0^2}\left(\nabla \cdot \boldsymbol{f} - \rho_0 \frac{D_0 q}{Dt}\right) \quad \text{for} \quad S = \text{ Constant} \tag{C.16}$$

When $U = 0$ Eq. (C.15) reduces to the following **inhomogeneous wave equation (for stationary medium)**:

$$\boxed{\nabla^2 p' - \frac{1}{c_0^2}\frac{\partial^2 p'}{\partial t^2} = \nabla \cdot \boldsymbol{f} - \rho_0 \frac{\partial q}{\partial t} \equiv -\gamma} \tag{C.17}$$

that form the basis of the field of classical acoustics.

Focusing on one particular class of fluid motion, considering the following hypothesis:

- **small amplitude fluctuations** of a potential nature
- **quiescent fluid medium**
- **absence of external sources of mass or momentum**

and thanks to the **potential nature of the acoustic motion**, it is possible to rewrite the already obtained form of the **system of linearized gas-dynamic equations**, in a simplified one such as the following, directly taken from Ref. [20]:

$$\begin{cases} \dfrac{\partial \rho'}{\partial t} + \rho_0 \nabla \cdot \mathbf{u'} = 0 \\ \rho_0 \dfrac{\partial \mathbf{u'}}{\partial t} + \nabla p' = 0 \\ \dfrac{\partial \mathbf{S'}}{\partial t} = 0 \\ p' = c_0^2 \rho' \end{cases} \tag{C.18}$$

It has to be noted though, that by doing this operation of linearization, an error is obviously introduced, and it has to be accounted for, somehow.

With all this in mind, it is possible to get to the **commonly used form of the wave equations** - either in density or pressure formulation - by using some mathematical elaborations and the constitutive equation - Eq. (C.18 - d) - :

$$\boxed{\frac{\partial^2 p'}{\partial t^2} - c_0^2 \, \Delta p' = 0} \tag{C.19}$$

$$\boxed{\frac{\partial^2 \rho'}{\partial t^2} - c_0^2 \, \Delta \rho' = 0} \tag{C.20}$$

The above equations describe any possible class of motion of such a fluid flow continuum.

Appendix D

Fundamentals of Digital Signal Processing (DSP)

D.1 Fourier Transform and Fourier Series

Basic connection between the two domains of *time* and *frequency* is the **Fourier transform**, which transforms the **time signal** $g(t)$ into the **frequency spectrum** $G(f)$, expressed with the following equation:

$$G(f) = \int_{-\infty}^{+\infty} g(t)\, e^{-i2\pi ft}\, dt \tag{D.1}$$

The inverse transform, i.e. the **Fourier anti-transform** function, permits to retriever the time signal $g(t)$ from the transformed signal $G(f)$ in the following way:

$$g(t) = \int_{-\infty}^{+\infty} G(f)\, e^{i2\pi ft}\, df \tag{D.2}$$

The two mentioned transformations share almost all the same properties, in particular, the **convolution theorem** that states the following:

$$g(t) = f(t) * h(t) = \int_{-\infty}^{+\infty} f(\tau)\, h(t-\tau)\, d\tau \tag{D.3}$$

$$G(f) = \Im\{f(t) * h(t)\} = F(f) \cdot H(f) \tag{D.4}$$

i.e. the *convolution* of two signals (expressed here with the operator asterisk $*$) in one of the two domains, corresponds to a *multiplication* of signals in the other; the $\Im\{..\}$ operator represents the Fourier transform of the argument, while the uppercase letters represent the Fourier transforms of the corresponding lowercase variables.

The operation in Eq. D.3 represents the output $g(t)$ of any physical system with **impulse response function** $h(t)$, subject to the **forcing function** $f(t)$; it is evident the simplicity in treating signals with Eq. D.4. rather than with Eq. D.3.

Equation D.1 only applies, strictly speaking, to **transient functions** i.e. functions whose integral over all time is finite; using the convolution theorem, it can be extended to the case of **periodic functions** when these are treated like being generated by convolving *one period of length* T with an infinite train of *unit delta functions* with spacing equal T. (see Ref. [16] for more in depth).

In **complex numbers form**, the Fourier series spectrum for a transient function $g(t)$ with Fourier transform $G(f)$, repeated with a period of T, can be calculated as follow:

$$G(f_k) = \frac{1}{T} G\left(\frac{k}{T}\right) = \frac{1}{T} \int_{-T/2}^{+T/2} g(t)\, e^{-i2\pi kt/T}\, dt \tag{D.5}$$

When the signal $g(t)$ is periodic, with frequencies zero or positive, it can be expressed in *terms of sine and cosine functions*, using the following series:

$$g(t) = \frac{a_0}{2} + \sum_{k=1}^{\infty} a_k\, cos\,(k\omega_0 t) + \sum_{k=1}^{\infty} b_k\, sin\,(k\omega_0 t) \tag{D.6}$$

where the coefficients a_k and b_k are expressed as follows:

$$a_k = \frac{2}{T} \int_{-T/2}^{+T/2} g(t) cos\,(k\omega_0 t)\, dt \tag{D.7}$$

$$b_k = \frac{2}{T} \int_{-T/2}^{+T/2} g(t) sin\,(k\omega_0 t)\, dt \tag{D.8}$$

meaning that:

$$G(f_k) = \frac{a_k}{2} - i\frac{b_k}{2} \tag{D.9}$$

Each **sinusoidal component** is made up of a sum of a positive and a negative frequency component, each with *half the amplitude* of the corresponding sinusoid, since when they

align, the total amplitude is double that of the individual components, as expressed in Eq. D.9 from Ref. [16].

D.2 DFT: the Discrete Fourier Transform

When treated signals are **discretely sampled**, Equations D.1 and D.2 can be replaced by the following expressions for the **direct** and **inverse** DFT functions:

• **Direct (or forward) DFT**:

$$G(k) = \left(\frac{1}{N}\right) \sum_{n=0}^{N-1} g(n)\, e^{-i2\pi kn/N} \tag{D.10}$$

• **Inverse DFT**:

$$g(n) = \left(\frac{1}{N}\right) \sum_{n=0}^{N-1} G(k)\, e^{i2\pi kn/N} \tag{D.11}$$

Amongst various things and properties that can be explored in Ref. [16], one important fact is that concerning the phenomenon of **Aliasing** and the **Shannon theorem of sampling**: i.e. a time signals sampled at a sampling frequency of f_s, *must not contain frequencies higher than half the sampling frequency, before digitalization.*

D.3 FFT: the Fast Fourier Transform

Instead of using a direct approach calculation of the just presented Fourier transform expressions, which would require a *number of operations* of the order of $\mathbf{N^2}$, it can be used another *variant of the computational algorithm* for the same computations but it calculates the **DFT in a more efficient way**, using only a number of operations of the order of $\mathbf{N \log_2 N}$. This means that, for a typical transform size of $\mathbf{2^{10} = 1024}$ DFT points, the FFT algorithm is more than 100 times faster. However, not everything comes without a price: the **FFT algorithm** presents the same pitfalls that has the DFT algorithm, namely:

1. **Aliasing**
2. **Leakage**

3. **Picket fence effect**

In the calculations made in this thesis project, some *conventional Matlab*© *algorithms* have been used, and some ad-hock written functions have been implemented.

In order to reduce one or more of these presented side effects, the signal record can be multiplied by a **"data window"** or **"weighting function"** in time domain, while in the frequency domain, this operation corresponds to a convolution with the Fourier transform of the window function, as it has already been pointed out because changing the nature of a signal in the time domain implicitly changes the nature of its spectrum in the frequency domain. The data window function acts like a **filter** and, in the frequency domain, the type of weighting obtained is determined by the *size* and *shape* of the window through which the analyzer sees the data in the time domain; the *choice of window* depends upon various parameters such as the type of analyzed signal and the specific application considered.

In Table D.1 are reported some **types of commonly used window functions** and their specifications. (see Ref. [16] and Ref. [7] for a more in-depth overview of the argument).

Window	NBW	HSL (dB)	SLRO (dB/decade)	PFFX (dB)
Rectangular	1.0	-13	20	3.9
Hanning	1.5	-33	60	1.4
Kaiser-Bessel	1.8	-60	20	0.8
Flat top	3.8	-70	20	<0.1

TABLE D.1: Types and properties of various window functions.

Where **NBW** is the noise bandwidth, **HSL** is the highest sidelobe, **SLRO** is the sidelobe rolloff and **PFFX** parameter is the picket fence effect.

In Figure D.1, taken from Ref. [16], are summarized the effects of FFT analyzers weighting process.

D.4 Correlation Functions: Cross-Correlation and Auto-correlation Functions

Correlation functions give a measure of how well two signals correlates one another, as a function of the *time displacement* between them.

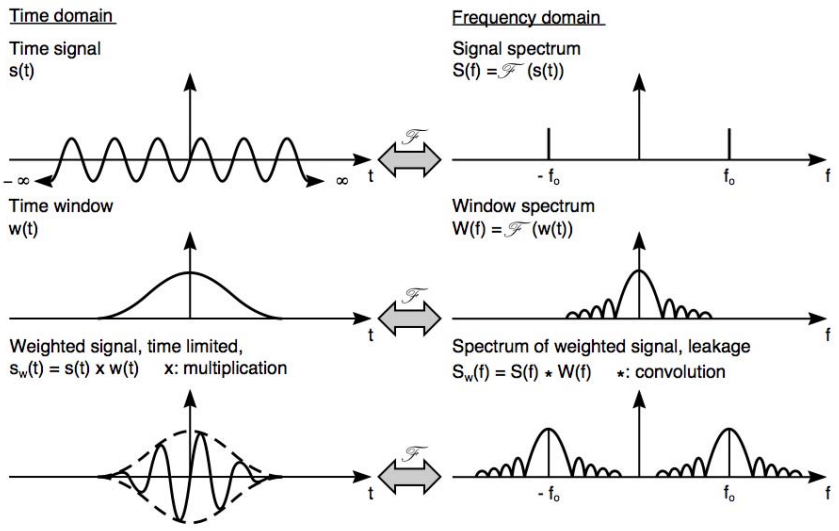

FIGURE D.1: FFT analyzers weighting effects on signals: frequency spectrum.

The following expression defines the **cross-correlation function** between two *non stationary signals* $x(t)$ and $y(t)$:

$$R_{xy}(t,\tau) = E\left[x(t-\tau/2)\, y(t+\tau/2)\right] \tag{D.12}$$

where t is the *time of centering*, τ the *total displacement* and $E[..]$ is the expected value or statistical average.

For *stationary processes* there is no statistical variation with time, so the time-averaging can be computed; if the cross correlation is defined in terms of *symmetrical time displacement*, it gets the following form:

$$R_{xy}(\tau) = \lim_{T\to\infty} \frac{1}{T} \int_{-T/2}^{+T/2} x(t-\tau/2)\, y(t+\tau/2)\, dt \tag{D.13}$$

while for *non-symmetrical interval*, it gets the following representation:

$$R_{xy}(\tau) = \lim_{T\to\infty} \frac{1}{T} \int_{-T/2}^{+T/2} x(t)\, y(t+\tau)\, dt \tag{D.14}$$

When the cross-correlation is computed between the same signal (i.e. when $x(t) = y(t)$) the so called **autocorrelation function** results; it is a measure of how well a signal correlates with itself as a function of displacement, and it is written as follows:

- for *non-stationary functions*:

$$R_{xx}(t,\tau) = E\left[x(t-\tau/2)\,x(t+\tau/2)\right] \tag{D.15}$$

• for *stationary functions* (with *non-symmetric* interval in this case):

$$R_{xx}(\tau) = \lim_{T\to\infty}\frac{1}{T}\int_{-T/2}^{+T/2} x(t)\,x(t+\tau)\,dt \tag{D.16}$$

It has to be noted though that limitations occur when using the autocorrelation function to detect *echoes* as well as when using the cross-correlation function to determine whether a signal is a *scaled, delayed version* of another.

D.5 Cross Spectrum

It can be shown that the Fourier transform of the *autocorrelation function* is equal to the **autospectrum** or **power spectrum**, while the Fourier transform of the *cross-correlation function* is the so called **cross-spectrum** computable as below, following the notation from Ref. [16]:

$$G_{xy}(f) = E\left[G_x^*(f)\cdot G_y(f)\right] \tag{D.17}$$

and it has the properties of having:

- an **amplitude** given by the *product of the amplitudes* of the two spectra, respectively at each frequency,
- a **phase** given by the *phase difference* between the two (i.e. the phase change between x and y)
- the effect of **additive random noise** tends to zero as a result of the *averaging operations*.

In Figure D.2, always taken from Ref. [16], are depicted the acutospectra and autocorrelations results for three signals, for comparison purposes.

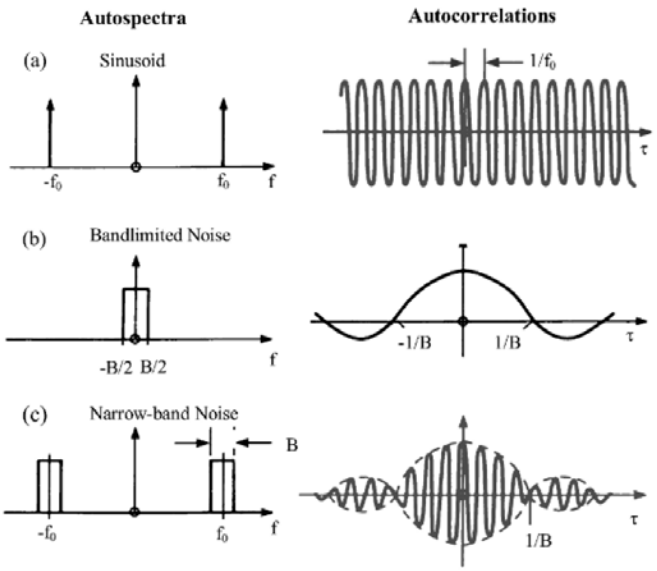

FIGURE D.2: Autospectra and autcorrelations comparisons for three signals.

D.6 Coherence

The **coherence** between two signals $x(t)$ and $y(t)$ is given by the following formula:

$$\gamma^2(f) = \frac{|G_{xy}(f)|^2}{G_{xx}G_{yy}} \tag{D.18}$$

Eq. D.18 is the square of the correlation coefficient between the frequency components as a function of frequency (how can be read in Ref. [16]); it has a value between zero and one and **measures the degree of linear relationship between the two signals as a function of frequency**. Coherence has a *low value*, towards zero, if the **relationship is not linear**, if there is any **noise addition** in either of the two signals or if a **delay** between equivalent parts of the two signals is present; while it presents a *high value*, towards one, if the **relationship is fully linear**.

In order to identify the sources of a measured spectrum, one can consider the **coherent power**, i.e. the product of *coherence* with the *autospectra* used to calculate it; this will **quantify the amount of autospectrum resulting from the linear part of the relationship** between $x(t)$ and $y(t)$.

Appendix E

WP Analytical Model Equations

E.1 Derivation of the Radiated Sound Field

The following is a re-adaptation of the original paper from Dr. A. Cavalieri titled: *"Calculation of the integral (observer in the far acoustic field)"*:

Making the following positions for *shortness*:

$$K_1 = \frac{\rho_0 U \tilde{u} D^2}{8|x|} \tag{E.1}$$

$$\Delta_y = \delta(y_2)\delta(y_3) \tag{E.2}$$

$$G_e = e^{i(\omega\tau - k y_1)} e^{\left(-y_1^2/L^2\right)} e^{\left(-\tau^2/\tau_c^2\right)} \tag{E.3}$$

it is possible to express the **approximated stress tensor** T_{11} and its *derivatives* with the following expressions:

$$T_{11}(\mathbf{y}, \tau) = \left(2\rho_0 U \tilde{u} \frac{\pi D^2}{4}\right) \Delta_y \left[G_e\right] \tag{E.4}$$

$$T_{11}(\mathbf{y}, \tau) = \rho_0 \tilde{u}^2 D^2 \Delta_y G_e \tag{E.5}$$

$$\frac{\partial T_{11}}{\partial y_1} = \rho_0 \tilde{u}^2 D^2 \Delta_y \left(-ik - \frac{2y_1}{L^2}\right)^2 G_e \tag{E.6}$$

$$\frac{\partial^2 T_{11}}{\partial y_1^2} = \rho_0 \tilde{u}^2 D^2 \Delta_y \left[\left(-ik - \frac{2y_1}{L^2} \right)^2 - \frac{2}{L^2} \right] G_e \tag{E.7}$$

Then the **pressure field** gets the following *analytical form*:

$$p(\mathbf{x},t) = \frac{\rho_0 U \tilde{u} D^2}{8} \iiint \int \frac{\partial^2 T_{11}}{\partial y_i \partial y_j}(\mathbf{y},\tau) \frac{\delta\left(t - \tau - \frac{|\mathbf{x}-\mathbf{y}|}{c}\right)}{|\mathbf{x}-\mathbf{y}|} d\tau d\mathbf{y} \tag{E.8}$$

$$p(\mathbf{x},t) = K_1 \iiint \int \frac{\partial^2 T_{ij}}{\partial y_i \partial y_j}(\mathbf{y},\tau) \delta\left(t - \tau - \frac{|\mathbf{x}-\mathbf{y}|}{c}\right) d\tau d\mathbf{y} \tag{E.9}$$

$$p(\mathbf{x},t) = K_1 \frac{\partial^2}{\partial x_1^2} \iiint \int \Delta_y \left[G_e\right] \delta\left(t - \tau - \frac{|\mathbf{x}-\mathbf{y}|}{c}\right) d\tau d\mathbf{y} \tag{E.10}$$

$$p(\mathbf{x},t) = K_1 \frac{\partial^2}{\partial x_1^2} \iiint \left[\Delta_y \left(G_e\right)\right]_{\tau = t - |\mathbf{x}-\mathbf{y}|/c} d\mathbf{y} \tag{E.11}$$

$$p(\mathbf{x},t) = K_1 \frac{\partial^2}{\partial x_1^2} \int \left[\left(G_e\right)\right]_{\tau = t - |\mathbf{x}-\mathbf{y}|/c} dy_1 \tag{E.12}$$

$$p(\mathbf{x},t) = K_1 \frac{\partial^2}{\partial x_1^2} \int \left[e^{i\left[\omega\left(t - \frac{|\mathbf{x}-\mathbf{y}|}{c}\right) - k y_1\right]} e^{\left(-y_1^2/L^2\right)} e^{\left[-\frac{\left(t - \frac{|\mathbf{x}-\mathbf{y}|}{c}\right)^2}{\tau_c^2}\right]} \right] dy_1 \tag{E.13}$$

After considerations on the **problem's geometry**, It is possible to write:

$$|\mathbf{x}-\mathbf{y}| = \sqrt{(x_1 - y_1)^2 + x_2^2 + x_3^2} = \sqrt{|x|^2 - 2x_1 y_1 + y_1^2} \tag{E.14}$$

concluding that:

$$|\mathbf{x}-\mathbf{y}| = |x| \sqrt{1 - \frac{2x_1 y_1}{|x|^2} + \frac{y_1^2}{|x|^2}} \tag{E.15}$$

This expression *approximates* to the following:

$$|\mathbf{x}-\mathbf{y}| \approx |x| \sqrt{1 - \frac{2x_1 y_1}{|x|^2}} \approx |x| \left(1 - \frac{x_1 y_1}{|x|^2}\right) \tag{E.16}$$

with the final result of the *approximation* being:

$$|\mathbf{x}-\mathbf{y}| \approx |x| - \frac{x_1 y_1}{|x|} \approx |x| - y_1 cos\theta \tag{E.17}$$

After some long analytical passages for reducing the expression it is possible, by setting the following *parameter* A:

$$A = -\frac{\rho_0 \tilde{u}^2 D^2}{4\pi|x|} e^{i\omega\left(t-\frac{|x|}{c}\right)} e^{\left(-\frac{\left(t-\frac{|x|}{c}\right)^2}{\tau_c^2}\right)} \tag{E.18}$$

to get this result for the **pressure field**:

$$p(\mathbf{x},t) = \frac{\partial^2}{\partial x_1^2}\left[A\int e^{i\left(\frac{\omega y_1 cos\theta}{c}-ky_1\right)} e^{\left(-\frac{y_1^2}{L^2}-\frac{(y_1 cos\theta)^2}{c^2\tau_c^2}\right)} e^{\left(-\frac{2\frac{y_1 cos\theta}{c}\left(t-\frac{|x|}{c}\right)}{\tau_c^2}\right)} dy_1\right] \tag{E.19}$$

Now, by considering also the following *equivalences*:

$$B = \exp\left[i\left(\frac{\omega y_1 cos\theta}{c} - ky_1\right)\right] \tag{E.20}$$

$$C = \exp\left[\frac{-y_1^2}{L^2} - \frac{(y_1 cos\theta)^2}{c^2\tau_c^2}\right] \tag{E.21}$$

$$D = \exp\left[\frac{2y_1 cos\theta\left(t-\frac{|x|}{c}\right)}{c\tau_c^2}\right] \tag{E.22}$$

It is possible to re-write the pressure field in a simplified form like the following:

$$p(\mathbf{x},t) = \frac{\partial^2}{\partial x_1^2}\left[A\int [B\cdot C\cdot D]\, dy_1\right] = \frac{\partial^2}{\partial x_1^2}\left[A\int \left[e^{(B+C+D)}\right] dy_1\right] \tag{E.23}$$

Which, integrated with *Mathematica*© gives, after setting respectively the parameters:

$$K_2 = \frac{i\tau_c c L\sqrt{\pi}}{2\sqrt{\tau_c^2 c^2 + L^2 cos^2\theta}} \tag{E.24}$$

$$E_1 = -\frac{L^2}{4\tau_c^4 c^4 \left(\tau_c^2 c^2 + L^2 cos^2\theta\right)} \tag{E.25}$$

$$F = \left[c\left(ck - \omega cos\theta\right)\tau_c^2 + 2icos\theta\left(|x| - ct\right)\right]^2 \tag{E.26}$$

the following *indefinite integral* :

$$I = -2iK_2 \cdot e^{(E_1 F)} \cdot (\epsilon) \tag{E.27}$$

Where ϵ is the *error function* defined below:

$$\epsilon = \text{erfi}\left[\frac{\tau_c^2 c\left(-ckL^2 + \omega cos\theta L^2 + 2icy_1 + 2iL^2 cos\theta\left(-|x| + ct + y_1 cos\theta\right)\right)}{2\tau_c cL\sqrt{\tau_c^2 c^2 + L2cos^2\theta}}\right] \tag{E.28}$$

$$\text{erfi}\left(i\infty\right) = i \tag{E.29}$$

$$\text{erfi}\left(-i\infty\right) = -i \tag{E.30}$$

It is possible to re-write the *integral* in the following way:

$$I = -2iK_2 e^{(E_1 F)} = \frac{K_2}{i} e^{\left(\tau_c^2 c^2 E_1 F\right)} \tag{E.31}$$

And by setting respectively these other parameters:

$$K_3 = -\frac{\rho_0 \tilde{u}^2 D^2 \tau_c cL}{4\sqrt{\pi}|x|\sqrt{\tau_c^2 c^2 + L^2 cos^2\theta}} \tag{E.32}$$

$$H = i\omega\left(t - \frac{|x|}{c}\right)^2 \tag{E.33}$$

$$J = -\frac{\left(t - \frac{|x|}{c}\right)^2}{\tau_c^2} \tag{E.34}$$

$$E_2 = \tau_c^2 c^2 E_1 \tag{E.35}$$

It is possible to rewrite the pressure field with this expression:

$$p(\mathbf{x}, t) = K_3 \frac{\partial^2}{\partial x_1^2} \left[e^{(H+J+E_2+F)} \right] \tag{E.36}$$

That, with the **hypothesis of far-field**, becomes

$$p(\mathbf{x}, t) = K_3 \left(\frac{cos^2\theta}{c^2} \right) \frac{\partial^2}{\partial t^2} \left[e^{(H+J+E_2+F)} \right] \tag{E.37}$$

If for sake of clarity one uses the following simplified notation:

$$\Omega = (H + J + E_2 + F) \tag{E.38}$$

It is evident the **dependence of the pressure field from the function of the angle** $cos^2\theta$:

$$p(\mathbf{x}, t) = K_3 \left(\frac{cos^2\theta}{c^2} \right) \frac{\partial^2}{\partial t^2} \left(e^{\Omega} \right) \tag{E.39}$$

$$H_2 = i\omega - 2\frac{\left(t - \frac{|x|}{c}\right)}{\tau_c^2} \tag{E.40}$$

$$J_2 = -2i\, c\, cos\theta \tag{E.41}$$

$$F_2 = \left[c\left(ck - \omega cos\theta\right) \tau_c^2 + 2icos\theta\left(|x| - ct\right) \right] \tag{E.42}$$

$$N = \left[\frac{2L^2 cos^2\theta}{\tau_c^2 \left(\tau_c^2 c^2 + L^2 cos^2\theta\right)} - \frac{2}{\tau_c^2} \right] \tag{E.43}$$

and the pressure field results from the following equation:

$$p(\mathbf{x}, t) = K_3 \left(\frac{cos^2\theta}{c^2} \right) \frac{\partial}{\partial t} \left[H_2 + E_2 J_2 F_2 \right] e^{\Omega} \tag{E.44}$$

by eliminating the time derivative it gives the **final expression for the pressure field**:

$$\boxed{p(\mathbf{x}, t) = K_3 \left(\frac{cos^2\theta}{c^2} \right) e^{\Omega} \cdot \left[H_2 + 2E_2 J_2 F_2 \right]^2 + N} \tag{E.45}$$

Bibliography

[1] Ilan Kroo and Juan Alonso. "Lectures from the course: AA-241 Aircraft Design, Synthesis and Analysis". http://adg.stanford.edu/aa241/, Aircraft Aerodynamics and Design Group.

[2] "Aircraft Noise Fundamentals". Noise Management Program; (Excerpt from the Oakland International Airport Master Plan Update), 2006.

[3] Airbus Customer Service. *"Getting to Grips with Aircraft Noise"*. Airbus, 1, rond-point Maurice Bellonte, BP 33 31707 BLAGNAC Cedex FRANCE Telephone (+33) 5 61 93 33 33 Telefax (+33) 5 61 93 29 68 Telex AIRBU 530526F SITA TLSBI7X, flight operations support & line assistance edition, 12 2003.

[4] Marvin E. Goldstein. *"Aeroacoustics"*. McGraw-Hill international Book Company, Lewis Research Center, 1976.

[5] U.S. NRAC. "Report on Jet Engine Noise Reduction". Technical report, U.S. Naval Research Advisory Committee (NRAC) Panel, April 2009.

[6] Yves Gervais. "ENSMA Graduate course in Aeroacoustics". Lectures from personal notes, 12 2012.

[7] Brüel & Kjær. "Acoustic Measurements and Applications. course notes, 2011-2012.

[8] D.G. Crighton. "Basic Principles of Aerodynamic Noise Generation". *Prog. Aerospace Sci.*, 16(1):pp. 31–96, 1975.

[9] M. Cerna and A.F. Harvey. "The Fundamentals of FFT-Based Signal Analysis and Measurement". Application Note 041, National Instruments, July 2000.

[10] A. K. M. Fazle Hussain. "Coherent Structures and Turbulence". *Journal of Fluid Mechanics*, 173:pp. 303–356, 1986.

[11] Garry L. Brown and Anatol Roshko. "On density effects and large structure in turbulent mixing layers". *Journal of Fluid Mechanics*, 64(04):pp 775 – 816, 1974.

[12] André V. G. Cavalieri. *"Wavepackets as Sound-Source Mechanisms in Subsonic Jets"*. PhD thesis, ENSIP Poitiers, Université de Poitiers, june 2012.

[13] J. Blauert and N. Xiang. *"Acoustics for Engineers"*. Springer-Verlag, second edition, 2009.

[14] T.D. Rossing, editor. *"Springer Handbook of Acoustics"*. Springer Science, 2007.

[15] Julius S. Bendat and Allan G. Piersol. *"Random Data Analysis and Measurement Procedures"*. John Wiley and Sons, fourth edition, 2010.

[16] D. Havelock, S. Kuwano, and M. Vorländer, editors. *"Handbook of Signal Processingin Acoustics"*, volume Vol. 1. Springer Science, 2008.

[17] Mohit Gupta. "Summer Internship Project Report on Simulation and Visualization of Various Acoustic Sources in Matlab". Master's thesis, Kungliga Tekniska Hogskolan Stockholm, Sweden, EU Asia-Link ASIE/2005/111000, 2006.

[18] N.D. Sandham, C.L. Morfey, and Z.W. Hu. "Sound Radiation from Exponentially Growing and Decaying Surface Waves". *Journal of Sound and Vibration*, 294 (1):355–361, 2006.

[19] S.C. Crow. "Acoustic Gain of a Turbulent Jet". *Physiological Society Meeting*, 6, 1972.

[20] Peter Jordan. "Notes from Aeroacoustic Lectures on Noise Sources Identification". Institut Pprime, UPR-CNRS-3346, Université de Poitiers, ENSMA, France, 2011-2012.

[21] Roberto Camussi, Alessandro Di Marco, Paolo Gardonio, Peter Jordan, Michel Roger, Philip J. Morris, K. Viswanathan, and Avraham Hirschberg. *"Noise Sources in Turbulent Shear Flows: Fundamentals and Applications"*, volume 545 of *CISM International Centre for Mechanical Sciences*. Springer Vienna, Udine 2013, 2013.

[22] C. H. Dykhuizen and et al. "Fail-Safe Aircraft Engine Mounting System". General Electrics Company patents. (EP-1561684-B1), September 2011.

[23] P. K. Beardsley and G. A. Knight. "Aeroengine Mount". Rolls-Royce plc patents. (EP-1852346-A1), November 2007.

[24] A. Michalke and H. V. Fuchs. "On turbulence and noise of an axisymmetric shear flow". *Journal of Fluid Mechanics*, 70(01):179–205, 1975.

[25] Peter Jordan and Yves Gervais. "Subsonic jet aeroacoustics: associating experiment, modelling and simulation". *Experiments in Fluids*, 44(1):1–21, 2008.

[26] Andre V. G. Cavalieri, Daniel Rodriguez, Peter Jordan, Tim Colonius, and Yves Gervais. "Wavepackets in the velocity field of turbulent jets". *Journal of Fluid Mechanics*, Draft Manuscript, 2012.

[27] A.V.G. Cavalieri, P. Jordan, Tim Colonius, and Y. Gervais. "Axisymmetric superdirectivity in subsonic jets". *Journal of Fluid Mechanics*, 704(AIAA 2011-2743):pp. 388–420, 2012.

[28] Peter Jordan and Tim Colonius. "Wave Packets and Turbulent Jet Noise". *Journal of Fluid Mechanics*, 45:173–195, 01 2013.

[29] C. Mead and P. Strange. "Under-wing installation effects on jet noise at sideline". *AIAA 98-2207*, 01 1963.

[30] J. E. Ffowcs Williams and L. H. Hall. "Aerodynamic sound generation by turbulent flow in the vicinity of a scattering half plane". *Journal of Fluid Mechanics*, 40(04):657–670, 1970.

[31] M. J. Lighthill. "On Sound Generated Aerodynamically. I. General Theory". *Proceedings of the Royal Society of London. Series A. Mathematical and Physical Sciences*, 211(1107):564–587, 03 1952.

[32] N. Curle. "The Influence of Solid Boundaries upon Aerodynamic Sound". *Proceedings of the Royal Society of London. Series A. Mathematical and Physical Sciences*, 231(1187):505–514, 09 1955.

[33] André V. G. Cavalieri, Peter Jordan, and Yves Gervais. "Scattering of wavepackets by a flat plate in the vicinity of a turbulent jet". 18th AIAA/CEAS Aeroacoustics Conference (33rd AIAA Aeroacoustics Conference), American Institute of Aeronautics and Astronautics, 06 2012.

[34] André V. G. Cavalieri, Peter Jordan, Anurag Agarwal, and Yves Gervais. "Jittering Wave-Packet Models for Subsonic Jet Noise". *Journal of Sound and Vibration*, 330:4474–4492, 06 2010.